

Polarizability-Dependent Induced-Charge  
Electroosmotic Flow of Dielectric Particles and  
Its Applications

by

Fang Zhang

A thesis  
presented to the University of Waterloo  
in fulfillment of the  
thesis requirement for the degree of  
Doctor of Philosophy  
in  
Mechanical Engineering

Waterloo, Ontario, Canada, 2015

©Fang Zhang 2015

## **AUTHOR'S DECLARATION**

I hereby declare that I am the sole author of this thesis. This is a true copy of the thesis, including any required final revisions, as accepted by my examiners.

I understand that my thesis may be made electronically available to the public.

## ABSTRACT

To break the limit of the knowledge of the induced-charge electroosmotic flow, this thesis provides a new theoretical and numerical study of the polarizability-dependent induced-charge electroosmotic flow (ICEOF) of dielectric particles. We derived the analytical expression of the induced surface potential on dielectric particles for the first time. Based on this solution, we conducted numerical investigation of the migration of homogeneous and inhomogeneous dielectric particles under the influence of the polarizability-dependent ICEOF. Corresponding applications were also studied and addressed.

We found interesting electrokinetic effects associated with the polarizability-dependent ICEOF. It is proved that the electrokinetic motion of single homogeneous particles is not affected by the ICEOF around the particles; however, the hydrodynamic interaction between the ICEOF around two closely located particles is sensitive to the polarizability of the particles. We also studied the ICEOF of heterogeneous particles consisting of multiple dielectric parts. The spatially varying ICEOF around a heterogeneous particle continuously generates a torque. At the same time, the linear slipping velocity on the particle gives rise to constant translational motion. Thus these heterogeneous particles move like micro-wheels.

Two novel particle separation methods based on the polarizability-dependent ICEOF were developed and studied numerically. The first is to separate homogeneous particles. A separation region was created in a channel by embedding a pair of conducting plates where strong vortices were generated after applying electric fields. Due to the hydrodynamic interaction between the ICEOF around particles and the nearby wall, particles can either pass by or be trapped into the vortices. We further developed a separation method for Janus particles whose surface has two

different dielectric properties. The asymmetric ICEOF drives the particle to rotate until line up with the electric field. Meanwhile, the interactions between the ICEOF and the walls locate the particle at an equilibrium distance from the wall depending on the polarizability ratios of the particles. As a result, Janus particles of different polarizability ratios can be collected into different outlet branches continuously and independently. The third application is the new self-propelled particle. A heterogeneous particle is assembled with two differently high-polarizable ends. Under a uniform electric field, the ICEOF around the two polarizable ends results in a driving force pointing to the lower-polarizable end and this driving effect was found a function of the polarizabilities of the two ends.

Over all, this thesis for the first time provides the mathematical description of the dependence of ICEOF on the polarizability of the particles. The fact that the strength of ICEOF varies with the polarizability of the particle gives rise to several new particle manipulation techniques. The new particle separation methods were proved more advantageous than their counter parts. Moreover, the self-propulsion effect of a heterogeneous particle can be used to diversify the motilities of the particles in electrophoretic separation operations to optimize separation efficiency.

## **ACKNOWLEDGEMENT**

I am really grateful to who has helped me and cared about me in my life and during my study. I appreciate the wise advices, careful concerns, and the understanding and support from my supervisor Dr. Li. I really enjoyed and benefit from the accompany of my former and current colleagues Yasaman Daghighi, Saeid Movahed, Xuan Weng, Hai Jiang, Xiaoling Zhang and Ran Peng. I want to thank my parents and my sweet sisters who have loved me and trust me all the time. I want to give special thanks to my little nephew who gives me lots of pleasure since he was born two years ago.

# TABLE OF CONTENTS

AUTHOR'S DECLARATION .....	ii
ABSTRACT .....	iii
ACKNOWLEDGEMENT .....	v
TABLE OF CONTENTS .....	vi
LIST OF FIGURES .....	ix
LIST OF TABLES.....	xiv
LIST OF ABBREVIATIONS .....	xv
NOMENCLATURE .....	xvi
Chapter 1.....	1
Background.....	1
1.2 Electrokinetic phenomena: electrophoresis, dielectrophoresis, classic electroosmotic flow, induced-charge electroosmotic flow.....	1
1.3 Motivation and objectives .....	8
1.4 Outline of this thesis .....	11
Chapter 2.....	14
Literature review.....	14
2.1 Induced-charge electroosmotic flow and induced-charge electrophoresis.....	14
2.2 Heterogeneous particle.....	16
2.3 Particle separation techniques-electrophoresis and dielectrophoresis .....	17
Chapter 3.....	20
Mathematical expressions and governing equations .....	20
3.1 The ICEOF on dielectric sphere and cylinder in uniform electric field .....	20
3.2 Comparison between the derived induced surface potential and current existing mathematical expressions .....	27
3.2 Method-numerical model.....	32
3.3 Summary .....	37
Chapter 4.....	38
Migration of suspended homogeneous dielectric particles in uniform electric field.....	38
4.1 The motion of single particles in a straight microchannel.....	38
4.2 The interaction between two dielectric particles in uniform electric field .....	46
4.3 Conclusions.....	54

Chapter 5.....	56
Motion of heterogeneous particles in uniform electric field .....	56
5.1 Induced surface potential and ICEOF on heterogeneous particles .....	56
5.2 Computational domain and dimensions.....	60
5.3 Simulation results and discussion .....	62
5.4 Conclusions.....	72
Chapter 6.....	74
A novel particle separation method based on polarizability-dependent induced-charge electroosmotic flow. ....	74
6.1 Geometry and dimensions.....	74
6.2 Results and discussion .....	76
6.3 2D simulation validation.....	84
6.4 Summary and conclusions .....	84
Chapter 7.....	87
Separation of heterogeneous dielectric particle-Janus particle.....	87
7.1 The immigration of dielectric Janus particle in a straight channel .....	87
7.2 2D numerical simulation validation.....	95
7.3 Geometry and dimensions.....	96
7.4 Results and discussion .....	98
7.5 Conclusions.....	104
Chapter 8.....	105
Self-propelled heterogeneous particle .....	105
8.1 Computational domain and dimensions.....	106
8.2 Results-immigration of homogeneous particle in uniform electric field .....	108
8.3 Results-immigration of heterogeneous particle in uniform electric field .....	110
8.4 2D numerical validation.....	116
8.5 Conclusions.....	117
Chapter 9.....	119
Conclusions and future work .....	119
9.1 Conclusions.....	119
9.2 Future work.....	121
References.....	123

Appendix.....	128
License agreement for Chapter 4.....	129
License agreement for Chapter 6.....	130
License agreement for Chapter 7.....	131



## LIST OF FIGURES

Figure 1-1 The electrical double layer at the interface of a plate solid surface and liquid electrolyte.....	2
Figure 1-2. The electrical double layer and the EOF induced by uniform electric field on a straight channel.....	6
Figure 1-3.The polarization of conducting sphere immersed in liquid electrolyte in electric field. (a) The field lines intersect perpendicularly to the metal surface, (b) when the charging is done, the electric field profile is that of an insulator.....	7
Figure 1-4. Streamlines of the ICEOF around a polarized particle. Due to the opposite signs of the charges in the induced electrical double layer, four symmetric vortices occur around the surface in opposite directions.....	8
Figure 1-5. The polarization of a dielectric particle immersed in a liquid electrolyte in uniform electric field (a) polarization of dipoles in a dielectric particle and the screening process (b) the external electric field and the induced electrical double layer at steady state. The surface charges have opposite signs on the two sides of the particle, and charges distribution along the surface is non-uniform. ....	11
Figure 3-1. The spherical coordinate and the ICEOF around a polarized dielectric sphere (a) EDL and electric field lines around a polarized particle. (b) Streamlines of ICEOF adjacent to a polarized particle with screening cloud.....	21
Figure 3-2. Induced surface potential. (a) The induced surface potential of the dielectric particle with a radius $a=10\mu\text{m}$ , in a uniform electric field $E_\infty=100\text{V/cm}$ aligned in the $x$ -direction. $\epsilon_m = 80$ . ....	24
Figure 3-3. Induced surface potential of a sphere of radius $a=10\mu\text{m}$ , under electric field strength $E_\infty=100\text{V/cm}$ . Results are induced surface potential of metal sphere calculated by Squires' expression: $\zeta_i = \frac{3}{2}E_\infty a \cos\theta$ [5], and Wu's expression: $\zeta_i = \frac{\int_s \phi dA}{A} - \phi$ [7], respectively, and the induced surface potential of dielectric sphere by the derived solution $\zeta_i = \frac{3}{2}CE_\infty a \cos\theta$ , $C = \frac{\epsilon_p}{\epsilon_p + 2\epsilon_m} = 0.5$ , ....	30
Figure 4-1. Schematic diagram of the computational domain. Electric field is applied along the length of the channel. The particle is initially placed in the center of the channel. $H = W = 100\mu\text{m}$ , $L = 600\mu\text{m}$ , $d = 20\mu\text{m}$ .....	41
Figure 4-2. Vortices around a dielectric sphere of $20\mu\text{m}$ in diameter, when $\zeta_w = -15\text{mV}$ , $\epsilon_m = 80$ , $\epsilon_p = 1000$ . (a) $E_\infty = 40\text{V/cm}$ , (b) $E_\infty = 70\text{V/cm}$ , (c) $E_\infty = 100\text{V/cm}$ .....	44
Figure 4-3. The velocity vector and $x$ -velocity contour at $t=0$ . $E_\infty = 100\text{V/cm}$ , $\zeta_w = -15\text{mV}$ .	45
Figure 4-4. The flow velocity in the $x$ direction around the particle surface at $t=0$ . $E_\infty=100\text{V/cm}$ , $\zeta_w=-15\text{mV}$ , $d=20\mu\text{m}$ .....	45

Figure 4-5. Streamlines of the flow field and positions of particles with different $\varepsilon_p$ , at time $t=0s$ and $t=2.5s$ , $E_\infty = 100V/cm$ , $\zeta_w = -15mV$ , $\varepsilon_m = 80$ , $d=20 \mu m$ .....	47
Figure 4-6. Schematic diagram of the simulation domain for studying the interaction of two dielectric particles due to ICEOF.....	49
Figure 4-7. In the presence of a parallel electric field, the flow field and the pressure field (a) around two identical particles, and (b) around two different dielectric particles. $d = 10\mu m$ .....	50
Figure 4-8. In the presence of perpendicular electric field, the flow field and the pressure field (a) around two identical dielectric particles ( $\varepsilon_p = 1000$ ), and (b) around two different particles, $\varepsilon_{p-left} = 100$ , $\varepsilon_{p-right} = 20000$ , respectively, $d=10\mu m$ .....	52
Figure 4-9. Displacement of two dielectric particles with $\varepsilon_{p-left} = 100$ , $\varepsilon_{p-right} = 20000$ , $\varepsilon_m = 80$ over a period of 3 seconds. Particles were initially separated by a distance of $l = 5d$ . Dashed dark line indicates the initial center line of the two particles. (a) Under a parallel electric field $E_\infty = 100V/cm$ . (b) Under a perpendicular electric field $E_\infty = 100V/cm$ .....	53
Figure 4-10. Forces exerted on the two particles as a function of $\varepsilon_{p-right}$ . Particles are initially separated by a distance $l = 5d$ . $E_\infty = 100V/cm$ , and $\varepsilon_{p-left} = 100$ , $d = 10\mu m$ , (a) in a parallel electric field, (b) in a perpendicular electric field. The positive force is in the direction from the left to the right. The negative force is in the direction from the right to the left.....	55
Figure 5-1. Heterogeneous particles made of two dielectric materials represented by two different colors. ....	58
Figure 5-2. The induced surface potential calculated by Eq. (3-9), and Eq. (5-1), and $C = \frac{\varepsilon_p}{\varepsilon_p + 2\varepsilon_m}$ . The values of the parameters are: $\varepsilon_{p-right} = 200$ , $\varepsilon_m = 80$ , $a=10 \mu m$ , $E_\infty=100V/cm$ .....	59
Figure 5-3. The polarization of the 6-parts heterogeneous particle in uniform electric field. Alternate polarizabilities: $C_1=1$ , $C_2=0.2$ , size $d=10 \mu m$ , $E_\infty=25V/cm$ . (a) The value of induced surface potential, (b) the streamlines of the ICEOF.....	60
Figure 5-4. The schematic diagram of the computational domain.....	62
Figure 5-5. The rotation of the 6-parts particle $d=20\mu m$ with $C_1=1$ , $C_2=0.2$ , $E_\infty =25V/cm$ . Starts from $t=0, \omega_p = 0$ . ....	64
Figure 5-6. Streamlines of the 4-parts particle at steady state $t=0.2s$ and $\alpha = 90^\circ$ . $E_\infty=25V/cm$ .....	66
Figure 5-7. The change of rotational speed of 6-parts particle with external electric field strength. $C_1=1$ , $C_2=0.2$ , $d=20 \mu m$ .....	68
Figure 5-8. Micro-wheel motion in uniform electric field. 6-parts heterogeneous particle, with $C_1=1$ , $C_2=0.2$ , $d=20 \mu m$ , $\zeta = -30mV$ and $E_\infty = 50V/cm$ . Cross signs indicate the initial location at $t=0$ . ....	69
Figure 5-9. The non-dimensional force $\overline{F}_x = \frac{F_x}{\varepsilon_0 \varepsilon_m E_\infty^2 d^2}$ exerted to the particle at the beginning of the migration.....	70

Figure 5-10. Streamlines and the x-velocity field at $t=1.05s$ . 6-parts heterogeneous particle, with $C_1=1, C_2=0.2, d=20 \mu m, \zeta = -30mV$ and $E_\infty = 50V/cm$ .....	71
Figure 5-11. The linear speed and the translational speed of the heterogeneous particles in various electric fields. The speeds of the two motions depend on the applied electric field. While $C_1=1, C_2=0.2, d=20\mu m$ , and the static potential on the particle is $\zeta = -30mV$ .....	73
Figure 6-1. Schematic diagram of the computational domain. Thicker red lines indicate the metal plates.....	76
Figure 6-2. The streamline of the ICEOF on a fully polarized metal plate embedded in an insulating wall. Thicker red line indicates the location of the polarized metal plate.....	78
Figure 6-3. An example of the simulated streamlines in the computational domain and the separation section at $E_\infty = 27V/cm, d = 10 \mu m, C = 0.7$ , and $t = 0$ .....	79
Figure 6-4. The trapping trace of a particle in the separation section with a relative polarizability $C=0.7, E_\infty=27V/cm, d=10 \mu m$ .....	79
Figure 6-5. The passing-through trace of a particle with a relative polarizability $C=0.6, E_\infty=27V/cm, d=10 \mu m$ .....	80
Figure 6-6. A summary of paths of particles of various polarizabilities under different electric field strengths.....	82
Figure 6-7. Streamlines of the flow on a surface in the center of the 3D computational domain. At $t=0, C=0.6, E_\infty=27V/cm, d=10 \mu m$ .....	85
Figure 7-1. The angle $\alpha$ between the equatorial plane of the Janus particle and applied electric field.....	89
Figure 7-2. The streamlines of the ICEOF around a dielectric Janus particle, $\varepsilon_{p1} > \varepsilon_{p1}, \alpha = 0^\circ$ , .....	89
Figure 7-3. The reorientation of a dielectric Janus particle in uniform DC electric field due to ICEOF, initial $\alpha = 60^\circ, E_\infty = 50V/cm$ , polarizability ratio $\frac{C_1}{C_2} = 3$ , particle diameter $d = 10\mu m$ .....	91
Figure 7-4. Final separation distance between a dielectric Janus particle and the channel wall. $E_\infty = 50V/cm$ , polarizability ratio $\frac{C_1}{C_2} = 3$ , particle diameter $d=10\mu m$ .....	93
Figure 7-5. The separation distance of Janus particles from the wall with time, for two types of dielectric Janus particles of diameter $d = 10 \mu m, \frac{C_1}{C_2} = 1.5$ , and $\frac{C_1}{C_2} = 3$ , under different electric field strengths $E_\infty = 50V/cm$ and $E_\infty = 80V/cm$ .....	94
Figure 7-6. The variation of the final separation distance $\bar{H}$ with particle polarizability ratio $\frac{C_1}{C_2}$ , where $E_\infty = 50V/cm, \varepsilon_m = 80, d = 10\mu m$ .....	95

Figure 7-7. Example of the variation of final separation distance $\bar{H}$ with particle size, for $\frac{c_1}{c_2} = 2$ , $E_\infty = 50V/cm$ , $\varepsilon_m=80$ .....	96
Figure 7-8. Final separation distance between a dielectric Janus particle and the channel wall. $E_\infty = 50V/cm$ , polarizability ratio $\frac{c_1}{c_2} = 3$ , particle diameter $d=10\mu m$ .....	97
Figure 7-9. Schematic diagram of model system of dielectric Janus particles in a microchannel.....	98
Figure 7-10. Separation of dielectric Janus particles in EOF in DC electric field. $E_\infty=50V/cm$ in the main channel, $E_\infty = 25V/cm$ in branch channels 1, $E_\infty = 12V/cm$ in branch channels 2. Polarizability ratios of the three particles: $P_1: \frac{c_1}{c_2} = 2$ $P_2: \frac{c_1}{c_2} = 3$ , $P_3: \frac{c_1}{c_2} = 1.5$ , $d=10\mu m$ . (a) particles are released in the channel center with a horizontal separation distance $10d$ , (b) the trajectories and positions of the particles in 10 seconds, (c), (d) particles are separated and collected into branch channels independently following their individual streamlines.....	102
Figure 7-11. Separation of dielectric Janus particles by size. $P_3$ and $P_4$ have the same polarizability ratio, $\frac{c_1}{c_2} = 2$ . The diameter of particle $P_3$ is $d=10\mu m$ , the diameter of particle $P_4$ is $d=5\mu m$ . $E_\infty=50V/cm$ . ....	104
Figure 8-1. The schematic diagram of the computational domain.....	108
Figure 8-2. Dielectric particle suspended in an electrolyte in a straight channel. The channel wall has a negative static zeta potential $\zeta_w$ , and the potential of the particle is $\zeta_p$ . Uniform electric field $E_\infty$ is applied though the channel. ....	109
Figure 8-3. The translational velocity of a particle with static potential $\zeta$ in EOF. Zeta potential on the wall $\zeta_w = -30mV$ . Electric field is applied in the $x$ -direction.....	110
Figure 8-4. Heterogeneous particle with non-polarizable cylinder in the middle, dielectric hemisphere $\varepsilon_{p1}$ on the right, and dielectric hemisphere $\varepsilon_{p2}$ on the left, (a) the length of the cylinder is $l$ and diameter is $d$ . (b) electric field around the particle and the induced charges on the particle. Uniform electric field $E_\infty$ is applied. The static zeta potential on the particle is a constant $\zeta$ , and the induced surface potential on the hemisphere on the right is $\zeta_{i-1}$ , and $\zeta_{i-2}$ on the other side. ....	112
Figure 8-5. Streamlines around the dielectric particle. Static zeta potential on the wall $\zeta_w = -30mV$ , static zeta potential on the particle $\zeta = -20mV$ , electric field $E_\infty = 60V/cm$ applied in the $x$ -direction. ....	113
Figure 8-6. The velocity of the immigration of the particle without ICEOF and with ICEOF of different strength on the two ends of the particle. Under zeta potential of the wall $\zeta_w = -30mV$ , zeta potential on the particle $\zeta = -20mV$ . With the combination of the defined polarizability ( $C_1=0.6$ , $C_2=0$ ), ( $C_1=0.8$ , $C_2=0.2$ ), and ( $C_1=0.8$ , $C_2=0$ ). The scale of the particle is $d=l=10\mu m$ .....	114

Figure 8-7. The velocity of the particle with different polarizable hemispheres in uniform electric field. Zeta potential on the wall and the particle are  $\zeta_w = -20\text{mV}$  and  $\zeta = -20\text{mV}$ , respectively. The motion of the particles is in the negative  $x$ -direction with  $(C_1=0.6, C_2=0)$ ,  $(C_1=0.6, C_2=0.4)$  and  $(C_1=0.8, C_2=0.2)$ . The size of the particle is  $d=l=10\ \mu\text{m}$  .....116

Figure 8-8. The velocity vector of the flow field. zeta potential on the channel wall:  $\zeta_w = -30\text{mV}$ ; zeta potential on the particle  $\zeta = -20\text{mV}$ ; the defined polarizability of the heterogeneous particle  $(C_1=0, C_2=0.8)$ .  $E_\infty = 100\text{V/cm}$ .....118

## LIST OF TABLES

Table 1-1. Examples of dielectric materials and the values of their relative permittivity.....	10
Table 4-1. Values of constants and parameters used in the simulations.....	42
Table 5-1. Discretization methods for the simulations conducted using COMSOL 3.5a.....	62
Table 5-2. Values of the constants and parameters used in the simulation.....	63
Table 5-3. Rotation periods of five types of heterogeneous particles, particle size $d=20\ \mu\text{m}$ , $C_1=1$ , $C_2=0.2$ , $E_\infty=25\text{V/cm}$ . Heterogeneous particles composed of 4, 6, 8, 10 and 12 equal parts, respectively.....	65
Table 5-4. Rotation periods of 6-parts particle with a variety of polarizability compositions, $E_\infty=25\text{V/cm}$ , $d=20\ \mu\text{m}$ .....	68
Table 6-1. Discretization methods for the simulations conducted using COMSOL 3.5a.....	76
Table 6-2. Values of constants and parameters used in the simulations.....	77
Table 6-3. Paths of particles of different sizes at $E_\infty=27\text{V/cm}$ .....	84
Table 7-1. The steady angles of Janus particles in uniform electric field.....	92
Table 7-2. Discretization methods for the simulations conducted using COMSOL 3.5a.....	98
Table 7-3. Values of constants and parameters used in the simulations.....	99
Table 8-1. Discretization methods for the simulations conducted using COMSOL 3.5a.....	108
Table 8-2. Values and ranges of constants and parameters in the simulations.....	108
Table 8-3. The translational velocity of the dielectric particle with two hemispheres of different polarizability at the ends. $E_\infty = 60\text{V/cm}$ , $\zeta_w = \zeta = -20\text{mV}$ .....	116

## **LIS OF ABBREVIATIONS**

EP	Electrophoresis
EOF	Electroosmotic flow
ICEOF	Induced-charge electroosmotic flow
DEP	Dielectrophoresis
EDL	Electrical double layer

## NOMENCLATURE

$\vec{V}$	Velocity of the fluid	$\phi_0$	Potential on the particle surface due to polarization
$\vec{U}_p$	Velocity of the particle	$\phi_{steady}$	Potential outside the induced electrical double layer at steady state
$\vec{U}_e$	Electrophoresis velocity	$D_{in}$	Electric displacement inside the particle
$\mu_e$	Electrophoretic mobility	$D_{out}$	Electric displacement outside the particle
$F_{DEP}$	Dielectrophoretic force	$\zeta_w$	Zeta potential on a wall
$\vec{\omega}_p$	Rotational velocity of the particle	$\zeta$	Zeta potential
$\vec{X}_p$	Centroid vector of the particle	$\zeta_i$	Induced surface potential
$\vec{x}_p$	Position vector on the particle	$\zeta_p$	Surface potential on a particle
$\vec{\sigma}_p$	Stress tensor on the particle	$\vec{r}$	Radial distance in spherical coordinate
$\vec{\Gamma}$	Torque	$\theta$	Polar angle
$m_p$	Mass of the particle	$\varphi$	Azimuthal angle
$J_p$	Inertia of the particle	$\varepsilon_p^*$	Complex permittivity of particle
$\bar{I}$	Identity factor	$\varepsilon_m^*$	Complex permittivity of liquid
$t$	Time	$\varepsilon_0$	Absolute permittivity of the vacuum
$\vec{F}$	Body force	$\varepsilon_r$	Relative permittivity
$P$	Pressure	$\varepsilon_p$	Relative permittivity of the particle
$\phi$	Electric potential	$\varepsilon_m$	Relative permittivity of the medium
$\phi_{in}$	Potential inside a particle	$C$	Defined non-dimensional polarizability
$\phi_{out}$	Potential outside a particle	$\mu$	Viscosity of the liquid solution
$P_k$	Legendre polynomial	$T$	Temperature



$\rho$	Density of the liquid
$n_0$	Bulk ionic concentration
$\rho_e$	Free charge density
$z$	Absolute value of the ion valence
$K_B$	Boltzmann constant
$\kappa^{-1}$	Electrical double layer thickness
$\lambda_D$	Electrical double layer thickness
$\Delta t$	Time step

$q$	Induced charge
$\rho_e$	Net charge density
$d$	Diameter of the particle
$a$	Radius of the particle
$T_r$	Rotation period of the particle
$\tau_c$	Time scale of induced electrical double layer
$L_{dev}$	Development length of laminar flow
Re	Reynolds number

# Chapter 1

## Background

Electrokinetics is a series of general and significant phenomenon in microfluidic systems. It is associated with externally applied electric field, liquid electrolyte, solid particles or microchannel. In microfluidics systems, electrokinetics has been used to generate the motion of liquid or micro particles. Among the family of the electrokinetics phenomena, the most common effects are: electrophoresis (EP), dielectrophoresis (DEP), classic electroosmotic flow (EOF), and induced-charge electroosmotic flow (ICEOF).

### **1.2 Electrokinetic phenomena: electrophoresis, dielectrophoresis, classic electroosmotic flow, induced-charge electroosmotic flow**

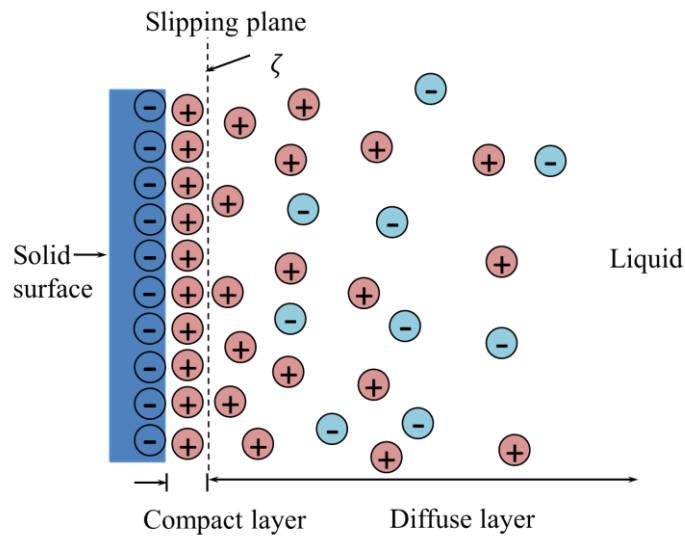
We first introduce the basis of several electrokinetic phenomena: the electrical double layer. In micro systems, the interface between a solid surface and an aqueous solution normally presents a layer of static charges. Since there are mobile ions in the surrounding solution, counter ions in the solution will be attracted to the solid surface to electrically screen the static charges and thus form a layer of counter charges. These two layers of charges are termed as electrical double layer (EDL). As shown in Figure 1-1, there is a layer of solute ions strongly attached to the surface. This layer is called compact layer. From the compact layer to the electrically neutral bulk solution, the concentration of the counter charges gradually reduces to the concentration of the bulk liquid. This region is termed as diffusion layer, wherein the counter ions are only loosely attracted to the surface and are mobile. The electric potential caused by the net charges in the double layer is termed as zeta potential  $\zeta$ , and is defined as the potential drop from the surface to the neutral liquid solution. The magnitude of the zeta potential at an interface in a microsystem

can be around or less than several tens of millivolts. Both the absolute value and the sign of the zeta potential are determined by the properties of the solid surface.

The thickness of the double layer in a symmetric electrolyte is expressed as [1]

$$\kappa^{-1} = \lambda_D = \sqrt{\frac{\epsilon_0 \epsilon_r k_B T}{2n_0 (ze)^2}} \quad (1-1)$$

Where  $k_B$  is the Boltzmann constant,  $T$  is the temperature  $n_0$  is the bulk ionic concentration, and  $z$  is the absolute value of the ion valence. Accordingly, the double layer thickness purely depends on the properties of the surrounding solution. In the common cases of the aqueous solutions in microfluidic systems, the thickness of the electrical double layer ranges from several tens of nanometers to several hundreds of nanometers.



**Figure 1-1. The electrical double layer at the interface of a solid plate and liquid electrolyte.**

### ***1.2.1 Electrophoresis***

Electrophoresis is the motion of dispersed micro particles in electric field. It results from the interaction between an external electric field and the static charges on the particle. In

microfluidic systems, static charges at the interface of two phases (e.g. at the particle surface which is surrounded by aqueous solution) are commonly apparent. The sign and absolute value of the net charges vary with the physical or chemical properties of the particles. When these particles are immersed in an aqueous solution and electric field is applied, the charged particles would experience Coulomb force from the local electric field. The electrophoretic velocity can be expressed as [2]

$$\vec{U}_e = \frac{\varepsilon_0 \varepsilon_r \zeta}{\mu} \vec{E} \quad (1-2)$$

Where  $\varepsilon_0$  is the permittivity of the vacuum and  $\varepsilon_r$  is the relative permittivity of the surrounding solution.  $\mu$  is the viscosity of the solution.  $\zeta$  is the static potential of the particle due to the static charges, and  $\vec{E}$  is the local electric field. The ratio of the electrophoretic velocity to the applied external electric field is defined as the electrophoretic mobility [2]:

$$\mu_e = \frac{\varepsilon_0 \varepsilon_r \zeta}{\mu} \quad (1-3)$$

Particles with different static potentials migrate at different velocities under the influence of an external uniform electric field. In particle manipulation technology, electrophoresis has been used to separate particles.

### ***1.2.2 Dielectrophoresis***

Dielectrophoresis describes the motion of dielectric particles. It is caused by the interaction between an externally applied non-uniform electric field and the induced charges on a dielectric particle. The particle doesn't have to be initially charged, instead, the dispersed dielectric particle will be polarized in response to the electric field, and result in net charges on the surface. The induced charges on the surface have opposite signs and are in equal amount. However, if the

external electric field is spatially non-uniform, the charge density varies in response to the gradient of the electric field, and leads to a net electrostatic Coulomb force exerted by the external electric field. The resulting net force drives the particle to move towards the high electric field region (positive dielectrophoresis) or low electric field region (negative dielectrophoresis) depending on the relative permittivity of the particle to the surrounding solution.

$$F_{\text{DEP}} = 2\pi a^3 \text{Re} \left\{ \frac{\epsilon_p^* - \epsilon_m^*}{\epsilon_p^* + 2\epsilon_m^*} \right\} \nabla |\vec{E}_\infty|^2 \quad (1-4)$$

Eq. (1-4) [3] is the expression of the dielectrophoretic force induced by electric field  $\vec{E}_\infty$  on a particle of radius  $a$  and complex permittivity  $\epsilon_p^*$  surrounded by a liquid solution with complex permittivity  $\epsilon_m^*$ . The complex permittivity of a dielectric materials is a function of the frequencies of the applied alternating currents. When dielectrophoresis is induced by direct current, static permittivity is employed instead. The dielectrophoretic force is highly dependent on the permittivity and the size of the dielectric particle and proportional to the second order of the electric field. Therefore, particles of different sizes or permittivity undergo dielectrophoretic forces of different strengths. Therefore, dielectrophoresis has been commonly used in particle separation technologies. In most cases, dielectrophoresis is actuated by alternating fields; accordingly, the dielectrophoretic force is also determined by the frequencies of the fields.

### ***1.2.3 Classic electroosmotic flow***

The electroosmotic flow (EOF) is the flow of an electrolyte solution in the close vicinity of an interface (e.g. the interface between micro channel and aqueous liquid or the interface between a

solid particle and the surrounding solution). It results from the interaction between an external electric field and net mobile charges in the electrical double layer (EDL) at the interface.

The existence of the static EDL does not require external electric fields. Nevertheless, when an external electric field is applied, the tangential electric field component exerts electrostatic Coulomb force on the net charges in the EDL. Since the mobile charges in the second layer are only loosely attached to the surface, the tangential electric field component would drive these mobile charges to move along the solid surface. The flow field is described by the Navier-Stokes equation:

$$\rho \frac{\partial \vec{V}}{\partial t} = -\nabla P + \mu \nabla^2 \vec{V} + \vec{F} \quad (1-5)$$

Here  $\rho$  and  $\mu$  are the density and viscosity of the liquid medium, and  $\vec{V}$  is the velocity of the liquid medium,  $P$  is the pressure, and  $F$  is the Coulomb force  $\vec{F} = \vec{E} \rho_e$ , induced by external electric field. The mathematical description of the potential generated by the net charges is given by Poisson's equation: [4]

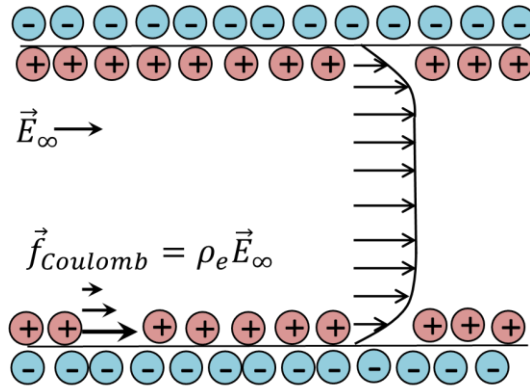
$$\nabla^2 \phi = -\frac{\rho_e}{\epsilon_0 \epsilon_r} \quad (1-6)$$

$\rho_e$  is the free charge density. The motion of the double layer would drag the bulk liquid to move along due to the viscosity of the solution, which is termed as the electroosmotic flow (EOF) (shown in Figure 1-2). When the thickness of the double layer is much smaller than the characteristic scale of the geometry, the EOF in a tube or square cross-section channel has a planar velocity profile. While solving the Navier-Stokes equation with Poisson-Boltzmann equation, Debye-Huckel approximation ( $\frac{ze\zeta}{k_b T} \ll 1$ ) is applied to linearize this set of equations.

The obtained analytical expression for the velocity is the classic Helmholtz–Smoluchowski slip formula [5].

$$\vec{V} = -\frac{\varepsilon_0 \varepsilon_r \zeta}{\mu} \vec{E}_{\parallel} \quad (1-7)$$

This expression shares the same form with the electrophoretic velocity expression except  $\vec{E}_{\parallel}$  stands for the tangential electric field. The value and the sign of the zeta potential of a solid surface can be various. Normally, the zeta potential on an isotropic solid surface that is exposed to liquid electrolyte is constant and the value is around several tens of millivolts. When the electrolyte solution in the microsystem is isotropic, the only factor that affects the EOF is the external electric field.

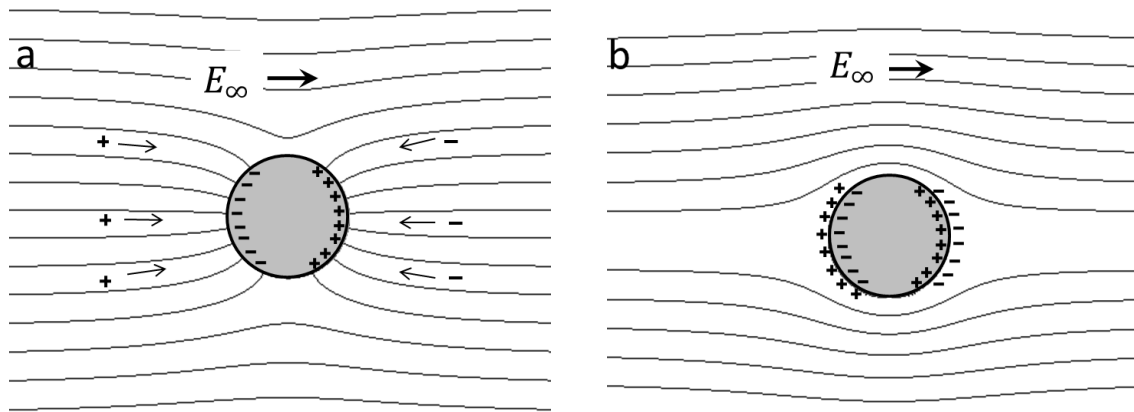


**Figure 1-2. The electrical double layer and the EOF induced by uniform electric field in a straight channel.**

#### ***1.2.4 Induced-charge electroosmotic flow on polarizable particle***

The induced-charge electroosmotic flow (ICEOF) is also referred as the secondary electroosmotic flow because the causing mechanism is analogous to that of the classic electroosmotic flow. The ICEOF is also the motion of liquid in the vicinity of a solid surface,

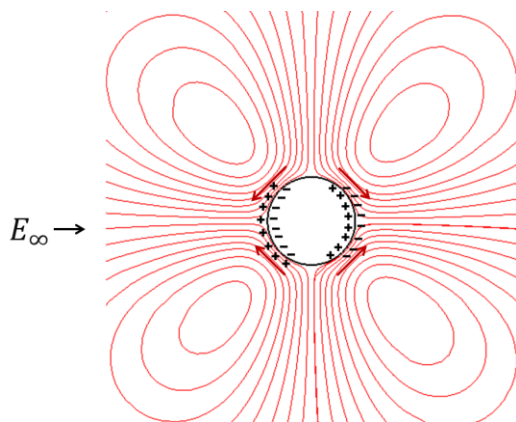
however, it occurs because of the interaction of the external electric field and net mobile charges in the induced electrical double layer. The solid surface involved in this phenomenon can be initially neutral, but polarizable. When the surface is polarized under the same mechanism as in dielectrophoresis, there are net charges distributed on the surface, with negative charges on one side facing the field source and positive charges on the opposite side. When the surface is fully polarizable or electrical conducting, the internal electric field generated by the induced charges will cancel the external electric field. The induced charge density is determined by the electric field, the dielectric property and the geometry of the surface. When the surface is exposed to liquid electrolyte, the induced charges would absorb free counter ions from the nearby liquid. Meanwhile, the electric field lines interacting on the particle also drive negative and positive ions to accumulate on the two sides of the particle (Figure 1-3 a). The accumulating process reaches a steady state when the particle is fully shielded from the outside electric field (Figure 1-3 b). The time scale for the charging process is on the order of  $\tau_c = 10^{-4}$ s [5]. Comparing with the characteristic time scale of general microfluidic processes, the charging process is negligible.



**Figure 1-3. The polarization of a conducting sphere immersed in liquid electrolyte in electric field, (a) the field lines intersect perpendicularly to the metal surface, (b) the external electric field profile when the charging is done.**



The screening cloud containing the solute ions is called the induced electrical double layer (EDL), which has the same configuration as the static EDL. The potential of this induced EDL in this study is termed as the induced surface potential  $\zeta_i$ . Since the charges on the two sides of the particle are opposite, the induced surface potential also has opposite signs on the two sides of the surface. Under the influence of the external electric field, the non-linear induced surface potential gives rise to non-linear slipping velocity of the double layer: the tangential electric field drives the mobile ions from the two “poles” towards the “equator”, resulting in four opposite but symmetric vortexes (as shown in Figure 1-4).



**Figure 1-4. Streamlines of the ICEOF around a polarized particle. Due to the opposite signs of the charges in the induced EDL, four symmetric vortexes occur around the surface in opposite directions.**

### 1.3 Motivation and objectives

The ICEOF in microsystems possesses interesting features. The vortexes of the ICEOF are able to introduce a convection regime into the classic linear microfluidic flow; low and high pressure regions are created at the joints of the vortexes on the polarized surface, and the flow direction changes at the vortexes.

Current knowledge of the ICEOF includes the mathematical expression of the induced surface potential on metal sphere and cylinder. The analytical expression is obtained by solving Laplace's equation with the appropriate physical boundary conditions. The first analytical expression was given by S. S. Dukhin [6], who obtained the induced surface potential  $(3/2)E_{\infty}a\cos\theta$  of metal spheres, where  $a$  is the radius of the particle, and  $E_{\infty}$  is the external electric field. T. M. Squires et al. [5] recently verifies this expression and also derived the induced surface potential for a metal cylinder:  $2E_{\infty}a\cos\theta$ . The analytical expression for the induced surface potential is only available for systems of simple geometries and uncomplicated boundary conditions due to the second-order partial derivatives of the Laplace's equation. To break this limit, Z. Wu [7] derived an integral formula  $\zeta_i = \frac{\int_S \phi dA}{A} - \phi$  based on the initial neutrality of a metal surface. The numerical result of the induced surface potential of a metal of arbitrary geometry can be obtained by applying the zero-current assumption at the geometry surface. In this integral formula,  $A$  is the surface area of the metal geometry, and  $\phi$  is the external electric potential.

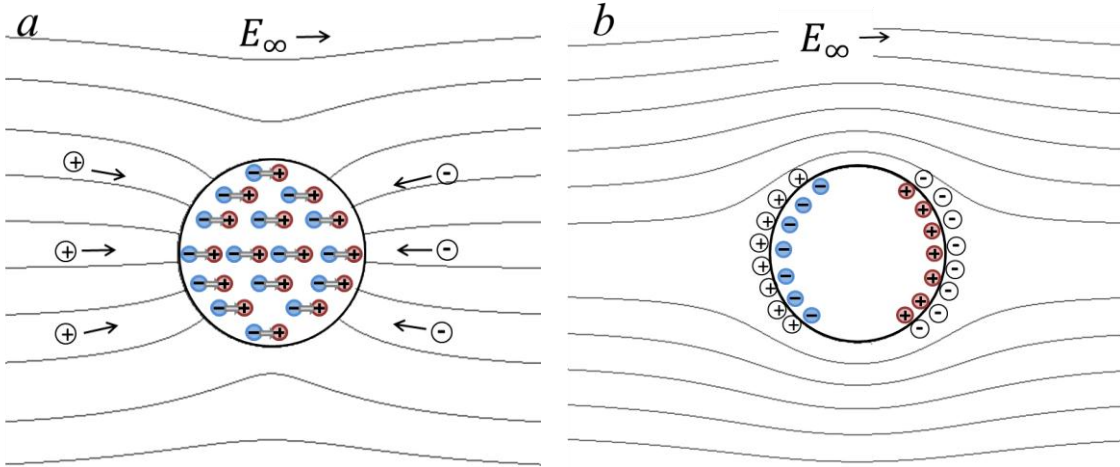
According to S. S. Dukhin [6], T. M. Squires [5] and Z. Wu's [7] theory, metal particles in the electrolyte are always ideally polarizable, and the external electric field will be completely diminished by the induced internal electric field. Accordingly, the induced surface potential is only determined by the external electric field and the geometry of the metal particle.

However, in microfluidic studies, a major part of the objects are partially polarizable dielectrics (Table 1-1). Though dielectric materials do not have mobile charges that can freely move when subjected to an electric field, the electric dipoles inside the dielectrics reorient in response to an external electric field (as shown in Figure 1-5). The polarizability of a dielectric describes how

easily the dielectric can be polarized in an external electric field. This property is measured by a dimensionless parameter—relative permittivity  $\epsilon_r$ [8-17], which is the ratio of the permittivity of a dielectric to the permittivity of vacuum  $\epsilon_0$ . The induced surface potential and the ICEOF of dielectrics are predicted to vary with the dielectric property of the dielectrics. To date, there is no systematic theoretical study of the dependence of the induced surface potential and the ICEOF on polarizability. This thesis aims to provide a better understanding of the polarizability-dependent induced surface potential and ICEOF of dielectric particles in microfluidic systems. The dependence of the ICEOF on dielectric polarizability could provide a diversity of vortex strengths. This feature will allow new flow control and particle manipulation methods.

Materials	Permittivity	References
Silicon	12	[8]
Ethylene glycol	37	[9]
Water	80	[10]
Hydrocyanic	2.3~158	[9]
Biological cells	104~151	[11]
Ceramic-powder polymer composite	200	[12]
Strontium titanate	2000	[13]
Barium titanate	5000	[14]
Copper titanate	~10,000	[15]
Conjugated polymers	210~240,000	[16]
Calcium copper titanate	>250,000	[17]

**Table 1-1. Examples of dielectric materials and the values of their relative permittivity.**



**Figure 1-5. The polarization of a dielectric particle immersed in a liquid electrolyte in uniform electric field, (a) the uniform array of dipoles inside the particle and the accumulation of the mobile ions from the surrounding electrolyte (b) the external electric field and the induced electrical double layer at steady state. The surface charges have opposite signs on the two sides of the particle, and charge distribution along the surface is non-uniform.**

#### 1.4 Outline of this thesis

This thesis consists of nine chapters.

In the first chapter, fundamental theories of the electrokinetic phenomena including the ICEOF in microfluidics are introduced. We summarize the current status of the study of ICEOF and explain the lack of knowledge of the ICEOF of dielectric systems. The objective of this research is to provide a systematic investigation of the polarizability-dependent ICEOF of dielectric particles.

The second chapter first offers a further detailed review of the research about ICEOF phenomena and the corresponding applications of ICEOF in microfluidics. We also reviewed the characteristic features of heterogeneous particles in chemical, biology and microfluidics areas,

and particularly demonstrate the motion of heterogeneous particles in response to external electric field due to polarizability. Finally, current particle separation methods are introduced including electrophoresis and dielectrophoresis techniques. The advantages and drawbacks of these separation methods are also summarized.

Chapter 3 involves the mathematical derivation of the essential formula of this thesis –the analytical expression of the polarizability-dependent induced surface potential. We also compare the mathematical derivation of our expression and the existing achievement established on metal surface. The mathematical models of the transient simulations in this thesis are also demonstrated. Governing equations for the electric field, the electrokinetic flow, and the motion of the particle and proper boundary conditions for each field are also given.

In the fourth chapter, we start the numerical study of the ICEOF for a homogeneous dielectric particle in a uniform electric field. We apply the derived mathematical expression of the induced surface potential and simulate the time-dependent motion of the dielectric particle in a liquid electrolyte subjected to a uniform electric field. Both the migration of single particles in a straight channel and the interaction between two closely spaced dielectric particles in a chamber are investigated.

In chapter 5, the research is carried forward to study heterogeneous particles composed of multiple equal parts of different polarizabilities with an alternate distribution. Simulation results found the rotational behavior of a heterogeneous particle. Meanwhile, the static zeta potential on the particle provides a linear translational motion parallel to the electric field. The resulting motion of heterogeneous particles under the two mechanisms appears as the motion of micro-wheels.

In chapter 6, we develop a novel particle separation method based on the polarizability-dependent ICEOF. We utilize the linear EOF of the bulk liquid and local strong vortexes around two metal plates embedded in the channel to create a separation section. The interaction between the ICEOF on a dielectric particle and the solid wall is able to deflect particle from the original path. Depending on the particle polarizability, the particle can either be trapped in the vortexes or pass on towards downstream. The transient numerical simulation results show that homogeneous particles in this microfluidic system can be separated by polarizability or size, and the separation result is highly sensitive to external electric field strengths.

In Chapter 7, I investigated the ICEOF on heterogeneous dielectric Janus particles that possesses two polarizabilities on the surface, and develop a Janus particle separation method. We did transient simulations of the self-alignment behavior of Janus particles in a uniform electric field and found that particles occupy different streamlines in the channel depending on their polarizability ratios. Thus, dielectric Janus particles of different polarizability ratios can be separated through the divergence of stream at downstream.

Chapter 8 examines the self-propulsion phenomenon of a heterogeneous particle. The heterogeneous particle is built by attaching two different-polarizable hemispheres to the ends of a non-polarizable cylinder. The unbalanced ICEOF around the particle offers a push effect, and the strength of this effect can be controlled by the electric field strength and dielectric polarizability. This push effect could help to modify the intrinsic mobility of the particle in an electrophoretic separation operation.

Chapter 9 summarizes the conclusions of this study. The contributions made in this thesis research are given in detail.

## Chapter 2

### Literature review

In this chapter, we review the literature relevant to this thesis research. This review focuses on: the current status of research on induced-charge electroosmotic flow; the latest achievements of particle separation techniques that utilize electrokinetic phenomena; the unique features of heterogeneous particles and the electrokinetic motion of heterogeneous particles in electric fields. This chapter demonstrated the limitation of existing studies of the ICEOF. It also summarizes the advantages and drawbacks of current particle separation methods.

#### 2.1 Induced-charge electroosmotic flow and induced-charge electrophoresis

##### *2.1.1 Induced-charge electroosmotic flow*

Induced-charge electroosmotic flow (ICEOF) was discovered since 1962 by Levich [18], and over the last two decades, ICEOF has attracted a lot of attention. Besides the theoretical analysis of the induced surface potential by Squires et al. [5], and Wu et al. [7], the flow features of this flow induced by DC electric fields and AC electric fields have also been studied [19-21]. The convective flow has found applications in microfluidic flow control and particle manipulation techniques. Depending on the external electric field strength and the geometry of the fixed metal plates in the micro channel, the local induced slipping velocity can be much higher than the general Stokes flow. The convection flow pattern on fixed metal plates [22-25] and suspended metal particles [26] provide promising mixing effects in microfluidic systems compared with diffusive mixing. The low and high pressure regions created by the ICEOF in response to a locally applied high electric field had been used to pump fluid flow or change flow directions [27-34]. Since the electric field is only locally applied, only low electric voltages are required.

### ***2.1.2 Induced-charge electrophoresis***

The motion of polarizable particles due to the hydrodynamic forces resulting from the ICEOF is known as induced-charge electrophoresis or the second-kind electrophoresis. The study of induced-charge electrophoresis started with the study of ideally polarizable metal particles. Dukhin [6] theoretically and experimentally studied the motion of full-polarizable particles in a uniform DC electric field. It was found [35, 37] that the transportation of a conducting sphere of symmetric geometry and homogenous property is not affected by the induced symmetric vortices, but dependent on the particle size and the strength of the electric field. On the other hand, Yossifon et al. [38] manifested asymmetric vortexes on the surface of a particle when the external electrical field is inclined to the spheroid axis of the particle. Particles of asymmetric geometry rotate in response to the direction of the applied electric field [39-44]. Saintillan et al. [35] and Saintillan [45], Rose et al. [46], Yariv [47] and Wu et al. [48] studied the repelling and attraction effects among particles due to ICEOF. It was demonstrated that stronger electric field and bigger particle sizes will result in stronger interactions, and this process is accompanied with rotation when the geometry is asymmetric.

The study of induced-charge electrophoresis of dielectric particles is relatively limited. Since the induced surface potential is polarizability-dependent, the corresponding strengths of the ICEOF are distinctive depending on the dielectric property of the dielectrics. There are studies of the self-alignment of non-electrically-conducting colloidal particles in AC electric fields in the vicinity of an electrode [49-53] and without the presence of the electrodes [54-56]. For example, Ristenpart et al. [53] considered the polarization of the electrolyte solution and the particle, and studied the distorted AC electric field near an electrode in the presence of a particle. Though he studied the effect of the conductivity of the particle to the electro hydrodynamic flow around the



particle, he did not relate this interaction to the properties of the colloidal particles. The numerical study of the electrokinetic motion of dielectric particles due to the ICEOF in a uniform electric field presents similar hydrodynamic effects as for metal particles, however, the degree of this effect is found to be a function of particle polarizability [57].

## **2.2 Heterogeneous particle**

Heterogeneous particles consisting of multiple physical or chemical properties have found applications in many fields such as biology, medicine diagnosis and microfluidics. The Janus particles can be fabricated with two sides functionalized or only one side functionalized, e.g. hydrophobic [58], pH-sensitive [59], biocompartment [60] or solvophilic and solvophobic surfaces [61]. In microfluidics, a Janus particle with a half catalytic surface gains an intrinsic propulsion velocity [62]. Janus particles carrying opposite electrostatic charges on the two hemispheres are able to assemble into a ring or chain structure in electrolyte solutions [63, 64]. External forces induced by applied electric field, magnetic field or light can control the spatial location, motion and orientation of Janus particles. When illuminated by light, the Au coated Janus particles start moving [65]. In magnetic fields, anisotropic magnetic Janus particles can arrange themselves to form chainlike or mesh-like structures [66]. Assembly of Janus particles made of metal and dielectric can also be actuated by AC electric field. At high ac frequency (above 10 kHz), the metallodielectric Janus particles form chains or 2d crystal depending on the frequencies of the fields [67]. Under non-uniform electric field, half-metal half-dielectric Janus particles undergo dielectrophoretic forces. The particles align their interfaces with the external electric field, and the orientation of the Janus particles can be controlled by the frequency [68] and the gradient [69] of the electric field.

Among the studies of induced-charge electrophoresis of heterogeneous particles, the first experimental research observed the motion of metallic Janus particles perpendicular to the uniform low-frequency AC electric field with the non-polarizable side facing forward [70]. The electrokinetic motion of Janus particles was theoretically studied by defining differing slip conditions at the particles' surface. The self-alignment behavior and the travelling velocity of Janus particles were found to be proportional to the slipping coefficient [71]. A mathematical model of the induced-charge electrophoresis of uncharged dielectric particles was built without limiting the EDL thickness. Solutions show that the mobility of the particles is a function of the permittivity of both the dielectric and metal halves [72]. While the dielectric half is charged, metallodielectric Janus particles travel with the interfaces perpendicular to the dielectric field, and the vortices around the metal hemisphere provides a driving effect pointing to the dielectric side [73]. The numerical results are in agreement with the experimental observation of the migration of the same particle [74]. Due to the characterized reorientation and vertical migration of spherical metallodielectric Janus particles, these particles function as micro-valves in circular cross-section channels [75].

### **2.3 Particle separation techniques-electrophoresis and dielectrophoresis**

Electrokinetic particle separation methods have been extensively developed and widely used. Typical separation methods associated with electrokinetic phenomena include electrophoresis technique and dielectrophoresis technique. When the electrophoretic or dielectrophoretic force acts on the particles along the flow of the carrier liquid, particles of different properties are subjected to different force strengths and migrate with different velocities. On the other hand, when the force exerted on the particle is perpendicular to the flow, particles of different properties deviate from the flow at different degrees.

The electrophoresis force can be induced by either a uniform DC electric field or a uniform AC electric field. Since particles of different charge to size ratios obtain various immigration velocities in responding to the external electric fields, particles can be separated spatially by charge to size ratios. In the flow free electrophoresis method [76, 77], electric field is applied perpendicular to the flow and the length scale of the separation chambers can be several millimeters or even centimeters. Capillary or gel electrophoresis methods are used more extensively to separate both micro- and nanoparticles [78-83]. Though the electrophoretic separation method is able to separate more than two components at one time, multiple process steps, long operation periods and long separation sections (normally long micro channels) are required to achieve high separation resolution [84, 85]. In addition, since the electric field is applied through long separation sections, high voltages are always required.

Dielectrophoretic separation, however, is mostly coupled with non-uniform alternating electric fields. According to Eq. (1-4) the parameters that influence the dielectrophoretic force include the size of the particle, the frequency-dependent permittivity and the electric field strength. Therefore, the dielectrophoretic separation is more versatile in AC fields. The dielectrophoretic forces are usually exerted perpendicular to the flow and thus particles suffering different force strengths in different directions [86-88] would be deflected from the flow. To exert a dielectrophoretic force on particles, a local spatially non-uniform electric field is required. Normally, complex electrodes arrays are designed and embedded in the channel to generate the electric field [89-91]. Alternatively, dielectrophoretic separation by size can also be induced by a DC electric field [92-94]. Usually insulating obstacles are fabricated in the channel to create electric field gradients. The advantages of DC dielectrophoresis are: electrolysis associated with metal electrodes embedded in the channels can be reduced, and DC electric field is able to drive

particle migration at the same time. Overall, comparing with electrophoretic separation, dielectrophoretic separation methods can be realized in a more compact structure with low voltages. However it usually demands complicated channel design and expensive fabrication of the microelectrode arrays.

## Chapter 3

### Mathematical expressions and governing equations

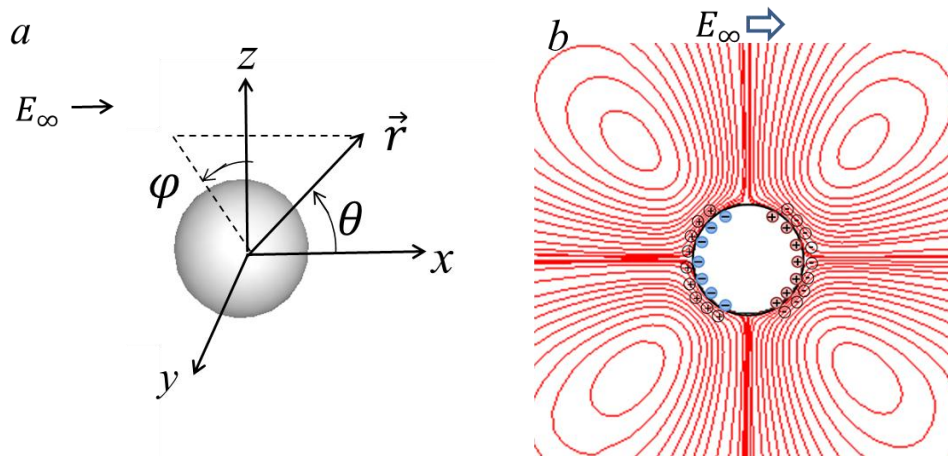
I first derive the induced surface potential of dielectric particles. This chapter provides the detailed derivation by solving Laplace's equation with appropriate boundary conditions. The result obtained describes the dependence of the induced surface potential on the polarizability of the particle. We also describe Squires' and Wu's work, and compared the derivation processes and the fundamental physical principles that are applied in Squires' and Wu's research with our derivation. This chapter also provides the governing equations of the numerical simulations in this thesis. The numerical study focuses on electrokinetic flow and the electrokinetic motion of suspended particles. The simulations of the liquid-particle coupled transient flow are accomplished through multi-physics model and moving grid technique.

#### 3.1 The ICEOF on dielectric sphere and cylinder in uniform electric field

##### *3.1.1 Induced surface potential and induced-charge electroosmotic flow of dielectric sphere*

There are two mechanisms that evoke the induced-charge electroosmotic flow (ICEOF) around dielectric particles. When a dielectric particle is subjected to an electric field, the external electric field exerts a Coulomb force on the randomly arranged dipoles in the particle. Under the effect of the Coulomb force, the dipoles shift from their original orientations and form an array of dipoles. The schematic diagram of the dipoles in a polarized dielectric sphere is shown in Figure 1-5a. As the dipoles are all aligned in the same direction, the charges on positive sides and negative sides of the dipoles inside the particle can be canceled and give rise to a surface charge on the particle. On one side of the particle, the surface charge is positive, and on the other side of the particle, the surface charge is negative.

While the dipoles are arranging themselves under the influence of the electric field, the mobile solute ions in the surrounding electrolyte also migrate along electric field lines. The mobile ions follow the electric field lines that interacting on the particle surface, and accumulate in the vicinity of the particles surface, with positive ions at one side of the surface facing the electric field, and negative ions accumulating at the opposite side of the surface. The charge cloud grows around the particle and shields the particle from the external bulk electric field. The accumulation process achieves a steady state when all the electric field lines are repelled from the particle. The surface charge and the corresponding screening cloud are termed as induced electrical double layer (EDL). As shown in Figure 3-1b, the distribution of the charges on the particle is non-uniform; both the surface charge and the screening cloud have opposite signs at the two sides of the sphere. The potential drop across the induced EDL is termed as the induced surface potential  $\zeta_i$  which is non-linear.



**Figure 3-1. The ICEOF around a dielectric particle, (a) the spherical coordinate (b) the induced EDL and streamlines of ICEOF adjacent to a polarized particle**

The tangential electric field around the particle surface drives the mobile ions in the EDL slip along the surface, which is the ICEOF. Assume the induced EDL is thin comparing with the

particle size. According to Helmholtz–Smoluchowski formula, the velocity of the ICEOF is a function of  $\zeta_i$ . Due to the lack of the analytical solutions of this induced surface potential of dielectric surfaces, this section will give the detailed mathematical derivation procedures of the induced surface potential of dielectric particles.

Assume a dielectric sphere of radius  $a$  is immersed in an electrolyte  $\epsilon_m$  and subjected to a uniform electric field:

$$\phi = -E_\infty x \quad (3-1)$$

The particle is polarized right away and the external electric field is distorted. The induced surface potential of the EDL  $\zeta_i$  is reflected by the potential drop across the double layer. We are going to solve Laplace's equation in a spherical coordinate system. Since the uniform electric field is applied in the  $x$ -direction, assume the electric potential  $\phi$  is independent of the azimuthal angle  $\varphi$ . The potential in a spherical coordinate system is expressed as:

$$\nabla^2 \phi = \frac{1}{r^2} \frac{\partial}{\partial r} \left( r^2 \frac{\partial \phi}{\partial r} \right) + \frac{1}{r^2 \sin \theta} \frac{\partial}{\partial \theta} \left( \sin \theta \frac{\partial \phi}{\partial \theta} \right) = 0 \quad (3-2)$$

Utilizing the method of separable variables one can obtain the general solution set to Laplace's equation in the following forms [95]:

$$\phi_{in} = \sum_{k=0}^{\infty} A_k r^k P_k(\cos \theta) \quad (3-3)$$

$$\phi_{out} = \sum_{k=0}^{\infty} B_k r^{-(k+1)} P_k(\cos \theta) \quad (3-4)$$

Where  $A_k$  and  $B_k$  are to-be-determined constants, and  $P_k(\cos \theta)$  are the Legendre polynomials.

Let the origin of coordinate be the center of the particle, and the electric field is infinite large.

The potential on the particle surface ( $r=a$ ) can be obtained by applying the following boundary conditions:

- 1) At infinity, the electric field should be equal to the applied external electric field, i.e., at  $r \rightarrow \infty, \phi_{out} = -E_{\infty} r \cos\theta$ ;
- 2) At the interface of the particle and the electrolyte,  $\phi_{in} = \phi_{out}$ ;
- 3) At the interface of the particle and the electrolyte,  $D_{in} = D_{out}$ , where  $D_{in} = -\varepsilon_0 \varepsilon_p \vec{E}_{in} \cdot \hat{n}$ ,  $D_{out} = -\varepsilon_0 \varepsilon_m \vec{E}_{out} \cdot \hat{n}$ .

The subscript ‘in’ means the fields inside the particle, and ‘out’ means the fields outside the particle.  $\hat{n}$  is the unit vector normal to the interface.  $\varepsilon_p$  is the relative permittivity of the particle and  $\varepsilon_m$  is the relative permittivity of the electrolyte.

Applying the above boundary conditions yields the specific solution of Laplace’s equation at  $r = a$ :

$$\phi_0 = -E_{\infty} a \cos\theta + \frac{\varepsilon_p - \varepsilon_m}{\varepsilon_p + 2\varepsilon_m} E_{\infty} a \cos\theta \quad (3-5)$$

Eq. (3-5) describes the potential at the surface of the particle after it is polarized as shown in Figure 1-5 a.

The potential out of the screening cloud can be obtained by applying a zero-current boundary condition, in other words, the electric field lines go around the particle.

Thus at  $r = \lambda_D + a$ , the boundary condition of the Laplace’s equation is  $(\frac{\partial \phi_{out}}{\partial r})_{r=a+\lambda_D} = 0$ .

Based on the thin double layer assumption, that is,  $\lambda_D \ll a$  and  $a + \lambda_D \approx a$ , the zero-current boundary condition is approximated by  $(\frac{\partial \phi_{out}}{\partial r})_{r=a} = 0$ . Then the following equation is obtained:

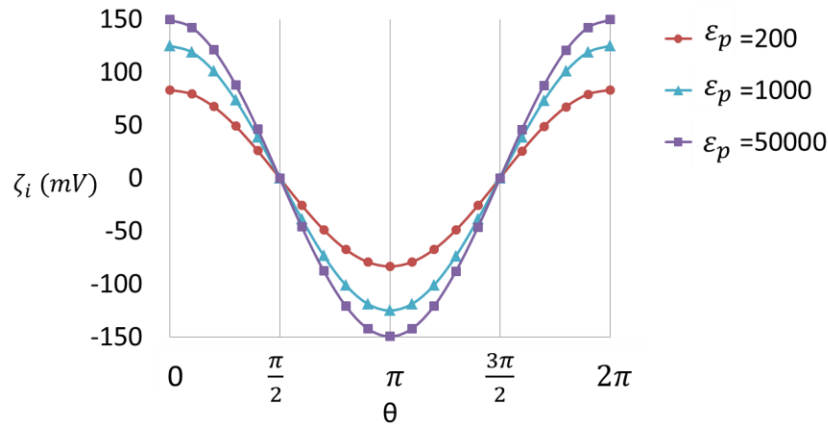
$$\phi_{steady} = -\frac{3}{2} E_{\infty} r \cos\theta \quad (3-6)$$



Eq. (3-6) is the potential out of the screening cloud. The potential drop across the double layer can be obtained from Eq. (3-5) and Eq. (3-6) [71].

$$\zeta_i = \phi_0 - \phi_{steady} = \frac{3\varepsilon_p}{2(\varepsilon_p + 2\varepsilon_m)} E_\infty a \cos\theta \quad (3-7)$$

As indicated in Eq. (3-7), the induced surface potential is a function of  $\theta$  and depends on the permittivity of the particle and the surrounding medium, the applied electric field and the size of the particle. Figure 3-2 shows the dependence of the induced surface potential of a dielectric particle on permittivity  $\varepsilon_p$  under a fixed permittivity of the medium  $\varepsilon_m$ .



**Figure 3-2. The induced surface potential of the dielectric particle with a radius  $a=10\mu\text{m}$ , in a uniform electric field  $E_\infty=100\text{V/cm}$  aligned in the  $x$ -direction.  $\varepsilon_m = 80$ .**

In Eq. (3-7), the coefficient  $\frac{\varepsilon_p}{\varepsilon_p + 2\varepsilon_m}$  describes how  $\zeta_i$  is dependent on the dielectric properties of the dielectric system. We define this coefficient as a non-dimensional polarizability  $C$ :

$$C = \frac{\varepsilon_p}{\varepsilon_p + 2\varepsilon_m} \quad (3-8)$$

which reflects how easily a dielectric sphere can be polarized in a dielectric system. The value of  $C$  ranges from 0 to 1.

Then the induced surface potential can be alternatively expressed by:

$$\zeta_i = \frac{3}{2}CE_\infty a \cos\theta \quad (3-9)$$

The generated ICEOF is driven by a similar physical mechanism to the classic electroosmotic flow. Based on the thin double layer and low potential assumptions, the Helmholtz–Smoluchowski equation is appropriate to describe the slipping velocity of the induced EDL:

$$\vec{V} = -\frac{\varepsilon_0\varepsilon_m\zeta_i}{\mu}\vec{E}_\parallel. \quad (3-10)$$

It should be noted that, the induced surface potential in this expression is proportional to the applied electric field as indicated by Eq. (3-7). Consequently, the velocity of the ICEOF is a function of the square of the electric field. Because of the dipolar nature of the induced electrical double layer around the particle, one half of the EDL is positive and the other half is negative. The direction of the ICEOF varies along the surface, and consequently vortices are generated around the particle. Figure 3-1 (b) shows the streamlines of the four vortices around the particle.

While the spherical particle is initially charged with static charges, the surface potential on the sphere is simply the superposition of the static zeta potential and the induced surface potential  $\zeta_p = \zeta + \zeta_i$ , and accordingly the slipping velocity of the double layer on the sphere is

$$\vec{V} = -\frac{\varepsilon_0\varepsilon_m\zeta_p}{\mu}\vec{E}_\parallel. \quad (3-11)$$

### ***3.1.2 Induced surface potential on a dielectric cylinder***

The analytical expression of the induced surface potential on a dielectric cylinder can be obtained by solving Laplace's equation. For simplicity, assume the particle is initially neutral, and the cylinder is long enough, so that the electric field around the cylinder can be considered as

2D. Once a uniform electric field is applied in the  $x$ -direction,  $\vec{E}_\infty = E_\infty \vec{x}$ , the cylinder with permittivity  $\varepsilon_p$  is polarized immediately. The potential field in the cylindrical coordinates is expressed as:

$$\frac{1}{r} \frac{\partial}{\partial r} \left( r \frac{\partial \phi}{\partial r} \right) + \frac{1}{r^2} \frac{\partial^2 \phi}{\partial \theta^2} = 0 \quad (3-12)$$

The physical boundary conditions of the electric field in this dielectric system are analogous as in the system of sphere and infinite surrounding medium. We apply the same boundary conditions as those in the last section:

- 1) At infinity, the electric field should be equal to the applied external electric field, i.e., at  $r \rightarrow \infty$ ,  $\phi_{out} = -E_\infty r \cos\theta$ .
- 2) At the interface of the particle and the electrolyte,  $\phi_{in} = \phi_{out}$ ,
- 3) At the interface of the particle and the electrolyte,  $D_{in} = D_{out}$ , where  $D_{in} = -\varepsilon_0 \varepsilon_p \vec{E}_{in} \cdot \hat{n}$ ,  $D_{out} = -\varepsilon_0 \varepsilon_m \vec{E}_{out} \cdot \hat{n}$ .

Then the potential at the cylinder surface at  $r=a$  is:

$$\phi_0 = -E_\infty a \cos\theta + \frac{\varepsilon_p - \varepsilon_m}{\varepsilon_p + \varepsilon_m} E_\infty a \cos\theta \quad (3-13)$$

and the potential outside the induced electrical double layer (EDL) is

$$\phi_{steady} = -2E_\infty a \cos\theta \quad (3-14)$$

thus the induced surface potential of the dielectric cylinder is:

$$\zeta_i = \phi_0 - \phi_{steady} = \frac{2\varepsilon_p}{\varepsilon_p + \varepsilon_m} E_\infty a \cos\theta \quad (3-15)$$

Comparing Eq. (3-15) and Eq. (3-7), the induced surface potential of a cylinder and a sphere has the similar form but with different factors. The factor  $\frac{\varepsilon_p}{\varepsilon_p + \varepsilon_m}$  in Eq. (3-15) describes how easily a dielectric cylinder can be polarized in an infinite dielectric medium. We define this factor as the non-dimensional polarizability of this cylinder in this dielectric system:

$$C = \frac{\varepsilon_p}{\varepsilon_p + \varepsilon_m} \quad (3-16)$$

Depending on the permittivity of this dielectric system, the value of this defined polarizability  $C$  ranges from 0 to 1.

Meanwhile, under the thin EDL assumption, the slipping velocity on a dielectric cylinder is expressed by the Helmholtz–Smoluchowski expression  $\vec{V} = -\frac{\varepsilon_0 \varepsilon_m \zeta_i}{\mu} \vec{E}_{\parallel}$ . Similarly, this non-linear slipping velocity also gives rise to four symmetric and opposite vortexes around the cylinder.

In the case where the cylinder initially carries static charges, the surface potential on the cylinder is simply the superposition of the static potential and the induced surface potential  $\zeta_p = \zeta + \zeta_i$ , and accordingly the slipping velocity on the cylinder is  $\vec{V} = -\frac{\varepsilon_0 \varepsilon_m \zeta_p}{\mu} \vec{E}_{\parallel}$ .

### **3.2 Comparison between the derived induced surface potential and current existing mathematical expressions**

Current mathematical expressions of the induced surface potential include the analytical expression of the induced surface potential of metal sphere and cylinder provided by Squires et al. [5], and the numerical result of induced surface potential of metal particle of arbitrary geometry provided by Wu et al. [7]. In this section, we will take spherical particles as an

example, and discuss the fundamental physical principles that are utilized to deduce the mathematical expressions in both the Squires' and Wu's works, and compare the results of the two expressions with the results from our derivation.

Squires [5] derived the induced surface potential of metal spherical and cylindrical particles by solving Laplace's equation analytically. Squires assumed that, after the initially uncharged metal particle polarized in the uniform electric field, the spherical surface corresponds to an equipotential surface; in other words, the electric field inside the particle is zero. Based on the fact that electric field lines interact with the particle at right-angles, which in the mathematical expression  $(\frac{\partial \phi_{out}}{\partial \theta})_{r=a} = 0$ , they obtained the analytical solution of Laplace's equation:

$$\phi_0 = -E_{\infty} r \cos \theta + E_{\infty} a^3 r^{-2} \cos \theta \quad (r \geq a) \quad (3-17)$$

Let  $r=a$  in Eq. (3-17), then the surface potential on the particle is:  $\phi_0 = 0$ .

They need one more analytical solution to describe the potential outside the screening EDL to identify the induced surface potential. The free ions from the solutions accumulate around the particle surface in the same manner as in the dielectric system, and the metal particle is totally shielded by the charges at the steady state. The potential outside the EDL can be obtained by employing the zero-current boundary condition:  $(\frac{\partial \phi_{out}}{\partial r})_{r=a} = 0$ .

Then the potential outside the EDL is expressed by the analytical solution of Laplace's equation

$$\phi_{steady} = -\frac{3}{2} E_{\infty} r \cos \theta \quad (r \geq a) \quad (3-18)$$

The difference between the potentials inside and outside the EDL gives the induced surface potential of the EDL:

$$\zeta_i = \frac{3}{2}E_\infty a \cos\theta \quad (3-19)$$

Eq. (3-19) is the analytical expression of the induced surface potential on a metal sphere. The derivation of the induced surface potential of a metal cylinder can be found in reference [5].

Wu on the other hand, obtained the induced surface potential of metal surface of arbitrary geometry by numerically solving Laplace's equation.

The metal surface is assumed to be an equipotential surface, which means the externally applied electric field is totally canceled by the internal electric field generated by the induced charges.

This is consistent with the assumption in Squires model:

$$E_i = -E_\infty \quad (E_i \text{ is the electric field generated by the induced charges}) \quad (3-20)$$

In another way:

$$\nabla\zeta_i = -\nabla\phi \quad \text{Here } \phi \text{ is the local external electric potential.} \quad (3-21)$$

If we integral Eq. (3-21) over the metal surface, we have:

$$\zeta_i = -\phi + c \quad (3-22)$$

c is a constant to be determined.

To determine c, one needs to note that, the induced surface potential and the induced charges are related by equation [5]

$$\zeta_i = \frac{q}{\epsilon_0 \epsilon_r \kappa} \quad (3-23)$$

q is the induced charge on the metal surface, and  $\kappa$  can be calculated by Eq. (1-1). Owing to the fact that, the induced negative and positive charges are in equal amount, the integration of the induced surface potential over the particle surface should be zero:

$$\int_S \zeta_i dA = \int_S \frac{q}{\epsilon_0 \epsilon_r \kappa} dA = 0, \quad (3-24)$$

Thus the integration of the right side of equation (3-22) yields:

$$\int_S (-\phi + c) dA = -\int_S \phi dA + cA = 0 \quad (3-25)$$

Thus,

$$c = \frac{\int_S \phi dA}{A} \quad (3-26)$$

Substitution of Eq. (3-26) into Eq. (3-22) gives

$$\zeta_i = -\phi + \frac{\int_S \phi dA}{A} \quad (3-27)$$

Here, the numerical results of the local external electric potential  $\phi$  can be obtained by solving Laplace's equation  $\nabla^2 \phi = 0$  with zero-current boundary condition  $(\frac{\partial \phi_{out}}{\partial r})_{r=a} = 0$  at the metal surface. Accordingly, the two terms in Eq. (3-27) represent the electric potential out of the EDL and the equilibrium potential on the particle surface inside the double layer, respectively.

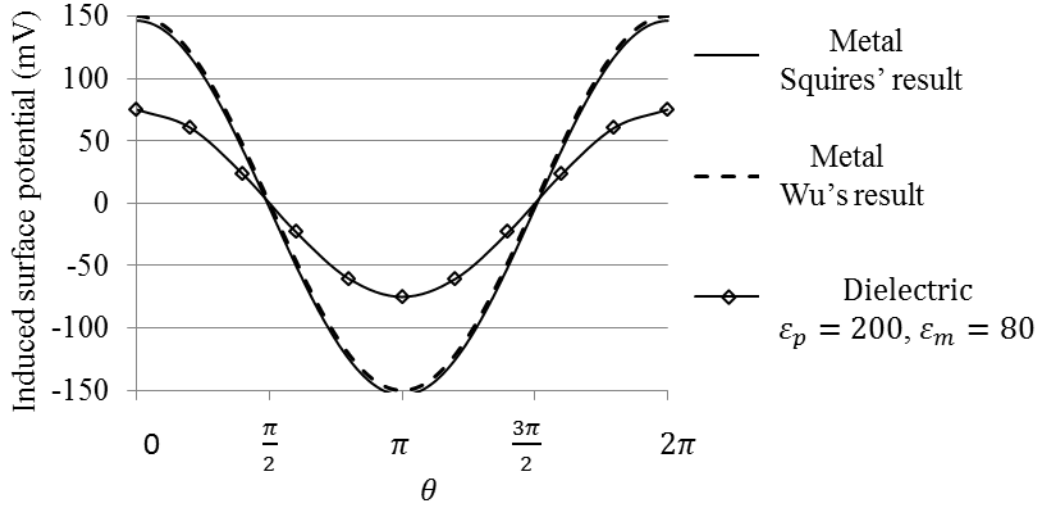
In conclusion, the two derivation procedures are subjected to the same boundary conditions and assumptions: equipotential particle surface after the polarization; zero-current boundary on the outer layer of the EDL. The difference is Wu's integral breaks the limit of the analytical solutions to the Laplace's equation, and provides numerical results for the induced surface potential on metal surfaces of any geometry.

In principle, the expressions from Squires et al., Wu et al. and this thesis research can all be decomposed into two terms: the potential out the EDL and the potential inside the EDL. The potential outside the EDL are obtained by solving Laplace's equation with zero-current boundary

condition. However, the solution to Laplace's equation inside the EDL on the dielectric surface satisfies different boundary conditions than the other two cases of metal sphere. In fact, the dielectric materials can only be partially polarized determined by the polarizability. As a result, the internal electric field only partially diminishes the external electric field. Comparing with a metal sphere, a dielectric sphere only generate an internal electric field strength reduced by a scale determined by the polarizability of the dielectric system. That is how the coefficient  $\frac{\varepsilon_p}{\varepsilon_p+2\varepsilon_m}$  was introduced into Eq. (3-7). The coefficient  $C = \frac{\varepsilon_p}{\varepsilon_p+2\varepsilon_m}$  describes how much the induced surface potential is reduced when the dielectric particle is partly polarizable. In an extreme case, wherein  $\varepsilon_p$  tends to be infinitely large, the polarizability-dependent coefficient  $\frac{\varepsilon_p}{\varepsilon_p+2\varepsilon_m}$  yields 1, which gives the induced surface potential  $\zeta_i = \frac{3}{2}E_\infty a \cos\theta$  identical to Squires' result.

The results of the induced surface potential of a sphere from these three derivations are plotted in Figure 3-3. Apparently, in the case of metal sphere, the results from Squires and Wu are in full agreement. In contrast, the reduced surface potential of the dielectric particle from the current derivation is the scaled version of the induced surface potential of a metal sphere by a ratio C.





**Figure 3-3.** Induced surface potential of a sphere of radius  $a=10\ \mu\text{m}$ , under electric field strength  $E_\infty=100\text{V/cm}$ . Results are induced surface potential of metal sphere calculated by Squires' expression:  $\zeta_i = \frac{3}{2}E_\infty a \cos\theta$  [5], and Wu's expression:  $\zeta_i = \frac{\int_S \phi dA}{A} - \phi$  [7], respectively, and the induced surface potential of dielectric sphere calculated by Eq. (3-7)  $\zeta_i = \frac{3}{2}CE_\infty a \cos\theta$ ,  $C = \frac{\epsilon_p}{\epsilon_p + 2\epsilon_m} = 0.5$ .

### 3.2 Method-numerical model

We studied the flow features of the polarizability-dependent ICEOF, and how this polarizability-dependent ICEOF affects the electrokinetic motion of dielectric particles. The physics that is involved in this study are electric field, which causes the classic EOF and the ICEOF; flow field, which describes the transient flow field; the motion of suspended particles, results from the hydrodynamic interaction between the particle and the surrounding aqueous solution. The coupled multi-physics theoretical model is described below:

### 3.2.1 Electric field

Assume the liquid filling the microchannel is isotropic and electrically neutral, and the electric field is governed by Laplace's equation.

$$\nabla^2 \phi = 0 \quad (3-28)$$

Where  $E_\infty$  is calculated by  $E_\infty = -\nabla\phi$

To apply a uniform electric field  $E_\infty$ , the boundary conditions are:

$$\hat{n} \cdot \nabla\phi = -E_\infty \text{ at the inlet,} \quad (3-29)$$

$$\phi = \phi' \text{ at the outlet.} \quad (3-30)$$

$$\hat{n} \cdot \nabla\phi = 0 \text{ at the channel walls,} \quad (3-31)$$

$$\hat{n} \cdot \nabla\phi = 0 \text{ at the polarized surface (e.g. dielectric particle, conducting plates).} \quad (3-32)$$

### 3.2.2 Flow field

The controlling equations for the flow field are the Navier-Stokes equation and the continuity equation.

$$\rho \frac{\partial \vec{V}}{\partial t} = -\nabla P + \mu \nabla^2 \vec{V} + \vec{F} \quad (3-33)$$

$$\nabla \cdot \vec{V} = 0 \quad (3-34)$$

The aqueous buffer solutions filled the channel or chamber is assumed to have the same physical properties as water. Additionally, the particle was assumed to have the same density as the liquid medium. So the buoyance effect is neglected (e.g. in the cases of several polymers). The body force in this case is purely provided by the electrostatic force exerted by the external electric field on the net charges in the electrical double layer. The channel was assumed to connect two

reservoirs that are open to the air, so there is no pressure difference between the inlet and the outlet of the channel. Accordingly, the inlet and outlets of a microchannel system utilize the following boundary conditions:

$$P=0, \text{ and } \vec{n} \cdot \nabla \vec{V} = 0. \quad (3-35a)$$

And for the open boundary conditions of the big chambers:

$$-P\vec{I} + \mu[\nabla \vec{V} + (\nabla \vec{V})^T] = 0 \quad (3-35b)$$

The initial velocity field through the computational domain is set as zero. The bulk liquid undertakes electroosmotic flow (EOF) because of the electrostatic charges on the channel wall. In most aqueous solutions, the thickness of the EDL is of the order of 10 nm, which is much smaller than the length scale of the microchannel (e.g., 100  $\mu\text{m}$ ). The details of the flow field inside such a thin double layer can be ignored; the effect of the electroosmotic flow originated from the thin EDL on the bulk liquid motion can be addressed by considering the thin EDL as a thin slipping flow layer at the channel wall. In this way, the electrostatic body force term in the momentum equation can be neglected; instead, a slipping velocity at the channel wall is introduced as a boundary condition for the flow. The slipping velocity is given by Helmholtz–Smoluchowski formula:

$$\vec{V} = -\frac{\varepsilon_0 \varepsilon_m \zeta_w}{\mu} \vec{E}_{\parallel} \quad (3-36)$$

where  $\vec{E}_{\parallel}$  is the local tangential electric field and  $\zeta_w$  is the zeta potential of the channel wall. Since the aqueous buffer solution is assumed to have the same property as water, so  $\varepsilon_m$  is assumed to be the relative permittivity of water at room temperature. B. J. Kirby, etc. [96, 97] summarized the range of the zeta potentials (0~120mV) of silicon and polymer microfluidic

substrates when the adjacent solutions have various solution concentrations. In this thesis, we use zeta potentials ranging from -15mV to -30mV. Here the potential  $\zeta_w$  is considered as a constant value based on the assumption that the electrolyte properties are uniform in the computational domain.

The flow around the surface of the particle is a little more complicated. On one hand, the particle is drifted by the liquid due to hydrodynamic force; on the other hand, there is a slip velocity on the surface of the particle. Accordingly, the velocity on the surface of the particle consists of two components, and is given by the following expressions [98]:

$$\vec{V} = \vec{U}_p + \vec{\omega}_p \times (\vec{x}_p - \vec{X}_p) - \frac{\varepsilon_0 \varepsilon_m \zeta_p}{\mu} \vec{E}_{\parallel} \quad (3-37)$$

In the above expression,  $\vec{U}_p$  is the translational velocity of the particle, and  $\vec{\omega}_p$  is the angular velocity of the particle. The centroid of the particle is located at  $X_p$ , and  $x_p$  is a position vector. The last term presents the slipping velocity resulted from the surface potential  $\zeta_p$  on the particle. When the particle is initially neutral,  $\zeta_p$  equals to the induced surface potential expressed by Eq. (3-7) or (3-26). When the particle presents a static zeta potential, then the surface potential of the particle is  $\zeta_p = \zeta + \zeta_i$ .

### ***3.2.3 Motion of particle***

In all the simulations in this thesis, the particle is considered to be a rigid body. Since no gravity is considered, the motion of the particle is only driven by hydrodynamic force. The total force and torque on the particle determine the motion of the particle.

The total force on the particle is [98-101]:

$$\vec{F} = \oint \vec{\sigma}_p \cdot \vec{n} dS \quad (3-38)$$

Where  $\bar{\sigma}_p$  is the stress tensor on the surface of the particle;  $\vec{n}$  is the unit vector normal to the surface S.

The total torque acting on the particle is:

$$\vec{\Gamma} = \oint (\vec{x}_p - \bar{X}_p) \times (\bar{\sigma}_p \cdot \vec{n}) dS \quad (3-39)$$

Where  $\vec{x}_p$  is the position vector of  $\bar{\sigma}_p$  and dS.

By using Newton's second law, the translational and angular velocities of the particle are expressed respectively as:

$$\frac{d\bar{U}_p}{dt} = \frac{\bar{F}}{m_p} \quad (3-40)$$

$$\frac{d\bar{\omega}_p}{dt} = \frac{\vec{\Gamma}}{J_p} \quad (3-41)$$

where  $\bar{\omega}_p$  is the angular velocity of the particle, and  $m_p$  and  $J_p$  are the mass and inertia of the particle, respectively.

The particle is initially released from location  $\bar{X}_0$ . The initial angular velocity and the initial translational velocity of the particle are zero. The position of the particle is determined by

$$\bar{X}_p = \int_0^t \bar{U}_p dt \quad (3-42)$$

The second-order Cartesian tensor  $\sigma_p$  is calculated by:

$$\bar{\sigma}_p = -P\bar{I} + \mu[\nabla\vec{V} + (\nabla\vec{V})^T] \quad (3-43)$$

where  $\bar{I}$  is the identity tensor. The first term of this equation is the stress tensor generated by a pressure gradient, and the second term is the deviatoric stress tensor result from viscosity.

Initially, the velocities of both the liquid and the particle are zero at  $t=0$ .

$$\vec{X}_p = \vec{X}_0, \vec{V} = 0, \vec{U}_p = 0, \vec{\omega}_p = 0 \text{ at } t=0. \quad (3-44)$$

### 3.3 Summary

In this thesis research, we focus on the electrokinetic flow in the computational domain, including the classic electroosmotic flow (EOF) all through the channel and local induced-charge electroosmotic flow (ICEOF) around polarizable surfaces. Suspended particles and fixed polarizable surfaces will be critical components of the models. The numerical simulations throughout this thesis are performed by solving the governing equations given in this chapter. Once the computational domain of each simulation is defined, meshes will be generated and mesh dependency will be studied. Depending on the models we studied, boundary conditions will be specifically applied and the corresponding values of the boundary conditions will be given in each chapter.

## Chapter 4

### **Migration of suspended homogeneous dielectric particles in uniform electric field**

The newly derived expression of the induced surface potential on spherical particle and the expression of the induced-charge electroosmotic flow (ICEOF) in chapter 3 describe the dependence of the ICEOF on the polarizability of the dielectric system, the electric field, and the particle size. In this chapter, we perform numerical simulations to investigate the impact of this ICEOF on the migration of micro particles dispersed in a liquid electrolyte where a uniform electric field is applied. We studied the flow field around single dielectric particles subjected to the local ICEOF and the bulk plug-like EOF in a straight channel. We also studied the flow field around closely located dielectric particles in a big chamber when the external electric field is applied in two different directions relative to the alignment of the particles. These two models provide an understanding of the influence of the ICEOF of a spherical particle on the particle itself and on the particles in adjacent areas. The simulations in this chapter are 3D transient simulations, and performed with Fluent 12.0 with finite volume method.

#### **4.1 The motion of single particles in a straight microchannel**

The migration of single dielectric particles in a straight channel is studied in this section. The straight channel is filled with liquid electrolyte and electric field is applied along the channel. A constant zeta potential is defined to the channel wall, which provides linear electroosmotic flow. The spherical particle suspended in the electrolyte is polarizable and ICEOF will be induced by the external electric field. The local ICEOF around the particle combines with the EOF of the bulk liquid and drives the suspended particle into motion. We numerically solved the flow field around the particle and in the channel, and monitored the migration of the particle in the straight

channel. Since the ICEOF on the dielectric particle is determined by several parameters, e.g. electric field, particle size and permittivity, the effects of these parameters on the motion of the particle were also studied.

#### ***4.1.1 Geometry and dimensions***

The simulation domain is shown in Figure 4-1. A uniform electric field  $\phi = -E_{\infty}x$  is applied along this straight channel. The channel section has a length  $L = 30 \times d$ , a width and a height  $W = H = 5 \times d$ . The particle with a diameter  $d = 20 \mu\text{m}$  is initially placed in the center of the channel. The length of the channel section is chosen to make sure both the bulk EOF and the local ICEOF around the particle are fully developed in the computational domain. According to F. Durst etc. [102], the entrance length for a fully developed laminar flow can be calculated by the following expression:

$$L_{dev} = 0.06 \times Re \times W \quad (4-1)$$

Where  $Re$  is the Reynolds number and is determined by

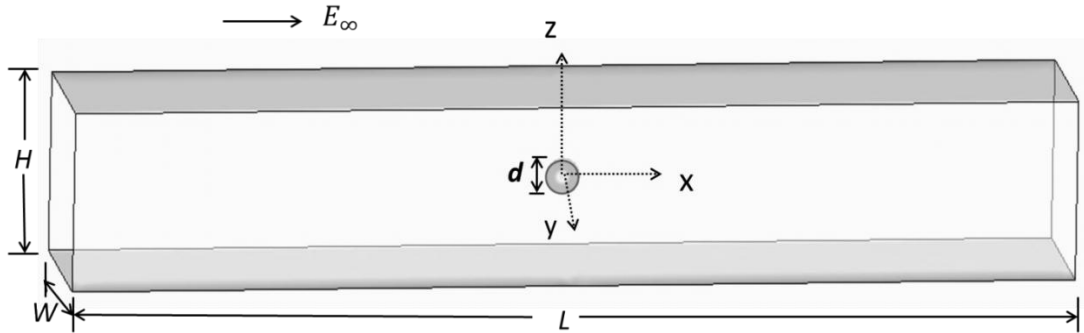
$$Re = \frac{\rho V D}{\mu} \quad (4-2)$$

Where  $V$  is the characteristic velocity of the fluid, which in our cases is either the velocity of EOF or the combination of EOF and ICEOF.  $D$  is the characteristic length scale of the geometry. In this chapter, the velocity of the liquid is of the order of several hundreds of micron per second. When  $V < 1000 \mu\text{m}/\text{s}$ , and let  $D=W$ , then the development length of the flow calculated by Eq. (4-1) is  $L_{dev} < 0.6 \times 10^{-6} \text{m}$ .

As mentioned in Chapter 3, we consider the density of the particle is the same as the surrounding aqueous solution, so the buoyancy effect is neglected. Different numbers of mesh



elements are tested. The computational domain is divided into 15,936, 17,264, 119,783, 156,637 and 174,856 elements respectively, and the translational velocity of the particle with permittivity  $\epsilon_p = 1000$ , under electric field  $E_\infty = 50\text{V/cm}$ , and  $\zeta_w = -30\text{mV}$  is tested. The value of  $U_p$  changes less than 0.5% when the computational domain contains more than 119,783 elements. Finally, 119,783 unstructured mesh elements are used. First order upwind spatial discretization and first order implicit transient simulation are utilized. The time step  $\Delta t$  for this series of simulations ranges from  $10^{-7}\text{s}$  to  $10^{-5}\text{s}$ . Small time steps are used during the acceleration process of the particle, and big time steps are applied after the particle reaches a steady velocity. The numerical error tolerance applied is  $10^{-6}$ . Table 4-1 summarizes the values of the parameters involved in the simulations. At  $t=0$ , both the flow and the particle are assumed static.



**Figure 4-1. Schematic diagram of the computational domain. Electric field is applied along the length of the channel. The particle is initially placed in the center of the channel.  $H = W = 5 \times d$ ,  $L = 30 \times d$ , particle diameter  $d$ .**

Definition	Constant/Parameters	Values/Range
Permittivity of the vacuum	$\varepsilon_0$ (F/ m)	$8.85 \times 10^{-12}$
Relative permittivity of the liquid medium	$\varepsilon_m$	80
Relative permittivity of the particle	$\varepsilon_p$	200~50000
Viscosity of the liquid	$\mu$ (kg/m s)	$0.9 \times 10^{-3}$
Density of liquid	$\rho$ (kg/m <sup>3</sup> )	998
Zeta potential of the wall	$\zeta_w$ (mV)	-15
Diameter of the particle	$d$ ( $\mu\text{m}$ )	10~20
External electric field	$E_\infty$ (V/cm)	23~31.5

**Table 4-1. Values of constants and parameters used in the simulations**

#### **4.1.2 Results and discussion**

The flow field in the domain consists of two flow components: the EOF of the main stream, and the local ICEOF flow around the spherical particle. The two individual flow field components are given by the following equations:

$$V_{\text{EOF}} = -\frac{\varepsilon_0 \varepsilon_m \zeta_w}{\mu} E_{\parallel}, \quad (4-3)$$

$$V_{\text{ICEOF}} = -\frac{\varepsilon_0 \varepsilon_m \zeta_i}{\mu} E_{\parallel}, \quad (4-4)$$

$$\text{where } \zeta_i = \frac{3\varepsilon_p}{2(\varepsilon_p + 2\varepsilon_m)} E_{\infty} a \cos\theta, \quad (4-5)$$

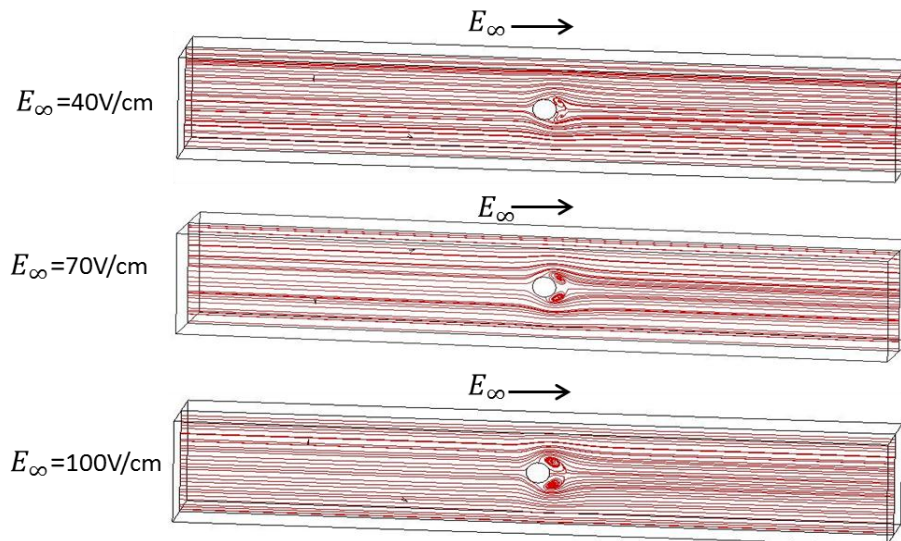
That is,

$$V_{\text{ICEOF}} = -\frac{\varepsilon_0 \varepsilon_m}{\mu} \frac{3\varepsilon_p}{2(\varepsilon_p + 2\varepsilon_m)} E_{\parallel} E_{\infty} a \cos\theta \quad (4-6)$$

where  $E_{\parallel}$  is the local tangential electric field.

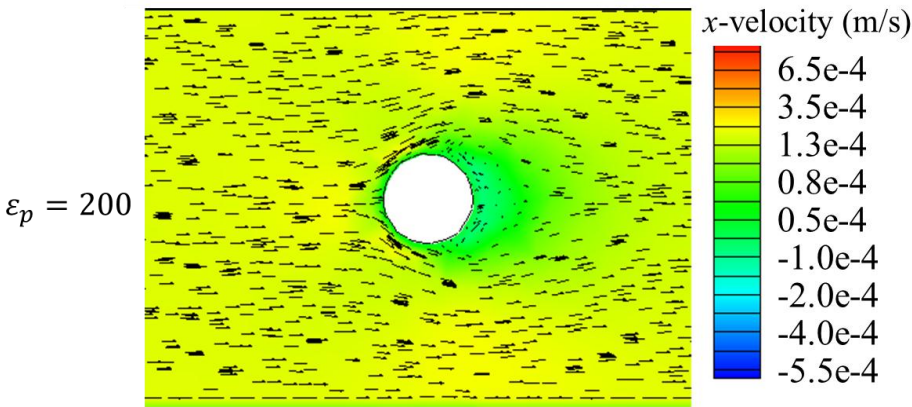
The two flow components are coupled in the flow field, and the effect of the flow field to the motion of the particle is considered. From the above expressions, the electrical field is obviously a critical factor determining the flow field and hence the motion of the particle. Meanwhile, the permittivity  $\epsilon_p$  also affects the ICEOF flow field which may influence the motion of the particle. Thus, the effect of the  $\epsilon_p$  and  $E_\infty$  on the flow field and the motion of the particle are studied by considering the value of  $\epsilon_p$  ranging from 200 to 50000, and the electric field  $E_\infty$  ranging from 40V/cm to 100V/cm.

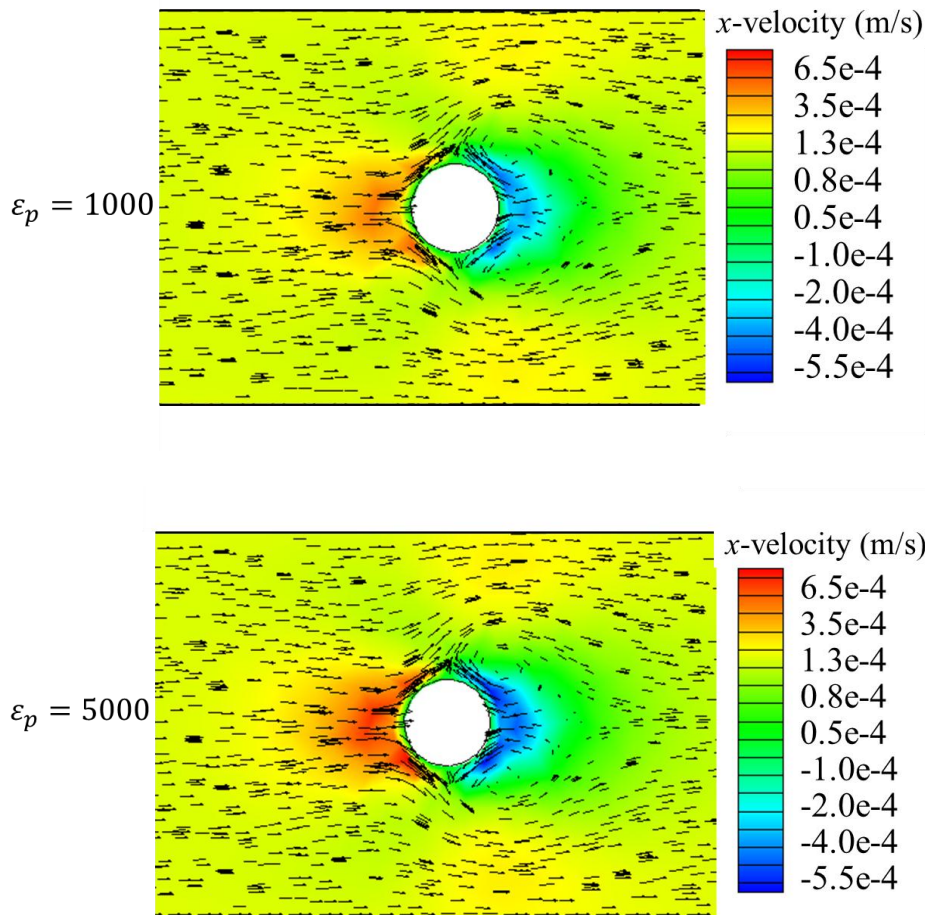
The flow fields around the dielectric particle under different electric field strengths are shown in Figure 4-2. As indicated in Eq. (4-6), the velocity of the ICEOF flow is proportional to  $E^2$ . Figure 4-2 shows the flow field around the particle under three different electric field strengths  $E_\infty = 40\text{V/cm}$ ,  $E_\infty = 70\text{V/cm}$  and  $E_\infty = 100\text{V/cm}$ . The vortices around the particle are more visible when higher electric field strengths are applied. The flow pattern around the dielectric particle is the result of the superposition of two flow field components: the four symmetric vortices of the ICEOF around the particle, and the planer EOF of the surrounding.



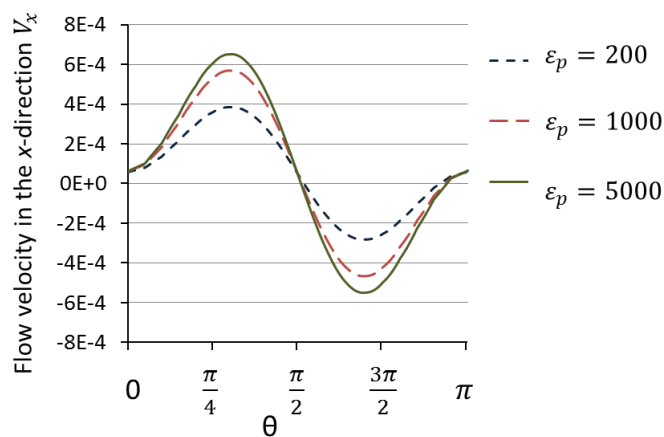
**Figure 4-2. Vortices around a dielectric sphere of  $d=20\mu\text{m}$  in diameter, when  $\zeta_w = -15\text{mV}$ ,  $\epsilon_m = 80$ ,  $\epsilon_p = 1000$ . (a)  $E_\infty = 40\text{V/cm}$ , (b)  $E_\infty = 70\text{V/cm}$ , (c)  $E_\infty = 100\text{V/cm}$ .**

As we discussed in the above section, the strength of the ICEOF is dependent on the permittivity of the particle  $\epsilon_p$ . Three different dielectrics ( $\epsilon_p = 200, \epsilon_p = 1000, \epsilon_p = 50000$ ) are chosen to study the effect of the permittivity on the flow field and the motion of the particle. As shown in Figure 4-3, the size of the vortices increases with the permittivity of the particle. When the permittivity of the particle is  $\epsilon_p = 200$ , and the permittivity of the liquid medium is  $\epsilon_m = 80$ , the ICEOF and the vortices are rather weak comparing with the electroosmotic flow of the liquid in the channel. However, when the particle's permittivity is  $\epsilon_p = 1000$  and  $\epsilon_p = 50000$ , ICEOF generates stronger vortices.





**Figure 4-3.** The velocity vector and  $x$ -velocity contour at  $t=0$ .  $E_\infty = 100\text{V/cm}$ ,  $\zeta_w = -15\text{mV}$ ,  $d=20\ \mu\text{m}$ .

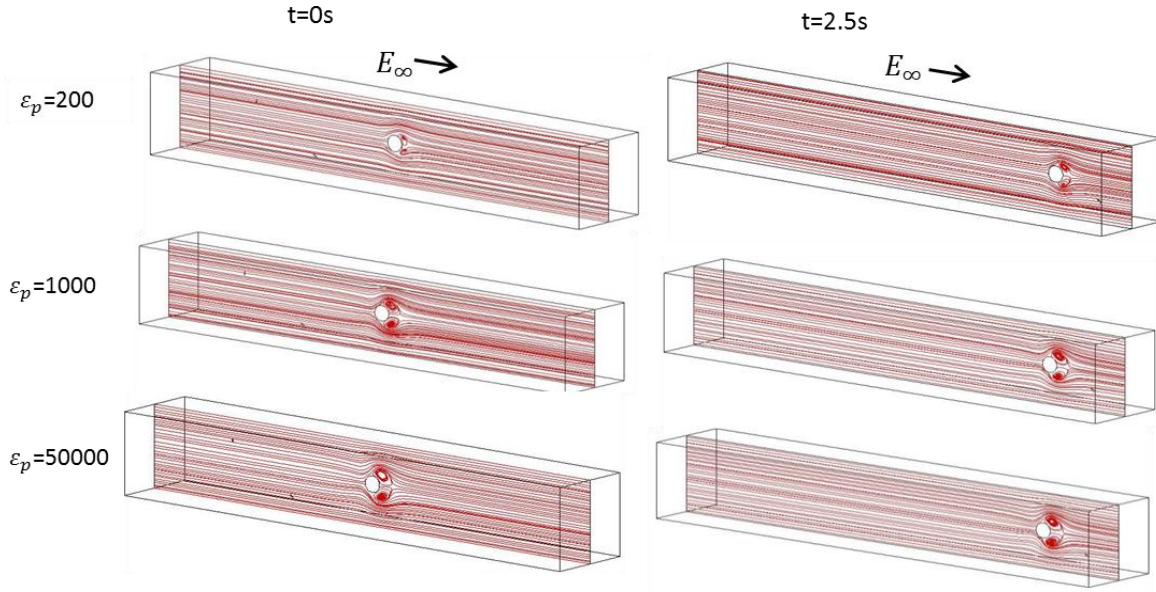


**Figure 4-4.** The flow velocity in the  $x$  direction around the particle surface at  $t=0$ .  $E_\infty = 100\text{V/cm}$ ,  $\zeta_w = -15\text{mV}$ ,  $d=20\ \mu\text{m}$ .

Figure 4-3 depicts the velocity vector of the combined EOF and ICEOF, and the contour of the  $x$ -velocity of the combined flow around three different particles  $\varepsilon_p = 200$ ,  $\varepsilon_p = 1000$  and  $\varepsilon_p = 5000$ . The velocity vectors indicate that, the two vortices at downstream are more visible when the polarizability of the particle is stronger. In the  $x$ -direction, due to the non-uniform ICEOF around the particle, a high positive  $x$ -velocity region at the front of the particle is always accompanied with a low negative  $x$ -velocity region at the back of the particle. The change of the value of the  $V_x$  around the particle in these three cases are shown in Figure 4-4. It is clear that, due to the polarizability-dependent ICEOF,  $V_x$  in the high positive region increases with the polarizability of the particle, however, the magnitude of the negative  $V_x$  at the back of the particle increases simultaneously by the same amount. Though the change of the polarizability of the particle always brings in variations to the flow field around the particle, the variations are always symmetric and opposite.

The motion of three particles of different permittivities is also shown in Figure 4-5. The particles were released from the center of the channel and traveled the same distance in  $t = 2.5$ s. Clearly, the dielectric particles with different permittivity  $\varepsilon_p$  have the same velocity in the microchannel when other parameters are the same. This is because the ICEOF around the particle has a symmetric structure (as shown in Figure 3-1 b). The direction of the two vortices upstream is opposite to the two vortices downstream, so that the four vortices make equal but opposite contributions to the motion of the particle. Therefore, even though the strength of the vortices changes with  $\varepsilon_p$ , the four vortices always make zero net contribution to the flow and hence the hydrodynamic force acting on the particle. A similar conclusion was found earlier by O'Brien et al. [35]. They studied the influence of the ion distribution, the electric field to the flow field, and found that the force on the particles is independent on the dielectric property of the dielectric

particles but depends on the particle size and shape, the initial static charges, and the strength of the electric field.



**Figure 4-5. Streamlines of the flow field and positions of particles with different  $\epsilon_p$ , at time  $t=0s$  and  $t=2.5s$ ,  $E_\infty = 100V/cm$ ,  $\zeta_w = -15mV$ ,  $\epsilon_m = 80$ ,  $d=20 \mu m$ .**

#### 4.2 The interaction between two dielectric particles in uniform electric field

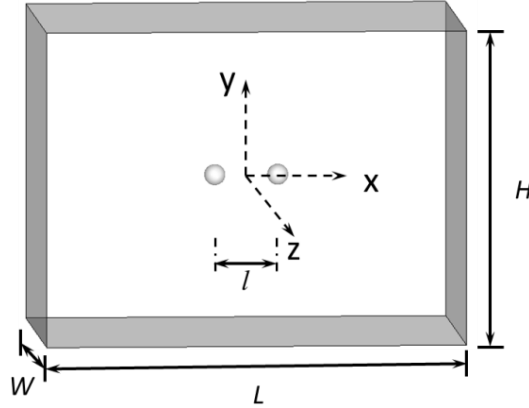
From Eq. (4-5) and (4-6), and the simulation results presented in the last section, it is easy to understand that the four vortices around the particle are indifferent directions, and the particles of different polarizabilities will give rise to ICEOF of different strengths. When two dielectric particles are close to each other, the vortices around the particles will interact with each other. To study the interaction of two dielectric particles due to the ICEOF, numerical simulations were performed. The same set of controlling equations are solved, including the continuity equation, Navier-Stokes equation, Laplace's equation, and the equations for the motion of the particles. The interaction between the particles and the relative displacements of the two particles are the

main concern of this section, so that the EOF generated at the channel walls is neglected. We assume that the particles are placed in a sufficiently large chamber, and the effect of solid boundary walls can be ignored. The computing domain is shown in Figure 4-4; the boundaries of the computing domain are open boundaries. The ICEOF on the surface of the two particles are indicated by applying a slipping velocity  $\vec{V} = \vec{U}_p + \vec{\omega}_p \times (\vec{x}_p - \vec{X}_p) - \frac{\varepsilon_0 \varepsilon_m \zeta_i}{\mu} \vec{E}_{\parallel}$ .

#### ***4.2.1 Geometry and dimensions***

The computational domain is shown in Figure 4-6. Two spherical particles with the same diameter  $d = 10\mu\text{m}$  are placed in the middle of the computation domain. The distance between the two particles is five times of the particle's diameter, i.e.,  $l = 5 \times d$ . The length, height and width of the computational domain are  $H = W = 15 \times d$ , and  $L = 20 \times d$ . The origin of the coordinate system is set at the center of the domain. The velocity of two identical particles of permittivity  $\varepsilon_p$  is tested under different mesh-elements numbers. It is found that, when the computational domain contains more than 130,925 mesh elements, the velocity of the particle changes less than 1%. Eventually, 130,925 unstructured mesh elements are originally defined in the computing domain by GAMBIT 2.40. The 3D transient simulation was performed using the commercial software FLUENT 12.0. First order upwind spatial discretization and first order implicit discretization methods are utilized. The particles are initially static. The time steps used in this serial of simulations range from  $10^{-7}\text{s}$  to  $10^{-5}\text{s}$ .



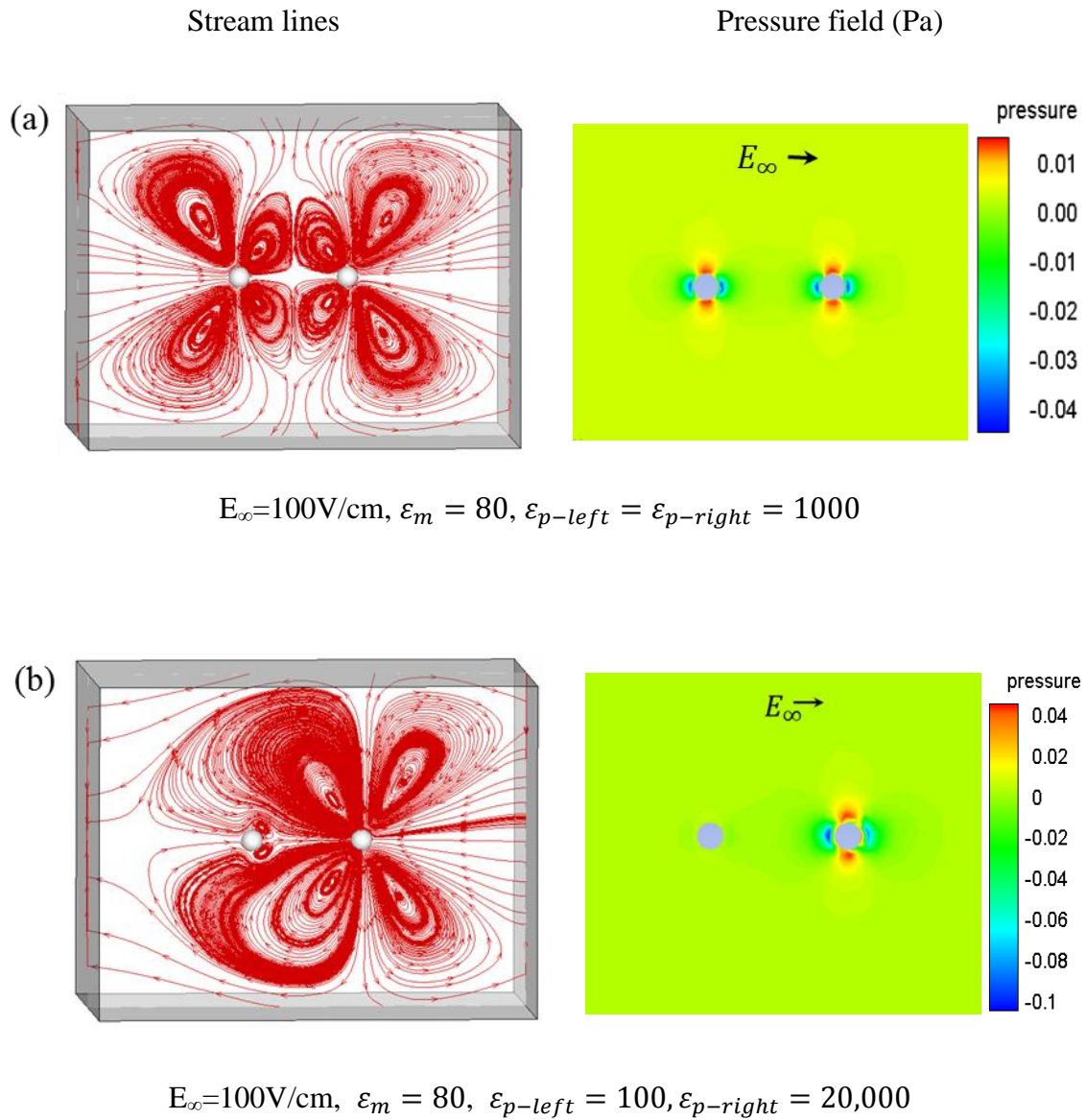


**Figure 4-6. Schematic diagram of the simulation domain for studying the interaction of two dielectric particles due to ICEOF.**

#### ***4.2.2 Results and discussion***

Figure 4-7 illustrates that at  $t=0s$ , the flow field and the pressure field around two particles with identical property and different polarizability in the presence of an electric field parallel to the alignment of the two particles. In Figure 4-7a, when the particles are identical, the vortices generate the same flow field and the same pressure field in the vicinity of the particles. The flow field and pressure field around the two particles are symmetric. However, in Figure 4-7b, when the two particles have different polarizabilities, the vortices around the two particles are of different strengths, and thus the flow field is not symmetric. The flow field (stream lines) and the pressure field near two different particles at the  $y = 0$  plane are shown in Figure 4-7b. In this case, the left-side particle has a permittivity of  $\epsilon_{p\text{-left}} = 100$  and the right-side particle has a permittivity of  $\epsilon_{p\text{-right}} = 20,000$ . It is clear that, the vortices around the right-side particles are much stronger than that around the left-side particle. That is because the particle with a permittivity  $\epsilon_{p\text{-right}} = 20,000$  generates a stronger induced surface potential than the left one

with  $\varepsilon_{p-left} = 100$  according to Eq. (4-5); therefore, the ICEOF is much stronger around the right-side particle according to Eq. (4-6),  $\vec{V} = -\frac{\varepsilon_0 \varepsilon_m \zeta_i}{\mu} \vec{E}_{\parallel}$ .



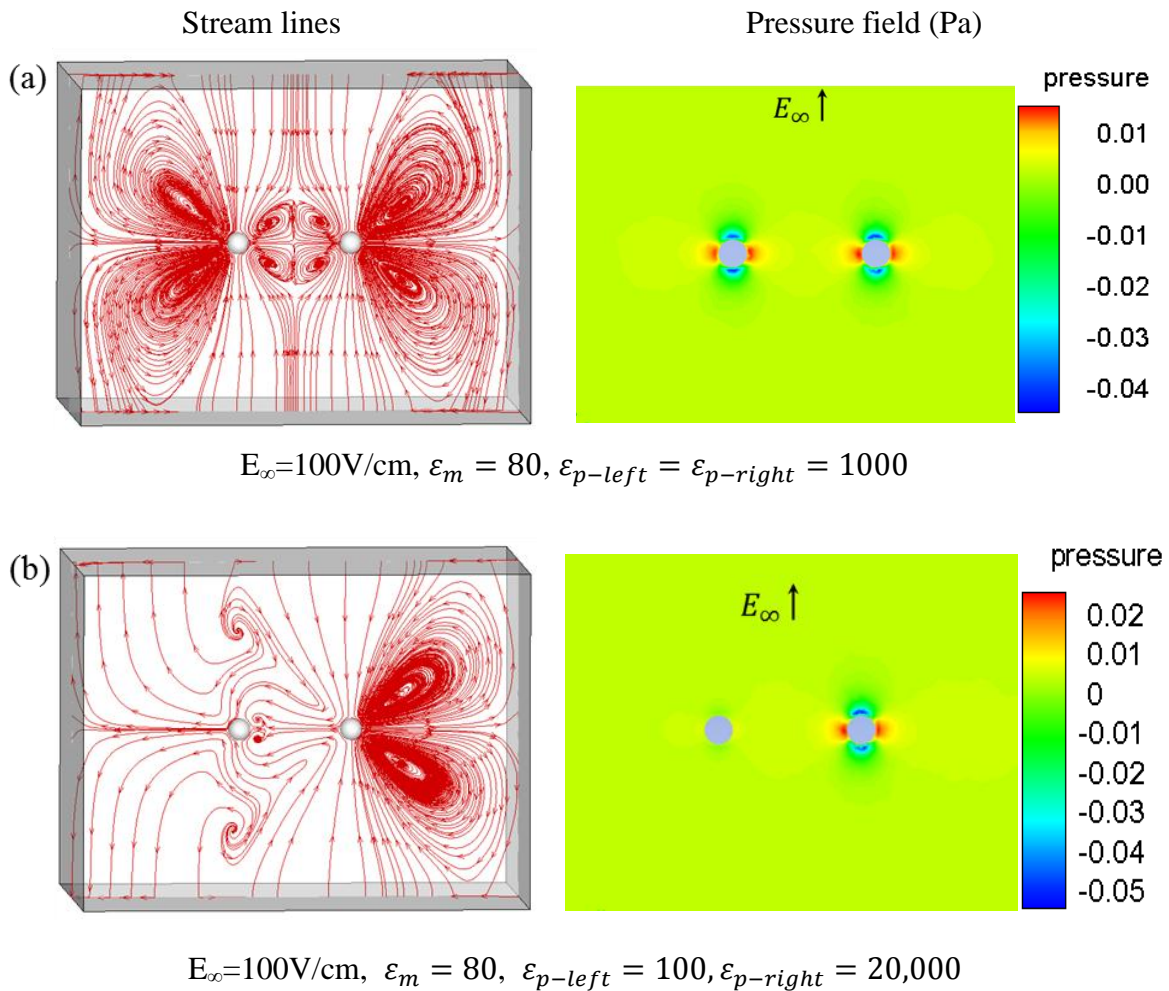
**Figure 4-7.** In the presence of a parallel electric field, the flow field and the pressure field (a) around two identical particles, and (b) around two different dielectric particles.  $d = 10\mu\text{m}$ .

It is noted that, the four vortices on the right-side particle with high permittivity are more visible, and the direction of the vortices are opposite between every two adjacent vortices; however, the vortices are symmetric to the straight line connecting the two particles. From the distribution of the vortices, it is easy to understand the distribution of the pressure field in the vicinity of the particles. There are high and low pressure regions near the particles. The pressure field around the right-side particle is almost symmetric corresponding to the flow field, so that the pressure on right-side particle is essentially balanced by itself. However, the pressure field around the left-side particle is significantly out of balance, the left-side particle experiences an attraction effect from the right-side particle due to the low pressure region in between them. Consequently the left-side particle will move towards the right-side particle.

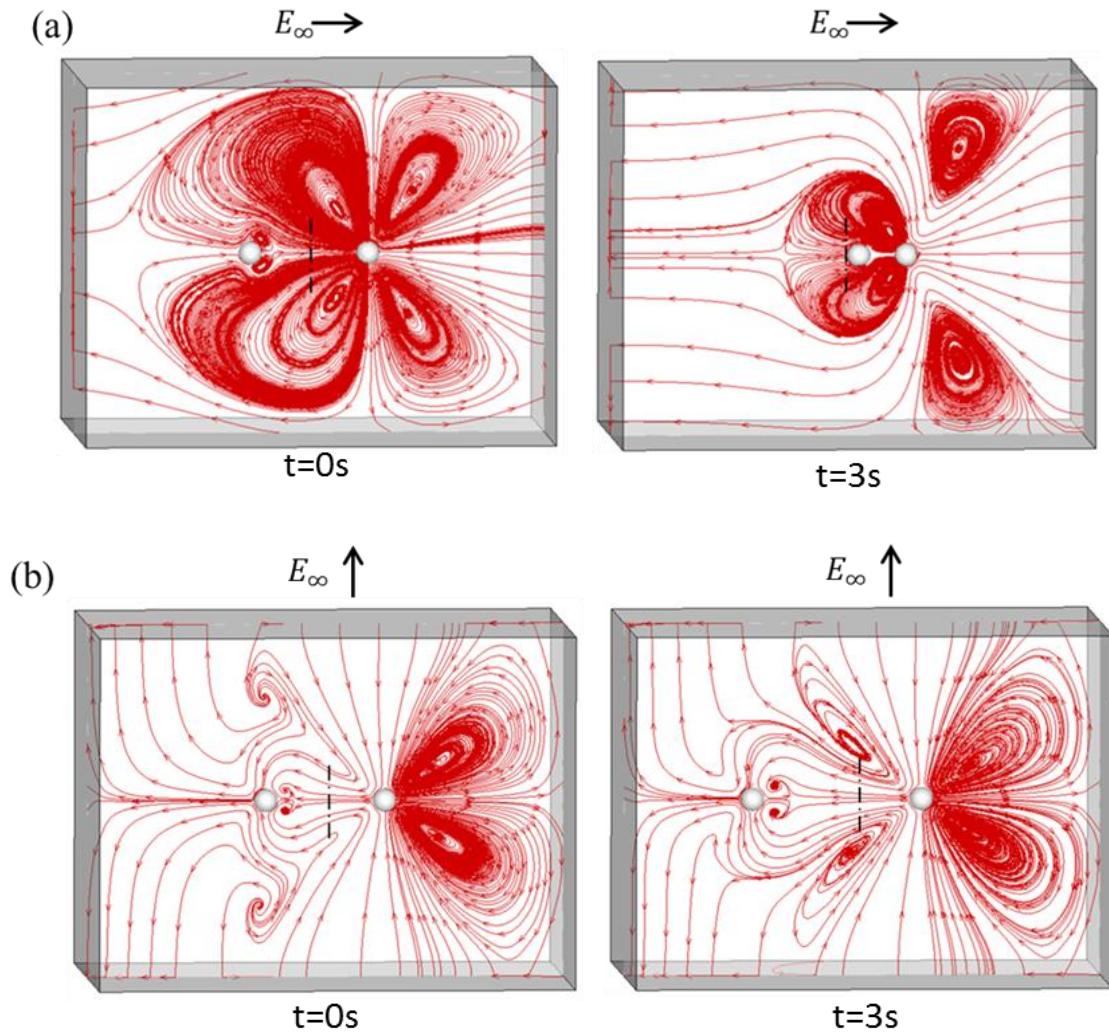
When the applied electric field is perpendicular to the alignments of the two particles, the flow field (stream lines) and the pressure field are shown in Figure 4-8. Figure 4-8a shows the streamlines and the pressure field around two identical particles. In spite of the deformation of the four vortices between the two particles, the streamlines in the whole domain are symmetric. As shown in Figure 4-8a, the four vortices are reversed in comparison with the vortices in Figure 4-8a. Accordingly, the high pressure and low pressure regions are also shifted. Meanwhile, the pressure still has a symmetric distribution in the whole field.

Figure 4-8b, on the other hand, shows the streamline and pressure field around two particles with different permittivity. Clearly, the vortices on the right-side particle with  $\epsilon_{p\text{-right}} = 20,000$  are much stronger than that of the left particle with a low permittivity. The featured four symmetric vortices of the ICEOF have been deformed. The two vortices on the left side of the right particle are merged with the vortices on the right side of the left-side particle, and thus the two vortices on the right side of the left particle are not apparent. This is very different from the symmetric

streamlines around two identical particles where all the four vortices on each of the particle are clearly seen (Figure 4-8a). Additionally, Figure 4-8b shows that the pressure fields in the vicinity of the two particles are not identical. The pressure around the right particle is approximately balanced. However, the high pressure between the two particles tends to push the left-side particle away from the right one.



**Figure 4-8. In the presence of perpendicular electric field, the flow field and the pressure field (a) around two identical dielectric particles ( $\epsilon_p = 1000$ ), and (b) around two different particles  $\epsilon_{p\text{-left}} = 100, \epsilon_{p\text{-right}} = 20,000$ , respectively,  $d = 10\mu\text{m}$ .**

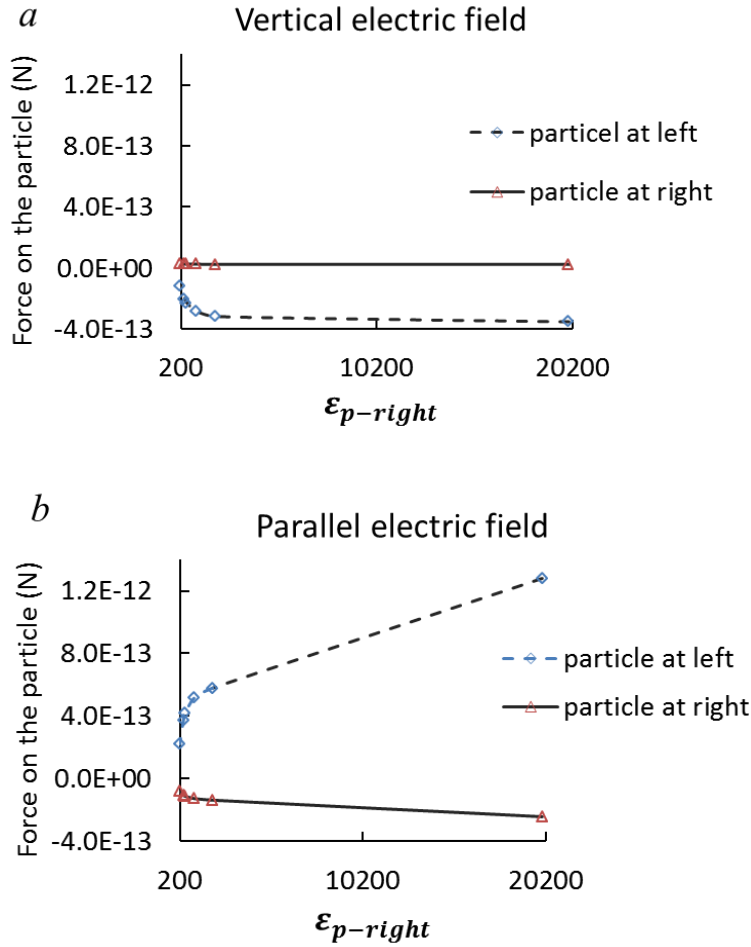


**Figure 4-9. Displacement of two dielectric particles with  $\epsilon_{p-left} = 100$ ,  $\epsilon_{p-right} = 20,000$ ,  $\epsilon_m = 80$  over a period of 3 seconds. Particles were initially separated by a distance of  $l = 5d$ ,  $d=10\mu\text{m}$ . Dashed dark line indicates the initial center line of the two particles. (a) Under a parallel electric field  $E_\infty=100\text{V/cm}$ . (b) Under a perpendicular electric field  $E_\infty=100\text{V/cm}$ .**

Because of the unbalanced pressure between the two dielectric particles, the particles will move in a certain direction at a specific velocity depending on the direction and strength of the applied electric field and the polarizabilities of the particles. Figure 4-9 shows the displacements of the two particles over a period of three seconds when an electric field  $E_\infty=100\text{V/cm}$  is applied

parallel or perpendicular to the alignment of the particles. The motions of the particles coincide with the pressure field described above: the right-side particle with a significantly higher permittivity barely moves and the left-side particle with a low permittivity moves toward (in the case of a parallel electrical field) or away from (in the case of a perpendicular electric field) the other particle. The velocity of the particles are  $U_{p\text{-left}} = 13\mu\text{m/s}$ ,  $U_{p\text{-right}} \cong 0$  when the particles are subjected to a parallel electric field  $E_{\infty}=100\text{V/cm}$ ; and  $U_{p\text{-left}} = -8\mu\text{m/s}$ ,  $U_{p\text{-right}} \cong 0$  when the particles are subjected to a perpendicular electric field  $E_{\infty}=100\text{V/cm}$ .

As shown in Figure 4-9, when the electric field is applied in different directions, not only the direction of the motion of the particles is reversed, but also the values of the velocities are not the same. The forces exerted on the particles when the particles are 5d apart are shown in Figure 4-10. In the case of a parallel electric field, with a fixed permittivity of the left-side particle, increasing the permittivity of the right-side particle will significantly increase the hydrodynamic interaction force on the left-side particle. Similarly, when the electric field is applied vertically, the effect of the interaction force on the left-side particle increases gradually with an increased polarizability of the right-side particle. Because the left-side particle is assumed to have a lower permittivity in all these cases, the symmetry of the field around the right-side particle is only slightly broken by the left-side particle. The force on the left-side particle caused by the interaction is always stronger than the force on the right-side particle. Additionally, Figure 4-10 indicates that, the interaction between the two particles is stronger when the electric field is parallel to the alignment of the two particles than the counter case. This is related to the induced pressure field in these cases. Comparing Figure 4-8b with Figure 4-8b the pressure difference in the presence of parallel electric field is stronger than the pressure difference when the electric field is vertically applied.



**Figure 4-10. Hydrodynamic forces exerted on the two particles as a function of  $\epsilon_{p-right}$ . Particles are initially separated by a distance  $l = 5d$ ,  $d=10\mu\text{m}$ ,  $E_\infty = 100\text{V/cm}$ , and  $\epsilon_{p-left} = 100$ . (a) In a parallel electric field, (b) in a perpendicular electric field. The positive force is in the direction from the left to the right. The negative force is in the direction from the right to the left.**

### 4.3 Conclusions

This chapter demonstrated the effects of polarizability of dielectric materials on the induced-charge electroosmotic flow (ICEOF). We introduced an analytical expression for the induced surface potential on dielectric particles as a function of permittivity of the particle and the

surrounding medium, particle size and the applied electrical field. This expression can also be used for metals with infinitely large permittivity  $\epsilon_p$ . The strength of the vortices of ICEOF is dependent on, in addition to the applied electrical field, the dielectric property of the particle and the surrounding medium. The transportation of a polarized particle in a microchannel flow is independent of the dielectric property of the particle, because the symmetric vortices of ICEOF contribute zero net force to the transportation. However, in the absence of the bulk liquid motion, the interaction of two dielectric particles by ICEOF presents interesting immigration phenomena. The vortices of two closely located particles give rise to high and low pressure regions near the particles. When the two particles have different dielectric properties, the vortices and pressure field around the two particles are not identical. Consequently, the two particles move toward or away from each other depending on the direction of the applied electrical field. In the case of two different particles, the particle with high permittivity is the dominant factor in the interaction between the two particles. The polarizability-dependent interaction of dielectric particles due to ICEOF may have the potential for developing novel particle separation and sorting technology.



## Chapter 5

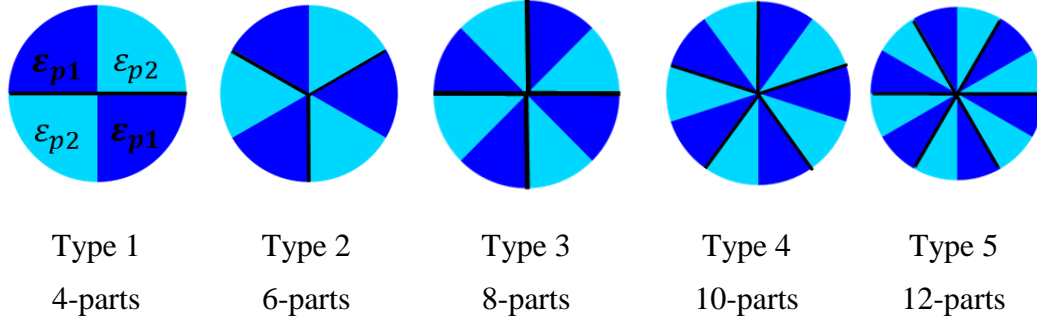
### Motion of heterogeneous particles in uniform electric field

In the last chapter, we studied the electrokinetic motion of homogeneous dielectric particles under the influence of uniform electric field. In this chapter, we study the motion of rotationally symmetrical heterogeneous dielectric cylinder particles composed of equal parts with alternate polarizabilities (e.g.  $\epsilon_{p1}$ ,  $\epsilon_{p2}$ , and  $\epsilon_{p1} > \epsilon_{p2}$ ) subjected to an external electric field. Depending on the polarizability of each dielectric component and the angle between each individual component and the electric field, the induced surface potential on a heterogeneous particle is spatially varying. Accordingly, the slipping ICEOF around the particle is also spatially varying. The particle suffers a continuous torque from the asymmetric slipping velocity of the ICEOF. Additionally, initial static charges on the particle result in linear electroosmotic flow on the heterogeneous particle and consequently provide a constant translational motion of the particle at the same time. As a result, the heterogeneous particles move like micro-wheels. The cylinder particles in this chapter are considered long enough in the third dimension, and the flow field around the particle can be described as 2D flow. Transient numerical 2D simulations are performed to investigate the rotation and translation of several types of heterogeneous particles under the influence of different polarizabilities and electric field strengths.

#### 5.1 Induced surface potential and ICEOF on heterogeneous particles

The heterogeneous dielectric particles shown in Figure 5-1 are made of two dielectrics  $\epsilon_{p1}$  and  $\epsilon_{p2}$  with alternate alignment. Each high polarizable part  $\epsilon_{p1}$  is paired with a low polarizable part  $\epsilon_{p2}$  on the right side. As shown in figure 5-1, particle type 1 is made of four equal parts, which

means two combinations of  $\varepsilon_{p1}$  and  $\varepsilon_{p2}$ , and Particle type 2 is made of 6 equal parts and contains 3 combinations of  $\varepsilon_{p1}$  and  $\varepsilon_{p2}$ , etc.

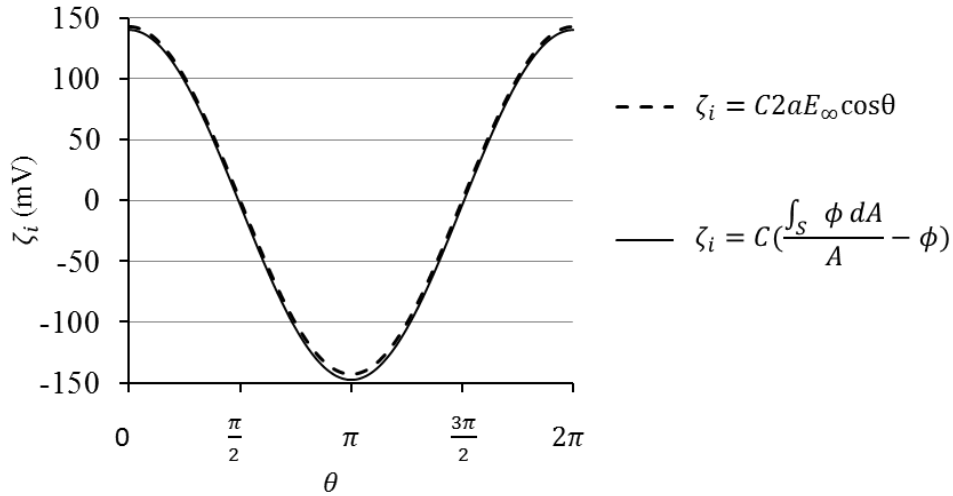


**Figure 5-1. Heterogeneous particles types made of two dielectric materials represented by two different colors.**

When a heterogeneous particle is suspended in aqueous solutions and electric field is applied, each individual combination is polarized independently. Since each combination is electrically neutral separately, the derived induced surface potential on a cylinder Eq. (3-15) does not apply to this non-spherical surface. We have claimed in Chapter 3 that the deduction of  $\zeta_i$  from the work of Wu et al. [7] obeys similar principles to the principles in our derivation (i.e. zero-current boundary out of the EDL, and internal electric field is induced to counterbalance the external field). The coefficient  $C = \frac{\varepsilon_p}{\varepsilon_p + \varepsilon_m}$  in our expression reflects the impact of the dielectric properties to the value of the induced surface potential. Additionally, Figure 3-3 demonstrates that, the coefficient C is the ratio of the induced surface potential on dielectric particles to that on metal particles. Based on the above facts, we combine the coefficient C in our derivation Eq. (3-15) with Wu's integral Eq. (3-21) [7], and obtained the following Eq. (5-1). Eq. (5-1) estimates the induced surface potential on dielectric surfaces of arbitrary geometries. Eq. (5-1) is not limited to

spherical surfaces. For a cylindrical particle, Eq. (5-1) yields the same value as Eq. (3-7) as shown in Figure 5-2.

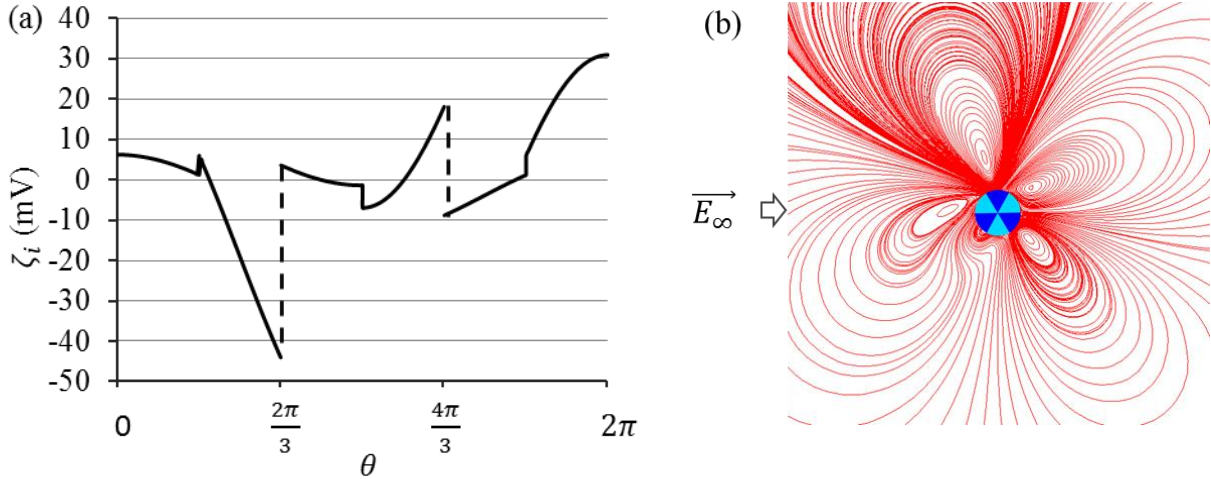
$$\zeta_i = C\left(-\phi + \frac{\int_S \phi dA}{A}\right), C = \frac{\varepsilon_p}{\varepsilon_p + \varepsilon_m} \quad (5-1)$$



**Figure 5-2. The induced surface potential on a sphere calculated by Eq. (3-15), and Eq. (5-1), and  $C = \frac{\varepsilon_p}{\varepsilon_p + \varepsilon_m}$ . The values of the parameters are:  $\varepsilon_p = 200$ ,  $\varepsilon_m = 80$ ,  $a=10 \mu\text{m}$ ,  $E_\infty=100\text{V/cm}$ .**

Since each dielectric pair is electrically neutral independently,  $A$  in Eq. (5-1) is the surface area of each individual dielectric pair. The distribution of the induced surface potential on a 6-part heterogeneous particle is illustrated in Figure 5-3a. As indicated in Figure 5-3b,  $\theta = 0 \sim \frac{\pi}{3}$  represents the dielectric surface  $C_2 = \frac{\varepsilon_{p2}}{\varepsilon_{p2} + \varepsilon_m} = 0.2$ , and  $\theta = \frac{\pi}{3} \sim \frac{2\pi}{3}$  represents the second dielectric part  $C_1 = \frac{\varepsilon_{p1}}{\varepsilon_{p1} + \varepsilon_m} = 1$  of this component ( $\theta$  is defined as in Figure 3-1). As seen in Figure 5-3a, because the polarizability on the left part of the component is larger than the polarizability on the

right part, the value of the induced surface potential  $\zeta_i$  on the left part of each component is more significant than the other part. The induced surface potential on each single component ( $1/3$  circle) is independent of the other two components, thus, the induced surface potential is not continuous at the joints of adjacent components.

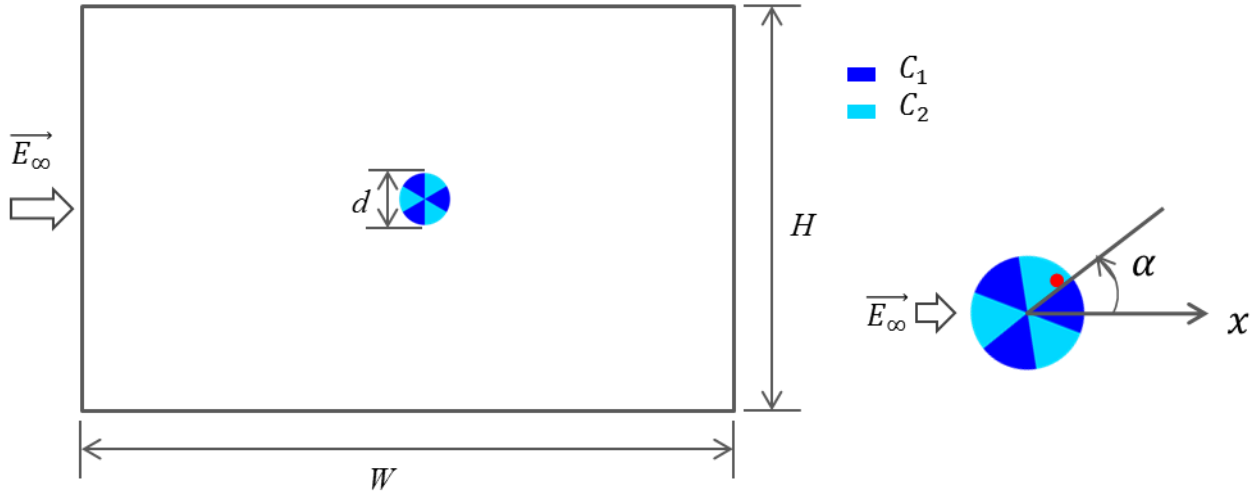


**Figure 5-3. The polarization of the 6-parts heterogeneous particle in uniform electric field. Alternate polarizabilities:  $C_1=1$ ,  $C_2=0.2$ , size  $d=10 \mu\text{m}$ ,  $E_\infty=25\text{V/cm}$ . (a) The value of the induced surface potential, (b) the streamlines of the ICEOF.**

Figure 5-3b depicts the streamlines of the corresponding ICEOF on the 6-parts heterogeneous particle. It is easy to understand that, since  $\zeta_i$  is larger on the left part of a component, the slipping ICEOF on the left part is also stronger than that on the right part. The rotationally symmetrical alignment of the dielectric components guarantees the ICEOF on each individual component contributes a torque on the particle in one consistent direction. In the next section, we will build numerical simulations to study the impact of the slipping ICEOF to the motion of the heterogeneous particle.

## 5.2 Computational domain and dimensions

Figure 5-4 shows the computational domain of the simulations in this chapter. A heterogeneous particle is suspended in a chamber, where uniform electric field is applied. Since the particles are heterogeneous, we define angle  $\alpha$  to represent the orientation of the particles relative to the uniform electric field as shown in Figure 5-4. The particle size is  $d$ , and the scale of the chamber is  $W \times H = 100d \times 150d$ . We studied the motion of the particles under the influence of the non-uniform slipping velocity on the particles, so the simulations are transient. Different numbers of mesh elements ranging from 1,513 to 4,562 are tested. We record the rotation periods of the 6-parts particle while  $E_\infty = 50\text{V/cm}$ , and  $C1=1$ ,  $C2=0.2$  and find that, when the number of volumes in the computational domain is larger than 2,370, the rotation period maintains a constant value (within 0.5% changes). Eventually, 3,102 mesh elements are generated for the simulations. Different mesh element numbers are applied to different types of particles. 4-parts: 2,765; 8-parts: 3,325; 10-parts: 3,798; 12-parts: 4,213. The 2D simulations are performed with COMSOL 3.5a. COMSOL is a finite-volume method based commercial software. The discretization methods used in the serial of simulations are given in Table 5-2. The numerical error tolerance applied is  $10^{-5}$ . The time steps for this transit motion should be small enough to guarantee an equilibrium rotation period of each particle under a fixed set of parameters. The times steps employed in this section ranges from  $\Delta t=0.02\text{s}$  to  $\Delta t=0.0001\text{s}$  depending on the rotational speed of the particles.



**Figure 5-4. The schematic diagram of the computational domain.  $\alpha$  is defined as the angle between the particle and the external electric field.**

Variables	Discretization method
Velocity	Second order
Pressure	First order
Electric potential	Second order
Displacement of the particle	Second order

**Table 5-1. Discretization methods used in the simulations.**

The governing equations in Chapter 3 were used for this series of numerical simulations. The scale of the chamber is much bigger than the particle size, thus the electroosmotic flow on the chamber is ignored. We first focused solely on the rotational motion of different heterogeneous particles resulted from the spatially varying induced surface potential. Then the static zeta potential on the heterogeneous particle was considered which leads to translational motion of the particle. The combination of the heterogeneous induced surface potential and the constant static zeta potential drives the particle into wheel-like motion.

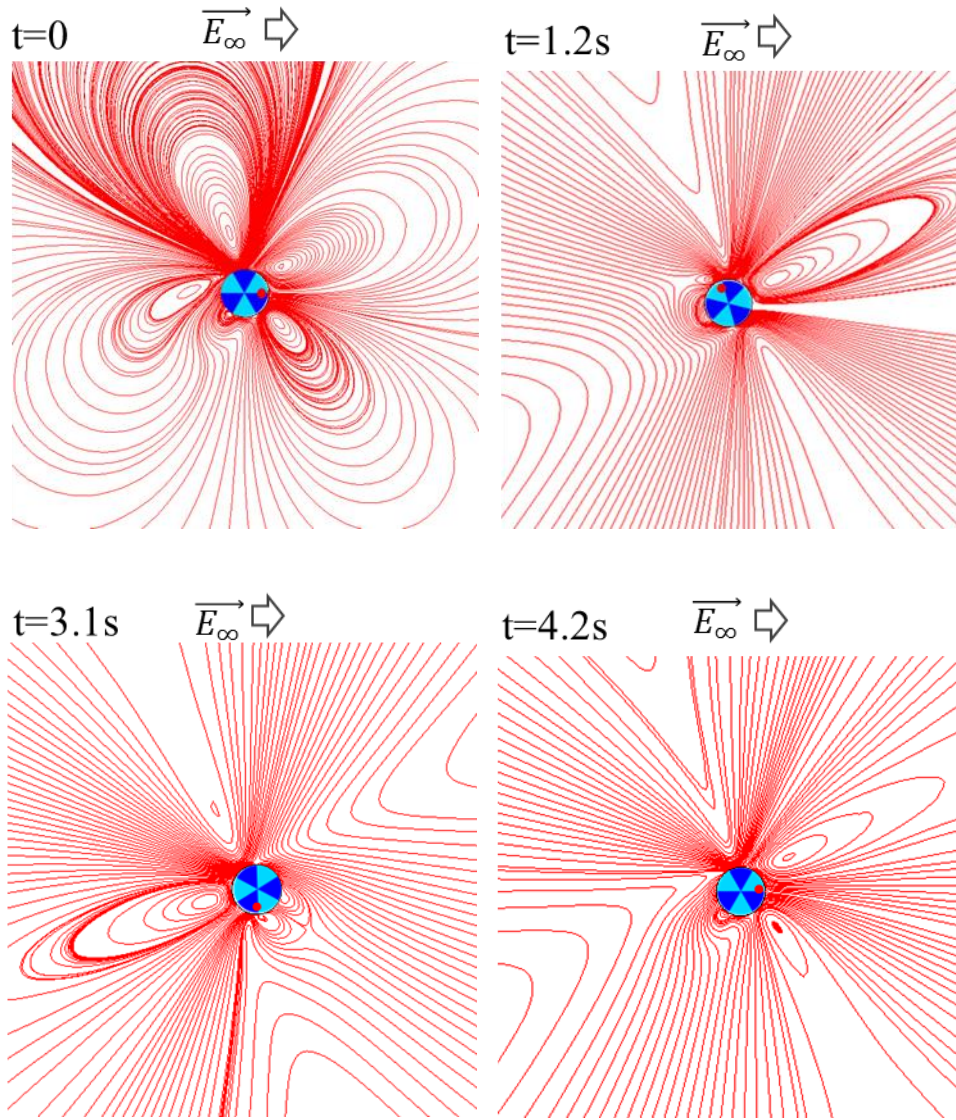
Definition	Constant/Parameters	Values/Range
Permittivity of the vacuum	$\epsilon_0$ (F/ m)	$8.85 \times 10^{-12}$
Relative permittivity of the liquid medium	$\epsilon_m$	80
Polarizability of the particle material	C	0.2~1
Viscosity of the liquid	$\mu$ (kg/m s)	$0.9 \times 10^{-3}$
Density of liquid	$\rho$ (kg/m <sup>3</sup> )	998
Zeta potential of the particle	$\zeta$ (mV)	-30
Diameter of the particle	$d$ ( $\mu$ m)	10~20
External electric field	$E_\infty$ (V/cm)	20~125

**Table 5-2. Values of the constants and parameters used in the simulations**

### 5.3 Simulation results and discussion

#### 5.3.1 Rotation of uncharged heterogeneous particles.

In this section, the particles are temporally assumed neutral and we purely studied the ICEOF caused rotation of the heterogeneous particle. A heterogeneous particle is placed in the center of the chamber and suspended in aqueous liquid. Assume the permittivity of the surrounding liquid is  $\epsilon_m = 80$ , then Eq. (3-8) gives the value of the defined non-dimensional polarizability of the two dielectric materials composing the particle:  $C_1 = \frac{\epsilon_{p1}}{\epsilon_{p1} + \epsilon_m}$ ,  $C_2 = \frac{\epsilon_{p2}}{\epsilon_{p2} + \epsilon_m}$ . Simulation results show that, once the electric field is applied, the resulted spatially varying ICEOF around the particle drives the particle to rotate. The rotation of the 6-parts particle of diameter  $d=20 \mu\text{m}$  while  $C_1=1$  and  $C_2=0$ , and the electric field strength is  $E_\infty=25\text{V/cm}$  is shown in Figure 5-5.



**Figure 5-5. The rotation of the 6-parts particle  $d=20\ \mu\text{m}$  with  $C_1=1$ ,  $C_2=0.2$ ,  $E_\infty=25\text{V/cm}$ . Starts from  $t=0$ ,  $\omega_p = 0$ .**

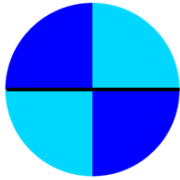

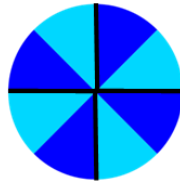
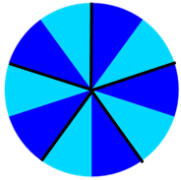
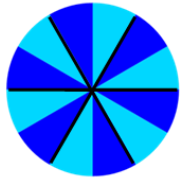
The rotation process in Figure 5-5 starts at  $t=0$  from static state, and finishes a full circle anticlockwise in  $t = 4.2\text{s}$  without deviation from the original location. The streamlines of the ICEOF around the heterogeneous particles indicate that, the ICEOF not only depends on the permittivity distribution but also the orientation of the particle relative to the external electric field. In principle, the induced charges always generate electric field in the electric field



direction. So the angle of each component surface relative to the electric field determines the distribution of the induced surface charges. While the particle is rotating, the angles between each single component surface and the external electric field vary, which results in the time-dependent ICEOF.

The time period for two circles starting from  $t=0$  in the case in Figure 5-5 is 8.4s, which is exactly two folds of the time of the first circle. Given the quick acceleration process of the particle, the time period of the first circle is considered as the rotation period. We study the rotation of five different types of particle containing 4, 6, 8, 10 and 12 components, respectively.

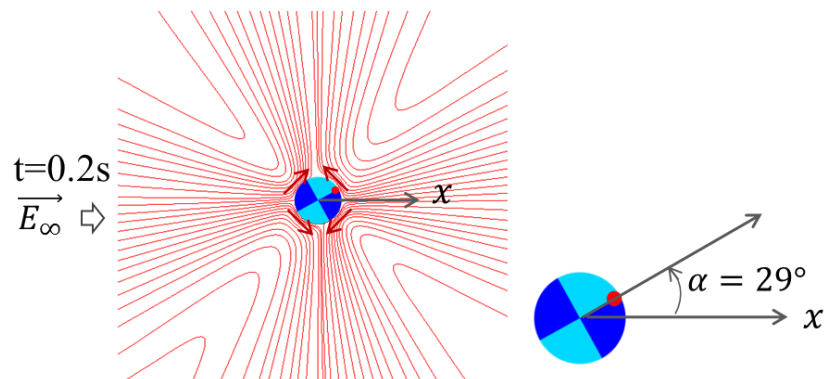
The rotation periods  $T_r$  of these five types of particle are given in Table 5-3.

Particle type					
$T_r$	--	4.2s	4.9s	5.8s	5.9s

**Table 5-3. Rotation period  $T_r$  of five types of heterogeneous particles. Particle size  $d=20 \mu m$ ,  $C_1=1$ ,  $C_2=0.2$ ,  $E_\infty=25V/cm$ . Heterogeneous particles are composed of 4, 6, 8, 10 and 12 equal parts, respectively.**

It is interesting that heterogeneous particles composed of more equal parts rotate slower (e. g. 12-parts particle) than particles consisting of less parts (e.g. 6-parts particle). Assume a heterogeneous particle is composed of infinite number of equal parts with alternate polarizability distribution, though the polarizability of each adjacent part is different, each part is physically infinitely small. The small individual surface results in weak ICEOF, consequently this particle is literally equivalent to a homogeneous particle, and barely rotates. Meanwhile, the simulation

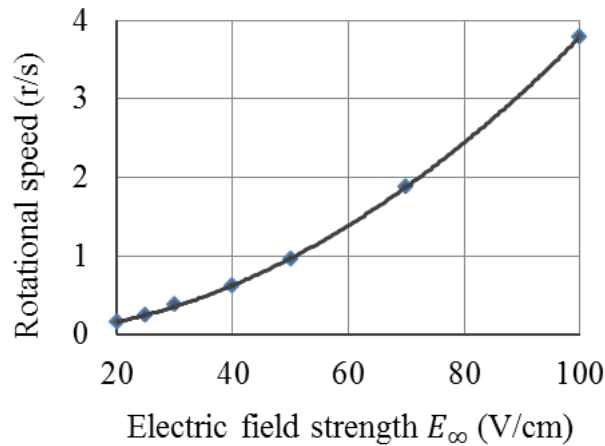
results show that, particle type 1 consisting of 4 parts could not rotate a full circle. Figure 5-6 shows the steady orientation of this particle in the uniform electric field. The particle is composed of two components of dielectrics  $C_1=1$  and  $C_2=0.2$ , and external electric field strength is  $E_\infty=25\text{V/cm}$ . The particle reaches a steady orientation while the angle between the particle and the electric field is  $\alpha = 29^\circ$ . The streamlines in Figure 5-5 clearly show that, at this position, the four vortexes around the particle are almost symmetric and in opposite directions, resulting zero-net torque to the particle. It is easy to understand that, a continuous rotation of the particle requires consistent torque acting on the particle. The moment resulted from the ICEOF around the particle type 1 reaches a balanced status at  $\alpha = 29^\circ$ , thus, the particle stops rotating at this orientation. In contrast, the time and space-dependent ICEOF in all the other 4 cases (the 6, 8, 10, and 12-parts particle) is able to generate consistent torques.



**Figure 5-6. Streamlines of the 4-parts particle at steady state  $t=0.2\text{s}$  and  $\alpha = 29^\circ$ .  $E_\infty=25\text{V/cm}$ .**

The influence of relevant parameters such as polarizability, electric field, and particle size to the rotational speed are studied. Figure 5-7 plots the change of rotational speed of 6-parts particle over the applied electric field strength. The heterogeneous particle exhibits higher rotational

speed at higher electric field strength. That's because the slipping velocity of the ICEOF is proportional to the second order of the electric field strength. Under a relatively high electric field strength e.g.  $E_\infty=100\text{V/cm}$ , the simulation result of the maximum slipping velocity on dielectric surface  $C_1=1$  is  $V=116\ \mu\text{m/s}$ , and the maximum velocity on the adjacent surface  $C_2=0.2$  is  $V=23\ \mu\text{m/s}$  (one fifth of the value of surface  $C_1=1$ ). The difference between the slipping velocity on two adjacent components is responsible for the rotational speed of the particles, and this difference is larger under stronger electric fields (e. g.  $E_\infty=100\text{V/cm}$ ).



**Figure 5-7. The change of rotational speed of 6-parts particle with external electric field strength.  $C_1=1$ ,  $C_2=0.2$ ,  $d=20\ \mu\text{m}$ .**

Table 5-4 gives the rotation periods of 6-parts particle with different dielectric polarizability compositions. It is easy to understand that, on each component, opposite signs of induced surface potential are generated, and the ICEOF slipping velocity is non-linear. Whenever the polarizability difference between the two dielectrics is significant (e.g.  $C_1=1$ ,  $C_2=0.2$ ), the resulted net torque on the particle is consequently remarkable. In contrast, when the adjacent parts have similar dielectric polarizabilities (e.g.  $C_1=1$ ,  $C_2=0.8$ ), the net torque is trivial, and the

particle rotates slowly. In an extreme case, when each pair of adjacent parts has the same dielectric polarizability, the particle is homogeneous, and doesn't rotate. This principle also applies to the other particle types.

$C_1/C_2$	1/0.8	1/0.5	1/0.2
$T_r$	16.8s	6.7s	4.2s

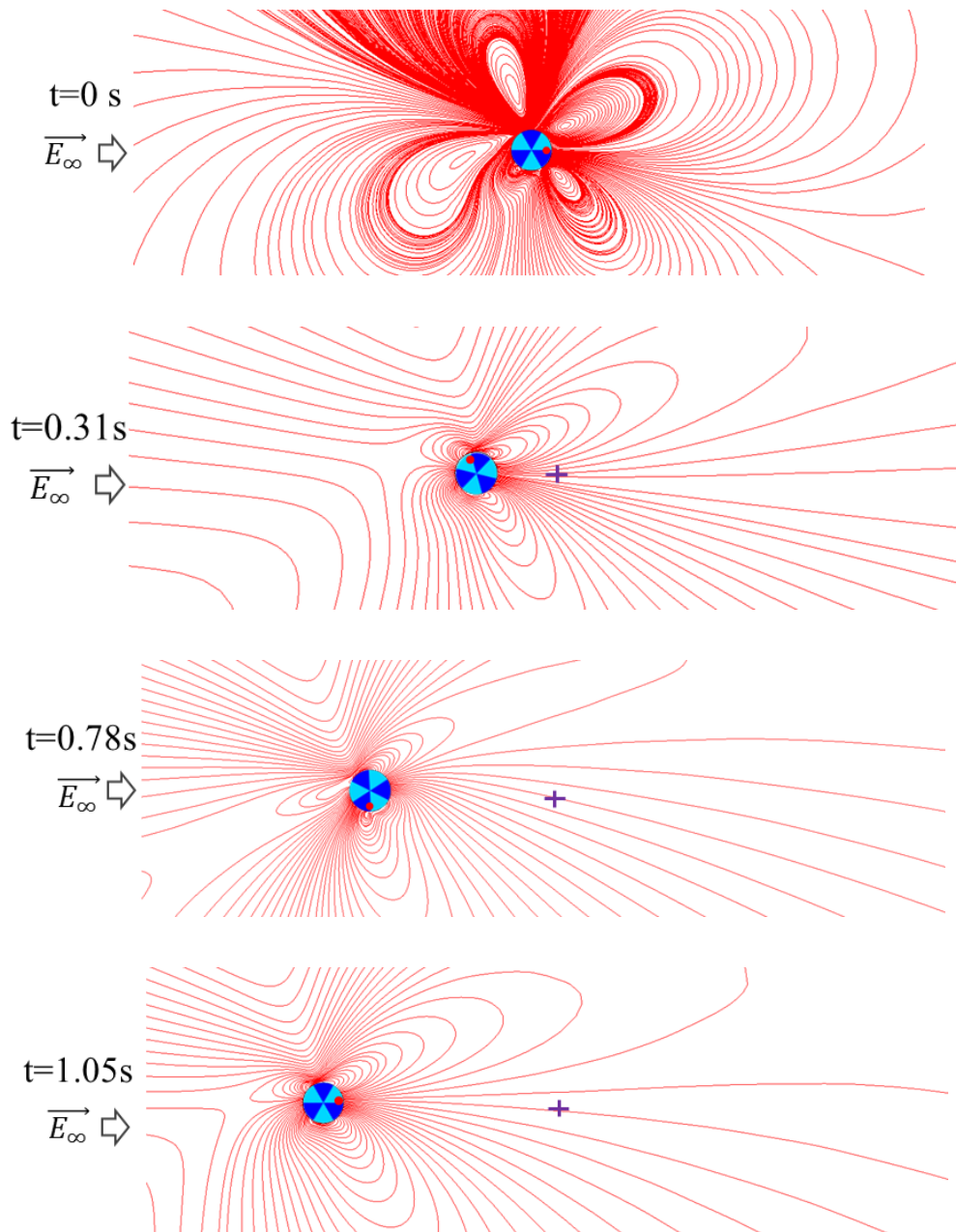
**Table 5-4. Rotation periods of 6-parts particle with a variety of polarizability compositions,  $E_\infty=25\text{V/cm}$ ,  $d=20\mu\text{m}$ .**

However, the simulation results also imply that, the particle size alone doesn't affect the rotational speed. The rotation period of 6-part particle with  $C_1=1$ ,  $C_2=0.2$ ,  $d=20\mu\text{m}$ , under  $E_\infty=25\text{V/cm}$  is 4.2s. Under the same parameters, it takes the 6-parts particle with a smaller size  $d=10\mu\text{m}$  exactly 4.2s to rotate one circle.

### 5.3.2 Micro-wheels

In the above section, the spatially varying ICEOF around the heterogeneous particles (except for the 4-parts particle) is proved to provide a consistent torque. Since the dielectrics in a micro system normally inherently presents a static zeta potential on the particle-electrolyte interface, in this section, we consider the initial zeta potential of the heterogeneous particle. Accordingly, the potential on the particle  $\zeta_p$  is the superposition of the uniform zeta potential  $\zeta$  and the nonlinear induced surface potential  $\zeta_i$ . In the following simulations, the value of the zeta potential on a particle is defined as one of the characteristic values in microfluidic system  $\zeta = -30\text{mV}$ . As a result, a linear EOF component will be generated on the particle surface besides the non-linear ICEOF. According to the classic electroosmotic flow formula  $\vec{V} = -\frac{\epsilon_0 \epsilon_r \zeta}{\mu} \vec{E}_\parallel$ , the EOF is

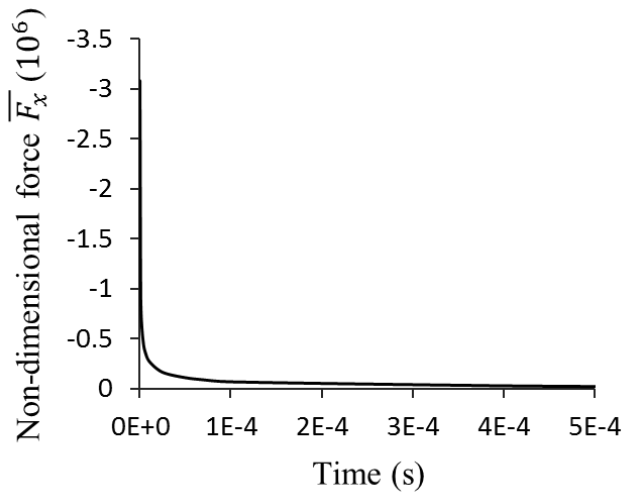
independent of the polarizability of the particle, but only a function of the static zeta potential on the particle, the permittivity of the liquid and the electric field strength.



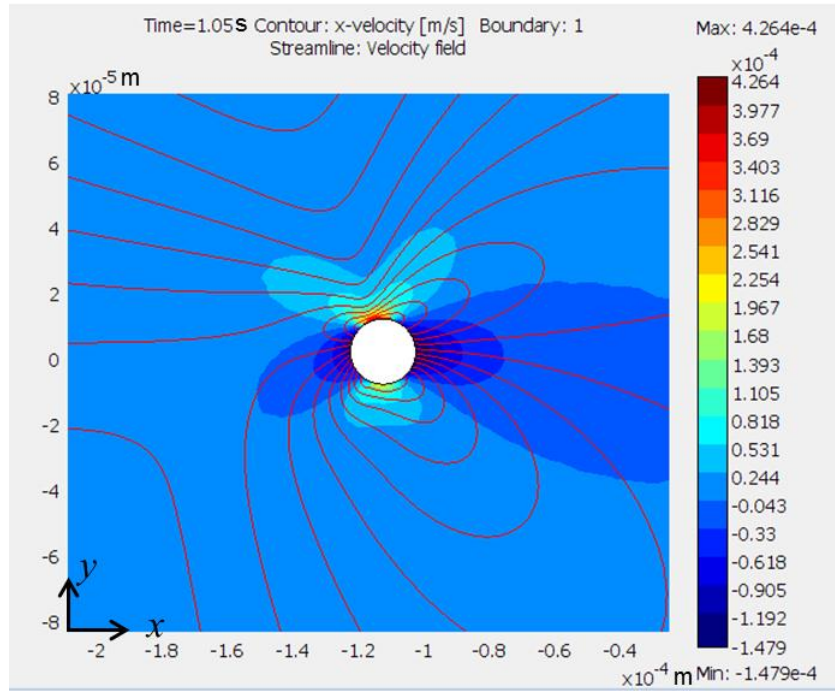
**Figure 5-8. Micro-wheel in uniform electric field. 6-parts heterogeneous particle, with  $C_1=1$ ,  $C_2=0.2$ ,  $d=20 \mu\text{m}$ ,  $\zeta = -30\text{mV}$  and  $E_\infty = 50\text{V/cm}$ . Cross signs indicate the initial location at  $t=0$ .**

Responding to the linear slipping EOF on the heterogeneous particle, the particle suffers a resistance effect from the adjacent liquid in the negative  $x$ -direction. Therefore, the heterogeneous particle undergoes constant translational motion while rotating. With a constant zeta potential and fixed dielectric properties of the dielectrics, the translational velocity is linear to the external electric field strength.

Figure 5-8 shows the rotation and translation motion of the heterogeneous 6-parts particle with  $C_1=1$ ,  $C_2=0.2$ ,  $d=20 \mu m$ , under electric field strength  $E_\infty = 50V/cm$ . Within  $T_r = 1.05$  seconds, the particle rotates a full circle and makes a displacement of  $109 \mu m$  in the negative  $x$ -direction. The rotational speed in this figure is the same as the rotational speed indicated in Figure 5-7 in the absence of EOF on the particle. The translational speed of the particle varies slightly while the particle rotates due to the time-dependent ICEOF. Therefore, the average translational speed in one full circle is defined as the translational speed. To identify the unit of the rotational speed with the unit of translational speed, the rotational speed is expressed with  $\pi\omega_p d$ .



**Figure 5-9.** The non-dimensional force  $\overline{F}_x = \frac{F_x}{\epsilon_0 \epsilon_m E_\infty^2 d^2}$  exerted to the particle at the beginning of the migration.



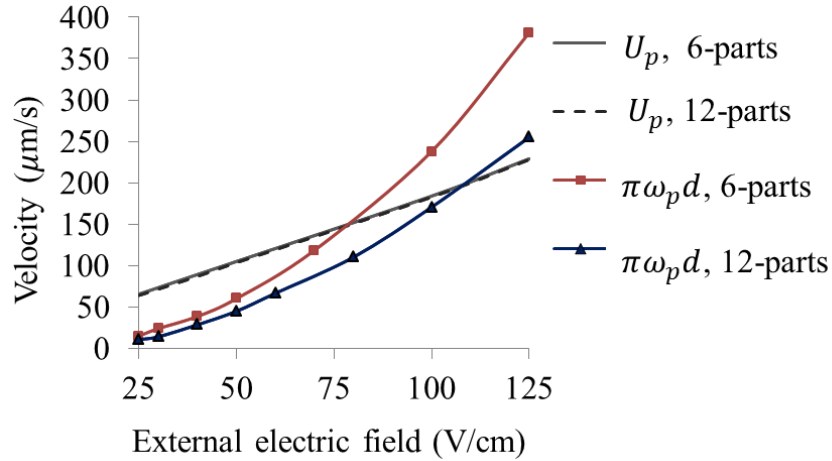
**Figure 5-10. Streamlines and the  $x$ -velocity field at  $t=1.05s$ . 6-parts heterogeneous particle, with  $C_1=1$ ,  $C_2=0.2$ ,  $d=20 \mu m$ ,  $\zeta = -30mV$  and  $E_\infty = 50V/cm$ .**

Figure 5-9 describes the non-dimensional net force exerted on the particle from  $t=0s$ . The non-dimensional hydrodynamic force  $\overline{F}_x = \frac{F_x}{\epsilon_0 \epsilon_m E_\infty^2 d^2}$  immediately decreases to zero at the beginning of this migration process. After the velocity of the particle has reached a steady status, the streamlines in Figure 5-10 depict the combined ICEOF and EOF around the particle, and the contour reflects the velocity of the combined ICEOF and EOF in the  $x$ -direction:  $V_x$ . The streamlines interact with the particle at the front and the back of the particle surface, which means the particle is moving with the liquid in the  $x$ -direction. Meanwhile, the two negative  $x$ -velocity regions in the front and at the back of the particle imply that, the particle is moving in the negative  $x$ -direction. The stream goes around the top and the bottom of the particle surface, and

two high positive x-velocity regions occur at the top and bottom of the particle which is caused by the EOF in the positive x-direction.

Figure 5-11 plots the linear speed and the corresponding translational speed of 6-parts particle and 12-parts particle under electric field strengths ranging from  $E_{\infty}=25\text{V/cm}\sim 125\text{V/cm}$ . The static zeta potential on the particle is  $\zeta = -30\text{mV}$ ,  $d=20\ \mu\text{m}$ , and the polarizability of the components are  $C_1=1$ ,  $C_2=0.2$ . The translational speed is linearly related to the external electric field strength which is consistent with the electroosmotic velocity formula  $\vec{V} = -\frac{\epsilon_0\epsilon_r\zeta}{\mu}\vec{E}_{\parallel}$ . Since the EOF is only related to the zeta potential of the particle, the translational velocity of the 6-parts particle and the 12-parts particle resulted from the local EOF are almost the same. In contrast, the linear speed of the 6-parts particle and the 12-parts particle are both proportional to the second order of the external electric field. At higher electric field strength  $E_{\infty}>75\text{V/cm}$ , the translational speed of the 6-parts particle is larger than the linear speed, whereas, for the 12-parts particle, the translational speed dominates when  $E_{\infty}< 110\text{V/cm}$ . Among the four heterogeneous particles which are able to rotate continuously, the 6-parts particle possesses the most significant rotational speed, and the 12-parts particle owns the lowest speed. The region between the two rotational speed curves in Figure 5-11 represents the rotational speeds that can be achieved by the four types of heterogeneous particles while  $C_1=1$ ,  $C_2=0.2$ ,  $d=20\ \mu\text{m}$ .





**Figure 5-11. The translational speed and the linear speed of the heterogeneous particles under various electric field strengths. The speeds of the two motions depend on the applied electric field. While  $C_1=1$ ,  $C_2=0.2$ ,  $d=20 \mu\text{m}$ , and the static potential on the particle is  $\zeta = -30\text{mV}$ .**

## 5.4 Conclusions

In this chapter, numerical simulations were performed to study the ICEOF of heterogeneous particles consisting of multi equal parts with alternate polarizabilities. Two dielectrics of different polarizabilities are alternated aligned. According to the expression for the induced surface potential on a dielectric surface, the induced surface potential and the ICEOF on are both dependent on the polarizability distribution, the angular position and the orientation of the particle. The results of the transient numerical simulations show that, the ICEOF induced by the non-linear induced surface potential continuously drives the particle to rotate, and bigger polarizability difference, stronger electric field and less components promise higher rotation speed (except the 4-parts particle). Meanwhile, in response to the external electric field, the uniform static zeta potential on the particle provides a translational speed of the particle. As a

result of the coupled EOF and ICEOF, the particles migrate in the uniform electric field like micro-wheels. The translational speed is proportional to the first order of the external electric field, and the rotational speed is a function of the second order of the external electric field. Under different electric field strengths, the translational speed can be equal to the rotational speed at a certain point for each heterogeneous particle.

These micro-wheels can be used as micro motors to stir and mix the aqueous solutions in the vicinity of the particles. The direction and velocity of the wheels can be controlled by the strength and direction of the external electric field.

## Chapter 6

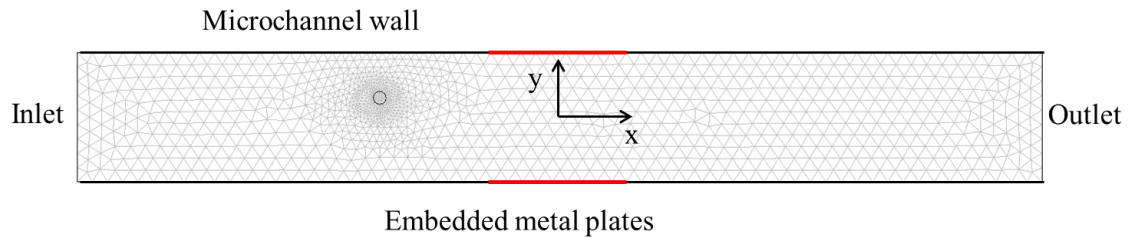
### **A novel particle separation method based on polarizability-dependent induced-charge electroosmotic flow.**

In this chapter, we propose a new particle separation method, which utilizes the induced-charge electroosmotic flow (ICEOF) on conducting plates embedded in the channel and the interaction between the channel wall and the ICEOF around dielectric particles. A pair of metal plates is embedded in a straight microchannel, and the microchannel is filled with aqueous liquid. Dielectric particles are suspended in the aqueous liquid. When electric field is applied through the channel, flow components occurring in the channel are: plug-like electroosmotic flow through the channel; local ICEOF adjacent to the metal plates; and local ICEOF around the dielectric particles. The big vortexes of the ICEOF on each metal plate push the stream against the wall. The dielectric particles following the stream will be pushed against the sidewalls as well. However, the vortexes on the dielectric particles would interact with the walls and the interaction deflects the particles from the original paths. Depending on the strength of this hydrodynamic interaction, a particle can either be trapped into the vortex or pass by the separation section and go downstream.

#### **6.1 Geometry and dimensions**

Figure 6-1 shows the 2D computational domain. The two metal plates have a length of  $L = 15 \times d$  and are embedded in a straight microchannel. The width of the channel is  $W = 10 \times d$ , and the length of the channel included in the computation domain is  $75 \times d$ . In this Chapter, the velocity of the flow is lower than  $V = 1000 \mu\text{m}/\text{s}$ . According to Eq. (4-1), the development lengths of the flows in this chapter are within  $0.6 \mu\text{m}$ . A dielectric particle of a diameter  $d = 10 \mu\text{m}$  is initially located at the upstream of the metal plates, and  $1.5 \times d$  away from the centerline of the channel.

Based on the mathematical models described in chapter 3, the numerical simulations were performed with COMSOL 3.5a. Mesh-independency is verified by dividing the computational domain into 1366, 2353, 2987 and 4970 elements, respectively. Critical separation polarizabilities under two different electric field strength  $E_{\infty} = 25\text{V/cm}$  and  $E_{\infty} = 30\text{V/cm}$  are identified when more than 2353 elements are formed. Eventually, 2,987 Lagrange finite elements are generated. The discretization methods applied are given in Table 6-1. The particle starts moving from static state and a time step  $\Delta t = 10^{-5}\text{s}$  is used for the transient simulations. The values of constants and parameters used in the simulations are listed in Table 6-2.



**Figure 6-1. Schematic diagram of the computational domain. Thicker red lines indicate the metal plates.**

Variables	Discretization method
Velocity	Second order
Pressure	First order
Electric potential	Second order
Displacement of the particle	Second order

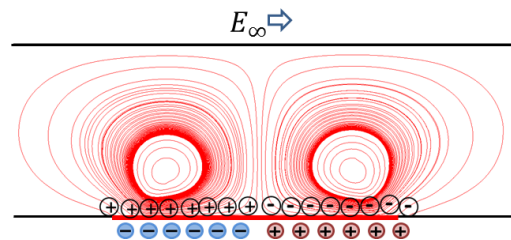
**Table 6-1. Discretization methods for the simulations conducted using COMSOL 3.5a**

Definition	Constant/Parameters	Values/Range
Permittivity of the vacuum	$\epsilon_0$ (F/ m)	$8.85 \times 10^{-12}$
Relative permittivity of the liquid medium	$\epsilon_m$	80
Defined non-dimensional polarizability of the sphere	$C$	0~1
Viscosity of the liquid	$\mu$ (kg/m s)	$0.9 \times 10^{-3}$
Density of liquid	$\rho$ (kg/m <sup>3</sup> )	998
Zeta potential of the wall	$\zeta_w$ (mV)	-30
Diameter of the particle	$d$ ( $\mu\text{m}$ )	5~15
External electric field	$E_\infty$ (V/cm)	23~32

**Table 6-2. Values of constants and parameters used in the simulations**

## 6.2 Results and discussion

Before we show the simulation result of the flow field in the channel, we first introduce the ICEOF on a flat metal plates subjected to a uniform electric field. In chapter 1, we have demonstrated the ICEOF on metal surfaces. For example the expression  $\zeta_i = -\phi + \frac{\oint_S \phi dS}{A}$  gives the induced surface potential on the metal surface of arbitrary geometry, and correspondently the induced slipping velocity on the metal surface is given by  $\vec{V} = -\frac{\epsilon_0 \epsilon_m \zeta_i}{\mu} \vec{E}$ . In the current case, the embedded conducting plates are polarized in the external uniform electric field, and the ICEOF profile in the vicinity of one plate is shown in Figure 6-2. The two vortexes are in opposite directions and of equal strength. Assuming a pair of metal plate embedded on the two sides of the wall, there would be four symmetric vortexes in opposite directions.

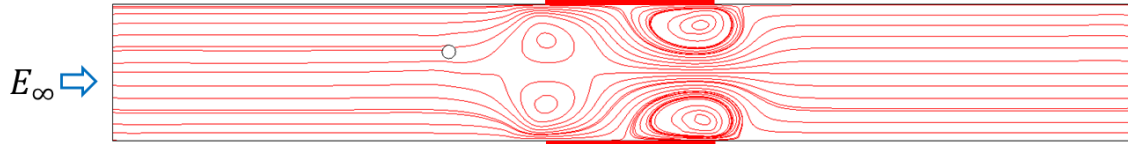


**Figure 6-2. The streamline of the ICEOF on a fully polarized metal plate embedded in an insulating wall. Thicker red line indicates the location of the polarized metal plate.**

When consider the fixed uniform zeta potential on the channel wall, the flow field in the channel would simply be the superposition of the associated linear electroosmotic flow and the local ICEOF around the conducting plates. Figure 6-3 is the preview of the flow field pattern at  $t=0$  when a uniform DC electric field is applied. The metal plates and the particle are polarized immediately under the influence of the external electric field. Clearly, there are four symmetric vortexes generated by the metal plates, and when the plug-like EOF from upstream comes to this section, the main stream splits and goes around the vortexes. The vortexes around the dielectric particle are invisible majorly because of the relatively small size. As indicated by Eq. (3-10) and Eq. (3-7), the strength of the ICEOF of the particle is proportional to the particle size. In the contract, the ICEOF of the conducting plates are locally dominant in between the two plates.

There are three components: the EOF of the bulk flow, the local ICEOF around the metal plates, and the local ICEOF around the particle. According to the mathematical expression of the EOF and ICEOF, impact factors to the flow are electric field, particle size and polarizability. We performed a series of simulations to study the flow and the trace of the particle in the flow while one of the dominant factors is changed.

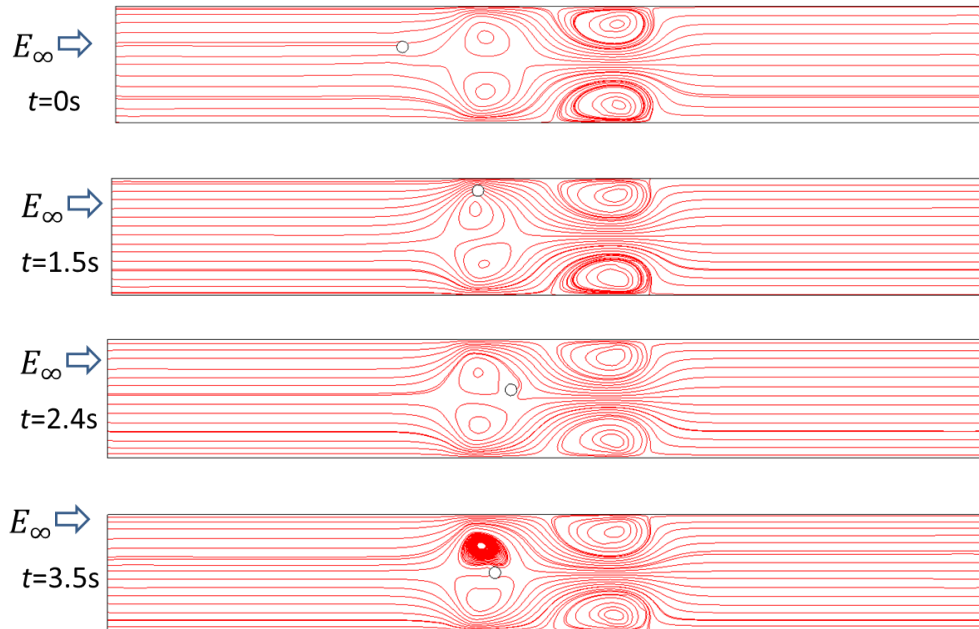
Several particle sizes  $d=5\mu\text{m}$ ,  $10\mu\text{m}$ ,  $15\mu\text{m}$  are tested. The dielectric property of the particles are expressed by the non-dimensional polarizability  $C = \frac{\epsilon_p}{\epsilon_p + 2\epsilon_m}$ , and the range of the value is  $C = 0 \sim 1$ . The EDL of both the static zeta potential and induced surface potential are assumed thin enough comparing with the particle and channel scale. The particles are assumed to have the same density as the surrounding liquid for simplicity.



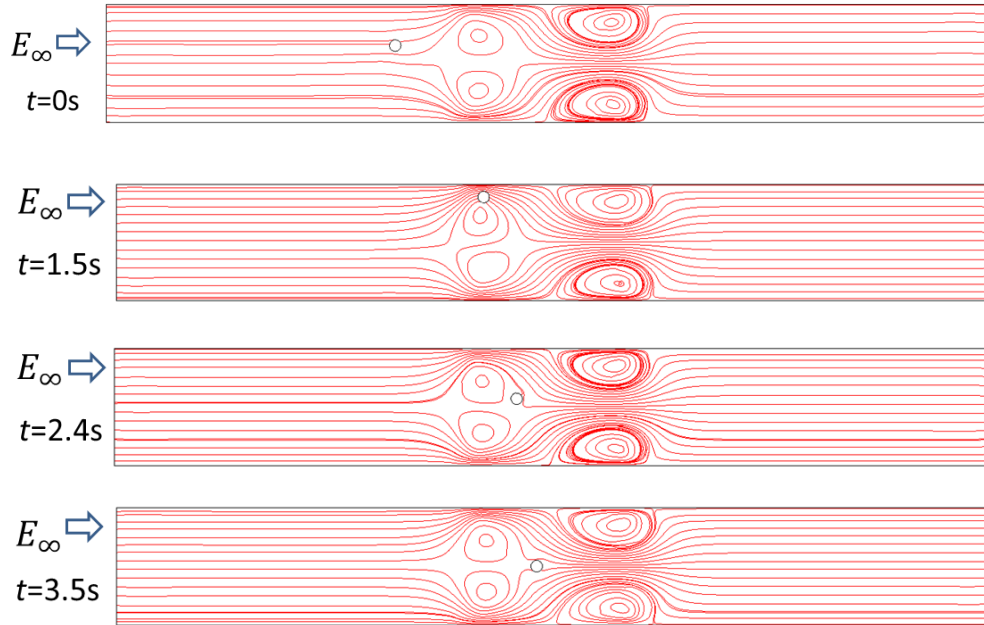
**Figure 6-3.** An example of the simulated streamlines in the computational domain and the separation section at  $E_{\infty} = 27\text{V/cm}$ ,  $d = 10 \mu\text{m}$ ,  $C = 0.7$ , and  $t = 0$ .

### 6.2.1 Effect of the particle's polarizability on the particle path

Figure 6-4 shows the path of a particle with a polarizability  $C = 0.7$  under electric field strength of  $E_{\infty} = 27\text{V/cm}$ . This particle is trapped in the vortices and cannot pass this section. Under the same condition, Figure 6-5 shows a particle with a relative polarizability  $C = 0.6$  passes in the vortices and moves towards downstream.



**Figure 6-4.** The trapping trace of a particle in the separation section with a relative polarizability  $C=0.7$ .  $E_{\infty}=27\text{V/cm}$ ,  $d=10 \mu\text{m}$ .



**Figure 6-5. The passing-through trace of a particle with a relative polarizability  $C=0.6$ ,  $E_{\infty}=27\text{V/cm}$ ,  $d=10\ \mu\text{m}$ .**

The phenomenon that particles of the same size but different polarizabilities under the same electric field take different paths can be explained by analyzing the flow field at the separation section. When the particle comes close to this section where the vortices generated by the metal plates are dominant, the particle follows the streamlines and tries to go around the front vortex. When the applied electric field is high and the vortices produced by the metal plates are strong enough, the space for the passing-through-flow streamlines in this section is very narrow. Thus the particle will be forced to move close to the wall when passing by the front vortex. As mentioned above, there are three flow components happening in this computational domain: the electroosmotic flow through the channel, the ICEOF created by the metal plates, and the ICEOF on the particle itself. Because the electric field in these two cases (in Figure 6-4 and Figure 6-5) is the same, the associated electroosmotic flow in the channel and the ICEOF generated by the



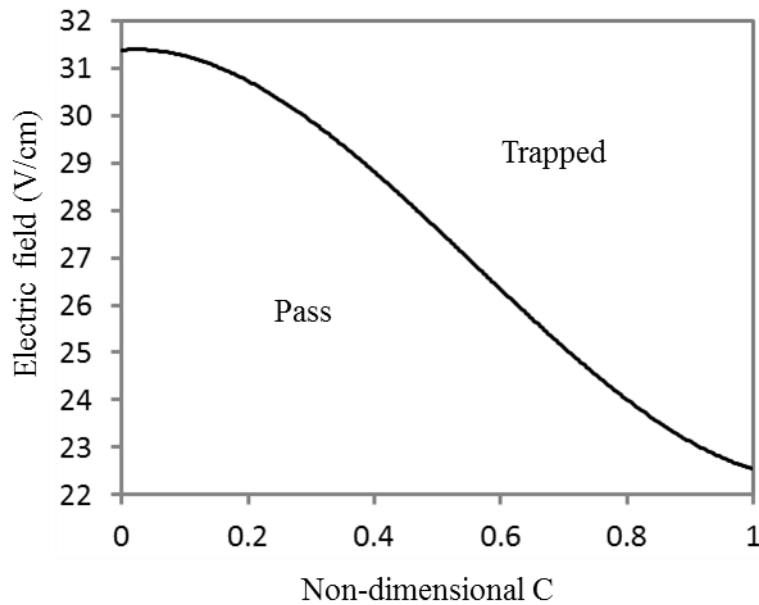
metal plates are the same. The only factor differs is the ICEOF on the particle itself. It should be realized that, when a polarized particle is close enough to an insulating channel wall, the ICEOF vortexes around the particle will interact with the wall and tend to push the particle away from the wall. This repelling effect depends only on the strength of the ICEOF of the particle, and hence depends only on the polarizability of the particle in the cases shown in Figure 6-4 and Figure 6-5. For the case presented in Figure 6-4,  $C = 0.7$ , when the particle is passing the narrow space between the large vortex and the channel wall, the stronger ICEOF vortexes around the particle push the particle away from the wall and break into the large vortex produced by the metal plate. This is a particle-trapping trace ended at the separation section. For the case shown in Figure 6-5,  $C = 0.6$ , the ICEOF vortexes around the particle is relatively weaker comparing with the particle in Figure 6-4, and its interaction with the channel wall is not strong enough to push the particle into the large vortex, consequently, the particle passes by the large vortex.

The simulation results illustrate that, particles released at the upstream of this channel can have two traces: be trapped into the vortexes at the separation section, and pass through the separation section and move to downstream with the main flow. While all other parameters are fixed, particles of different polarizability may take different paths.

### ***6.2.2 Effect of electric field strength on the paths of the particles***

A series of numerical studies were conducted to examine the effects of the electric field strength on the path of the particle for a fixed particle size,  $d = 10\mu\text{m}$ , and the results are summarized in Figure 6-6. Under a given electric field, there is a critical dielectric polarizability. Above this critical polarizability, particles of  $10\mu\text{m}$  in diameter will all be trapped in the vortex in the separation section. Below this critical polarizability, all particles of  $10\mu\text{m}$  in diameter will pass

the vortex and go to the downstream. The critical polarizability varies with the strength of the externally applied electric field. According to the chart, particles of non-dimensional polarizability  $C=0\sim 1$  can be separated by their polarizabilities. For example, under an electric field strength  $E_{\infty} = 27\text{V/cm}$ , the critical polarizability is between 0.6 and 0.7, as indicated in Figure 6-6. That is, particles that have a smaller polarizability than  $C = 0.6$  can be separated from particles with a polarizability larger than  $C = 0.7$ . At higher electric field strength, particles can be separated by a smaller polarizability. For example, when the electric field strength is  $E_{\infty} = 27.5\text{V/cm}$ , the critical polarizability is between 0.6 and 0.5.



**Figure 6-6. A summary of paths of particles of various polarizabilities under different electric field strengths.**

Figure 6-6 also implies the high sensitivity and selectivity of this novel separation method. For example, when the applied electric field strength is  $E_{\infty} = 27\text{V/cm}$ , all particles of polarizability  $C \leq 0.6$  will pass through the separation section; however, slightly increase the electric field to

$E_{\infty} = 27.5\text{V/cm}$ , particles with polarizability  $C = 0.6$  will be trapped, and only particles with polarizability  $C \leq 0.5$  pass through the separation section. In addition, to separate particles of polarizability ranging from  $C = 0 \sim 1$ , the required electric field ranges from  $E_{\infty}=24\text{V/cm}$  to  $E_{\infty}=32\text{V/cm}$ . This is relatively small electric field strength in the microfluidic study. This feature is able to find applications in biology study where the target bio-cells and molecules are usually vulnerable to strong electric field.

Furthermore, Figure 6-6 also indicates that, it is easier to trap particles at higher electric field strength. From a theoretical point of view, the ICEOF is proportional to  $E_{\infty}^2$ . As a result, when the electric field strength  $E_{\infty}$  increases, both the ICEOF on the particle and the ICEOF generated on the metal plates increase exponentially. On one hand, bigger ICEOF vortices produced by the metal plates induce narrower passages between the channel wall and the vortices. On the other hand, stronger ICEOF vortices around the particle push the particle more hardly towards the circular streamlines of the big vortices generated by the metal plates when passing through the passage between the channel wall and the big vortices. Both these factors make it more possible for the particle to be deflected from its original streamline and trapped into the circular streamlines of the big vortices.

One needs to be noted that, particles can be extremely close to the wall when passing the separation section. Among all the cases simulated in this study, the closest distance the particle could reach to the wall is around  $3.7 \mu\text{m}$  in the case of  $C=0$ , and  $E_{\infty} = 32\text{V/cm}$ . While consider the possibility of the double layer effect, since the thickness of the double layer assumed in this study is tens of nano-meter which is a normal case, the particle is still not close enough to consider the double layer effect.

### 6.2.3 Effect of particle size on the paths of the particles

As indicated by Eq. (3-10) and Eq. (3-7), the strength of the ICEOF increases linearly with the size of the particle. Therefore, the size of the dielectric particles will affect the trap-pass behavior. The paths of particles of different sizes (5, 10 and 15  $\mu\text{m}$ ) were studied under the same external electric field. Table 6-3 shows the results. Clearly the particle dimension affects the path of the particle.

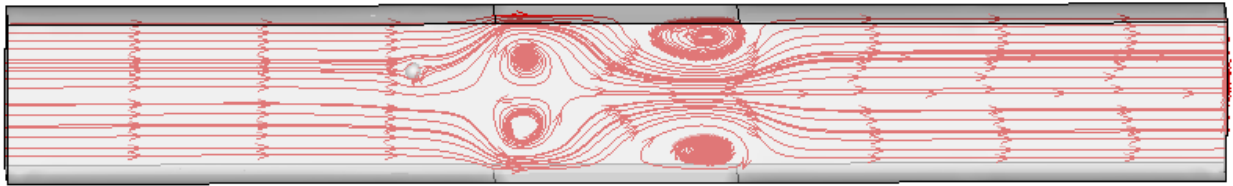
	C=0.7	C=0.6
d=5 $\mu\text{m}$	Pass	Pass
d=10 $\mu\text{m}$	Trapped	Pass
d=15 $\mu\text{m}$	Trapped	Trapped

**Table 6-3. Paths of particles of different sizes at  $E_{\infty}=27\text{V/cm}$ .**

The critical polarizability for d=10  $\mu\text{m}$  particle under electric field  $E_{\infty}=27\text{V/cm}$  is between C =0.6 and C =0.7. Under the same electric field strength, when the particle size is 5  $\mu\text{m}$ , particles with C=0.6 and C =0.7 both pass the separation section. In contrast, for a bigger particle size of 15  $\mu\text{m}$ , particles of polarizability C =0.6 and C =0.7 are all trapped. As explained previously, bigger particles have stronger ICEOF vortices, and experience stronger pushing force when passing the passage between the channel wall and the big vortices, and consequently are trapped by the big vortexes. These results demonstrate that, under an appropriate electric field, this method is capable of separating particles of the same material by size; and bigger particles are more likely to be trapped in the vortexes than smaller ones.

### 6.3 2D simulation validation

Two 3D numerical models are built to validate 2D simulation results. As shown in Figure 6-7, after mesh-independency study, 12,862 unstructured meshes are generated by GAMBIT 4.20. The 3D transient numerical simulations are performed by FLUENT 12.0. First order upwind spatial discretization and first order implicit transient simulation are utilized. The numerical error tolerance is  $10^{-6}$ . The dimensions are the same as in the 2D simulations, and the third dimension of the channel is  $50 \times d$ . Two sets of parameters are studied:  $C=0.6$ ,  $E_{\infty}=27\text{V/cm}$ ,  $d=10\ \mu\text{m}$ ; and  $C=0.7$ ,  $E_{\infty}=27\text{V/cm}$ ,  $d=10\ \mu\text{m}$ . According to the 2D studies, particles of polarizability  $C=0.6$  and  $C=0.7$  would be separated at electric field strength  $E_{\infty}=27\text{V/cm}$ . In contrast, the 3D transient study of the traces of the  $C=0.6$  particle and  $C=0.7$  particle demonstrate that, particle  $C=0.6$  is trapped into the front vortex, and  $C=0.7$  passes the vortices and goes downstream.



**Figure 6-7. Streamlines of the flow on a surface in the center of the 3D computational domain. At  $t=0$ ,  $C=0.6$ ,  $E_{\infty}=27\text{V/cm}$ ,  $d=10\ \mu\text{m}$ .**

### 6.4 Summary and conclusions

This chapter demonstrated theoretically a novel, simple and sensitive microfluidic method for particle separation. Particles suspended in an electrolyte solution in a straight microchannel can be separated based on size and polarizability by utilizing the ICEOF. This separation method requires only a straight microchannel with a pair of embedded metal plates on the sidewalls to

form a separation section. The carrying liquid filling the channel is electrolyte. Once apply DC electric field, there are induced vortexes on the plates and on the particle. Owing to the large size and high polarizability, the large vortexes on the plates would push the passing-through streamlines against the wall. While particles passing by the wall, the interaction between the particle and the wall would deflect the particle from the original streamline and switch to one of the two paths. And the critical condition is determined by the polarizability and size of the particle and the electric field strength. The non-dimensional polarizability  $C = \frac{\epsilon_p}{\epsilon_p + 2\epsilon_m}$  ranges from 0 to 1 was examined and particle size of  $d=5\mu\text{m}$ ,  $10\mu\text{m}$  and  $15\mu\text{m}$  were tested. The results proved that, in one operation, particles can be separated into two groups by polarizability or size. Moreover, relatively small electric field strength is used in this method. The separation result is very sensitive to the electric field strength, to separate particles of polarizability  $C = 0\sim 1$ , only a small range of electric field is required ( $E_{\infty}=24\text{V/cm}\sim 32\text{V/cm}$ ).

In practical, dielectric particles in this separation method can be used as carriers of biological cells. Particularly, when the objective cells have no distinctive difference in size, density or static charges, etc., it is hard to realize the separation through directly operating on the particles. However, biological cells can selectively bond with artificial particles via chemical reactions. Biological particles of different chemical properties can be separated by this method. Additionally, the low electric field required for this separation methodology is relatively safe for living cells. This separation method can be optimized by integrating a series of separation sections into one device. In this way, multiple components that have been sorted at the first separation section can be further sorted for a second time in a next separation section. Comparing with existing particle separation methods, in which, electrophoresis and dielectrophoresis are

mostly used, the method in this study is advanced in terms of simple and compact structure, and automatic operation.

## Chapter 7

### Separation of heterogeneous dielectric particle-Janus particle

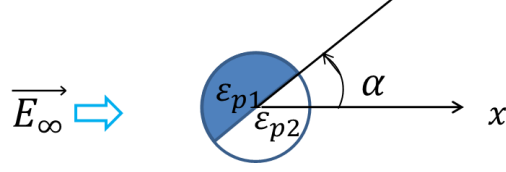
In chapter 3, we derived the induced surface potential of homogeneous dielectric particles in uniform electric field, and found out the dependence of the induced-charge electroosmotic flow (ICEOF) on polarizability. In chapter 5, we studied the spatially varying induced-surface potential and the ICEOF on heterogeneous dielectric particles. The asymmetric ICEOF generates unbalanced hydrodynamic effect on the particle and drives the particle to rotate and migrate. In this chapter, we employ the electrokinetic motion of the heterogeneous particles and propose a heterogeneous particle separation method. We study the ICEOF on heterogeneous dielectric particles-Janus particles with half hemisphere of dielectric  $\epsilon_{p1}$  and the other  $\epsilon_{p2}$ , ( $\epsilon_{p1} > \epsilon_{p2}$ ). Due to the dependence of the ICEOF on the polarizability, the ICEOF around the Janus particle is asymmetric. The ICEOF pattern is also significantly influenced by the orientation of the particle relative to the electric field. We examine the characterized rotation and self-alignment behavior of the Janus particles in the uniform electric field. We employ these characterized phenomena to separate dielectric Janus particles in uniform electric field, and this separation method is proved a promising, advanced, reliable technique.

#### 7.1 The immigration of dielectric Janus particle in a straight channel

##### 7.1.1 The ICEOF on dielectric Janus particle

As demonstrated in chapter 3, the induced surface potential and the ICEOF on a dielectric particle surface is polarizability-dependent. Since the dielectric particle is inhomogeneous, an angle  $\alpha$  is defined to describe the orientation of the Janus particle relative to the electric field. Shown as in Figure 7-1.





**Figure 7-1.**  $\alpha$  is defined as the angle between the equatorial plane of the Janus particle and the applied electric field.

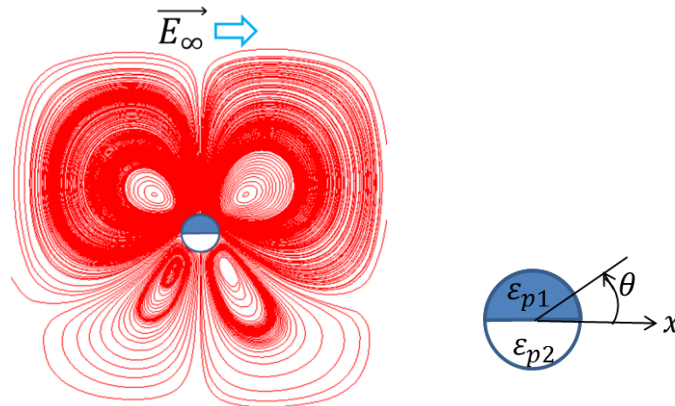
The induced surface potential on a dielectric Janus particles of radius  $a$  with permittivity  $\varepsilon_{p1}$  in one hemisphere and  $\varepsilon_{p2}$  in the other hemisphere should be asymmetric. In a uniform electric field, the induced surface potential on the surface of one hemisphere ( $\varepsilon_{p1}$ ) is given by

$$\zeta_i = \frac{3}{2} C_1 E_{\infty} a \cos\theta, \quad (C_1 = \frac{\varepsilon_{p1}}{\varepsilon_{p1} + 2\varepsilon_m}), \quad (7-1)$$

and the induced surface potential on the surface of the 2<sup>nd</sup> hemisphere ( $\varepsilon_{p2}$ ) is given by

$$\zeta_i = \frac{3}{2} C_2 E_{\infty} a \cos\theta, \quad (C_2 = \frac{\varepsilon_{p2}}{\varepsilon_{p2} + 2\varepsilon_m}). \quad (7-2)$$

Accordingly, the strengths of the ICEOF on the two sides of the particle are different. Assume  $\varepsilon_{p1} > \varepsilon_{p2}$ , Figure 7-2 shows the four vortices of the induced electroosmotic flows around such a Janus particle.



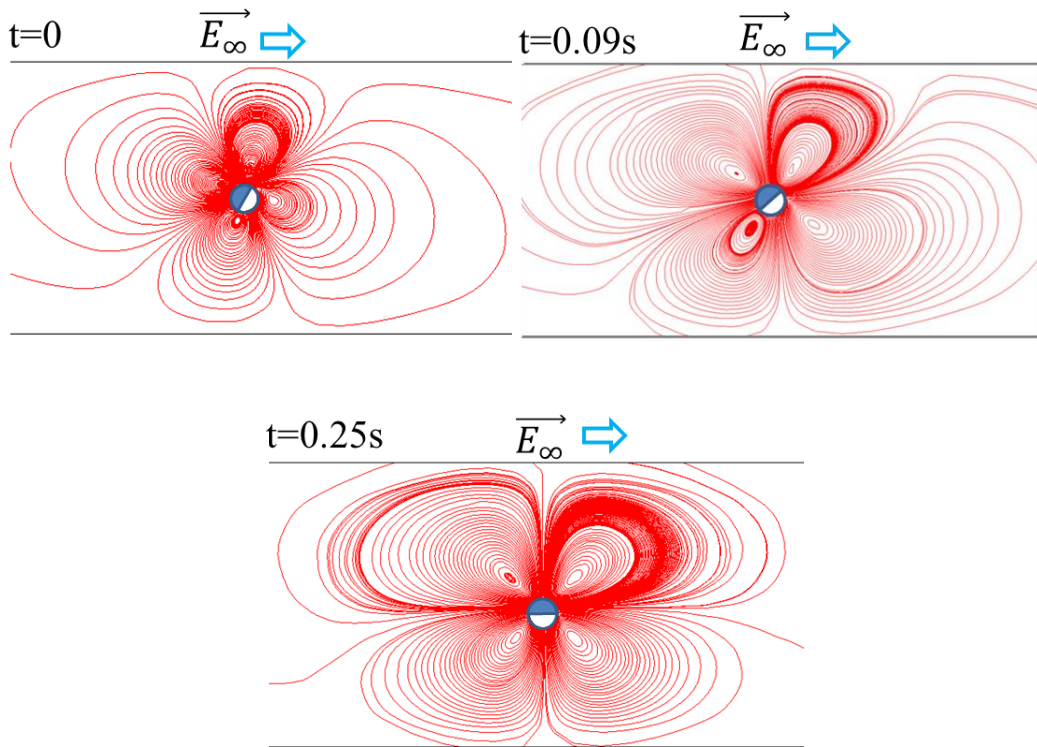
**Figure 7-2.** The streamlines of the ICEOF around a dielectric Janus particle,  $\varepsilon_{p1} > \varepsilon_{p2}$ ,  $\alpha = 0$ .

When the surrounding medium is isotonic, the dielectric property of the Janus particle can be characterized by the ratio of the relative polarizability  $\frac{C_1}{C_2}$ . Dielectric materials have a wide range of permittivity. For example, titanate dioxides have high relative permittivity ranging from  $\epsilon_r = 110$  to  $\epsilon_r = 17,000$  depending on chemical components and the percentage of each component. The  $\text{TiO}_2$  has a permittivity of 110 [103]. The permittivity of the  $\text{PbTiO}_3$  ranges from 200 to 400 [104]. Strontium titanate  $\text{SrTiO}_3$  [104] has a relative permittivity  $\epsilon_r = 300$ , and barium strontium titanate (BST) has a relative permittivity in the range of 200-450 [105].  $\text{Sr}_{0.99925}\text{Cr}_{0.0005}\text{TiO}_3$  [106] has a permittivity as high as  $\epsilon_r = 17,000$ . When the permittivity of the surrounding mediums (e.g., as water) is the same, the relative polarizability ratio of a Janus particle made of  $\text{Sr}_{0.99925}\text{Cr}_{0.0005}\text{TiO}_3$  and  $\text{PbTiO}_3$  is  $\frac{C_1}{C_2} = 2$ , and a Janus particle made of  $\text{SrTiO}_3$  and  $\text{TiO}_2$  has a permittivity ratio  $\frac{C_1}{C_2} = 1.5$ .

### ***7.1.2 The motion of dielectric Janus particle***

Assume the surrounding aqueous solution has a permittivity of  $\epsilon_m = 80$ , and the Janus particles are made of two materials with  $\epsilon_{p1}$  and  $\epsilon_{p2}$ , respectively, and  $\epsilon_{p1} > \epsilon_{p2}$ . After electric field is applied, there are two flow components in the channel, the EOF of the bulk liquid, and the ICEOF around each particle. As indicated by Eq. (3-7) and Eq. (3-10), the strength of the ICEOF around a particle depends on the size of the particle, the permittivity of the particle, and the electric field strength. Since the EOF of the bulk liquid contributes only to the translational motion of the particles in the channel, in this subsection, in order to understand the unique behavior of Janus particles in the electric field, the EOF of bulk liquid is not considered and only the ICEOF around each dielectric Janus particle is examined.

Generally, when a Janus particle is located in the liquid, the particle may be in a random position relative to the electrical field direction. That is, the particle's equatorial plane (dividing the two hemispheres of different dielectric materials) may have angle  $\alpha$  with the applied electrical field (in the x-axis direction), as shown in Figure 7-1. For convenience, let us consider when  $\alpha = 0^\circ$ , the particle's equatorial plane is parallel to the electric field lines with the hemisphere  $\epsilon_{p1}$  on the top, and the induced surface potential and the ICEOF slip velocity on the front side of the surface and the back side of the surface of each hemisphere are symmetric, respectively. When  $\alpha \neq 0$ , the distributions of the induced surface potential and the ICEOF slip velocity on the front side of the surface and the back side of the surface of each hemisphere are asymmetric, respectively.



**Figure 7-3. The reorientation process of a dielectric Janus particle in uniform DC electric field due to ICEOF, initially  $\alpha = 60^\circ$ ,  $E_\infty = 50V/cm$ , polarizability ratio  $\frac{c_1}{c_2} = 3$ , particle diameter  $d = 10\mu m$ .**

Figure 7-3 shows the reorientation process of a dielectric Janus particle with a polarizability ratio  $\frac{c_1}{c_2} = 3$  under the influence of an electric field  $E_\infty = 50V/cm$ . At  $t = 0$ , the angle between particle's equatorial plane and the electric field direction is  $\alpha = 60^\circ$ , and the vortices around the particle are asymmetric. The asymmetric vortices result in a torque on the particle that makes the particle rotates clockwise. Under the uniform electric field, the particle rotates until aligns with the external electric field in 0.25 seconds. The steady state of the particle is achieved when  $\alpha = 0^\circ$ .

The rotation of dielectric Janus particle with  $\frac{c_1}{c_2} = 3$  under electric field strength  $E_\infty = 50V/cm$  with a random initial angle is studied. Table 7-1 lists the final angles that the Janus particle would reach with the reorientation process. In summary, except two initial angles, the dielectric Janus particles will rotate to reach one of the two steady angles:  $\alpha = 0^\circ$  or  $\alpha = 180^\circ$  with the equatorial plane parallel to the external electric field direction.

Initial angles	$0^\circ \leq \alpha < 90^\circ$	$90^\circ$	$90^\circ < \alpha < 270^\circ$	$270^\circ$	$270^\circ < \alpha \leq 360^\circ$
Steady angle	$0^\circ$	$90^\circ$	$180^\circ$	$270^\circ$	$0^\circ$

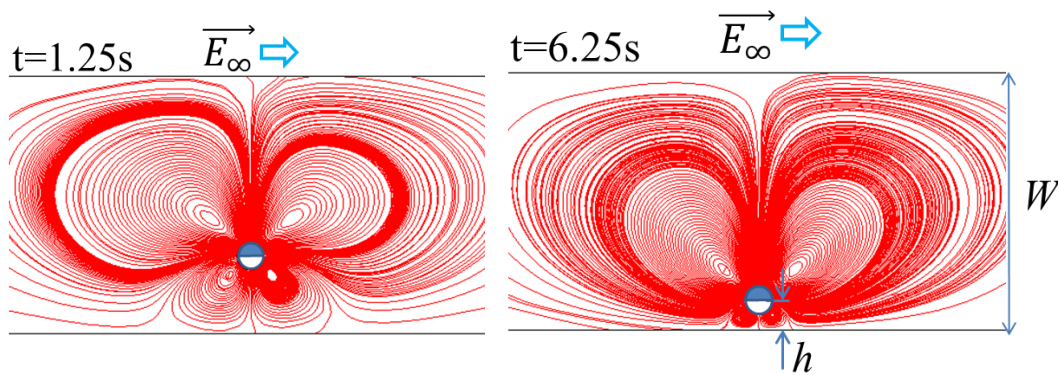
**Table 7-1. The steady angles of Janus particles in uniform electric field**

Besides the transient rotation process, the particles undergo simultaneous translational migration caused by the individual ICEOF. Due to the asymmetric vortices around the Janus particle, the particle will move away from the centerline of the channel towards one side channel wall. The vertical migration of the Janus particle takes longer time to reach the final position than the rotation. After the particle stops rotating, the particle is aligned parallel to the electric field. There are two vortices on each hemisphere, and these vortices interact with the channel walls

respectively. Because the two vortices on the  $\varepsilon_{p1}$  side are stronger than the vortices on the  $\varepsilon_{p2}$  hemisphere side, the particle will be pushed away from the wall on the  $\varepsilon_{p1}$  side. While the particle migrating vertically to the wall on the  $\varepsilon_{p2}$  side, the interaction between the vortices and the wall on the  $\varepsilon_{p1}$  side becomes weaker and the interaction between the vortices and the wall on the  $\varepsilon_{p2}$  side becomes stronger. This migration of the particle is perpendicular to the electric field and stops when the vortices-wall interactions on the two sides are balanced. The final distance between the particle and the wall is defined as a non-dimensional parameter  $\bar{H}$ ,

$$\bar{H} = \frac{2h}{W} \quad 0 < \bar{H} \leq 1 \quad (7-3)$$

Where  $h$  is the distance from the center of the particle to the wall closer to the particle as shown in Figure 7-4.

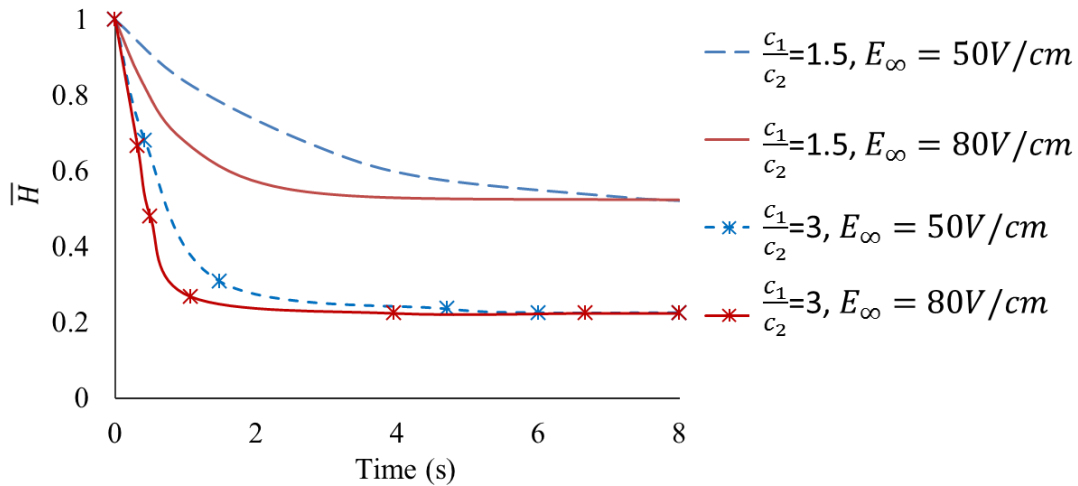


**Figure 7-4. Final separation distance between a dielectric Janus particle and the channel wall.  $E_\infty = 50V/cm$ , polarizability ratio  $\frac{c_1}{c_2} = 3$ , particle diameter  $d = 10\mu m$ .**

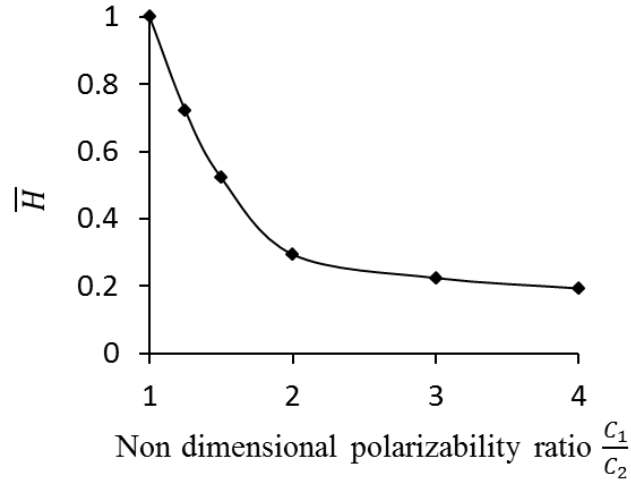
Since the strengths of the induced-vortices are dependent on the size and the dielectric property of the particle and the electric field strength, the influences of these three parameters on the separation distance  $\bar{H}$  were studied. The numerical simulations were performed by releasing a

single dielectric Janus particle at the center of the channel with the initial angle  $\alpha = 0^\circ$  in the absence of bulk liquid electroosmotic flow, and monitoring the migration of the particle until it stops moving.

Figure 7-5 illustrates the vertical migration of two Janus particles of different polarizability ratios,  $\frac{c_1}{c_2} = 1.5$  and  $\frac{c_1}{c_2} = 3$ , with time. Figure 7-5 shows that, for the same particle (i.e., the same polarizability ratio), while the final separation distance is the same under different electrical fields, the particle will reach the final separation distance in a shorter time under a higher electrical field. Under the same electrical field, the particle with a higher polarizability ratio will have smaller final separation distance, and reach the final separation distance faster.



**Figure 7-5. The separation distance of Janus particles from the wall with time, for two types of dielectric Janus particles of diameter  $d = 10 \mu\text{m}$ ,  $\frac{c_1}{c_2} = 1.5$ , and  $\frac{c_1}{c_2} = 3$ , under different electric field strengths  $E_\infty = 50V/cm$ , and  $E_\infty = 80V/cm$ .**



**Figure 7-6. The variation of the final separation distance  $\bar{H}$  with particle polarizability ratio  $\frac{C_1}{C_2}$ , where  $E_\infty = 50V/cm$ ,  $\varepsilon_m=80$ ,  $d = 10\mu m$ .**

Figure 7-6 shows the influence of the polarizability ratio on the separation distance. It is easy to understand that, if a particle is homogeneous, the vortices around the particle are symmetric and the forces on the particle are balanced, thus, the particle stays at the center of the channel.

However, for a Janus particle, the relative polarizability of the two hemispheres,  $C_1 = \frac{\varepsilon_{p1} - \varepsilon_m}{\varepsilon_{p1} + 2\varepsilon_m}$

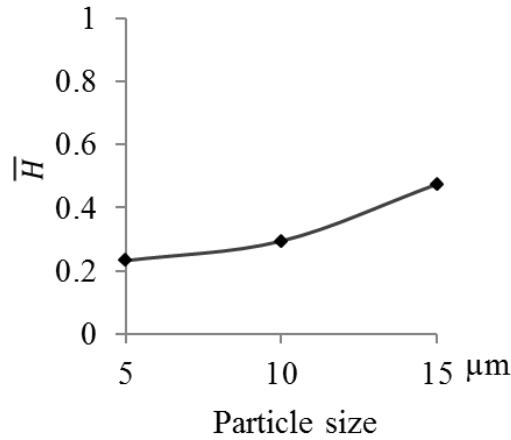
and  $C_2 = \frac{\varepsilon_{p2} - \varepsilon_m}{\varepsilon_{p2} + 2\varepsilon_m}$ , are not equal, consequently, the vortices on one hemisphere are stronger than

the vortices on the other hemisphere. Therefore, the Janus particles will tend to move to one side channel wall. The larger the polarizability ratio  $\frac{C_1}{C_2}$  is, the closer the particle will reach the wall.

As shown in Figure 7-7, the separation distance can be predicted. For example, when the channel width  $W$  is  $100\mu m$ , according to Eq. (7-3), the separation distance for a  $10\mu m$  Janus particle of

$\frac{C_1}{C_2} = 1.5$  is  $26\mu m$ , and the separation distance for a  $10\mu m$  Janus particle of  $\frac{C_1}{C_2} = 2$  is  $15\mu m$ ;

that is, these two particles of the same size but different polarizability ratios are  $11\mu\text{m}$  apart vertically from the channel wall.



**Figure 7-7. Example of the variation of final separation distance  $\bar{H}$  with particle size, for  $\frac{c_1}{c_2} = 2$ ,  $E_\infty = 50V/cm$ ,  $\epsilon_m=80$ .**

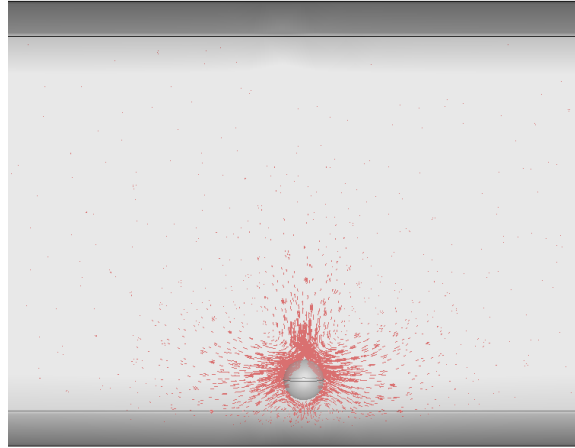
Figure 7-7 shows an example of the change of the final separation distance  $\bar{H}$  with particle size for a given polarizability ratio and a given electrical field. Comparing the case of a particle size  $d = 15\mu\text{m}$  with the case of a particle size  $d = 5\mu\text{m}$ , the difference in the final separation distance  $\bar{H}$  is significant. Based on the definition of the separation distance, Eq. (7-3), when the microchannel width  $W$  is  $100\mu\text{m}$ , the two Janus particles of the same polarizability ratio but different sizes,  $d = 5\mu\text{m}$  and  $d = 15\mu\text{m}$ , are  $22\mu\text{m}$  apart vertically from the channel wall.

## 7.2 2D numerical simulation validation

A transient 3D numerical model is built to validate the 2D simulation results. As shown in figure 7-8, after mesh-independency study, 9,236 unstructured meshes are generated by GAMBIT 4.20. The 3D transient simulation of the self-alignment of a Janus particle in a straight channel is performed with FLUENT 12.0. First order upwind spatial discretization and first order implicit transient simulation are utilized. The numerical error tolerance is  $10^{-6}$ . The dimensions of the



computational domain are: length:  $50 \times d$ , width:  $10 \times d$ , height:  $10 \times d$ . The simulation results indicate that, the Janus particle reaches a steady separation distance  $\bar{H} = 0.234$  within 7.2s as shown in figure 7-8. Comparing with the equilibrium distance in Figure 7-4 wherein  $\bar{H} = 0.225$ , the difference between the results from the 2D and 3D simulations is 4%.

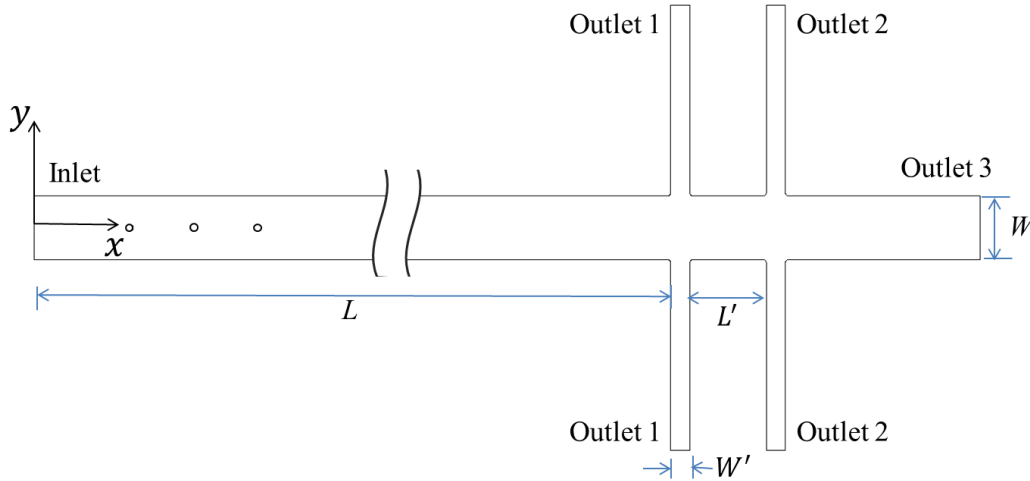


**Figure 7-8. Final separation distance between a dielectric Janus particle and the channel wall in 3D model.  $E_{\infty} = 50V/cm$ , polarizability ratio  $\frac{c_1}{c_2} = 3$ , particle diameter  $d = 10\mu m$ .**

### 7.3 Geometry and dimensions

Figure 7-9 shows the diagram of the microchannel system with suspended dielectric Janus particles. Janus particles are released at the centerline of a straight channel, and there are two pairs of branch channels at downstream. Electric field is applied through the channel by setting voltages at the inlet and outlets. The average size of the object particles in this chapter is  $d$ . The width of the channel is  $W = 10 \times d$ , and the length of the main channel section is  $L = 160 \times d$  which is assumed long enough for the particles to reach the final steady distance to the wall. The width of the branch channels are  $W' = 3 \times d$  and the spacing between two branch channels on each side is  $L' = 15 \times d$ . To perform a further study of the rotation and alignment behavior described

before, a series of numerical simulations of the rotation and transportation of dielectric Janus particles in uniform DC electric field were conducted in this chapter. The transient 2D simulation is performed by COMSOL 3.5a. We test the final steady distance of a Janus particle  $\frac{c_1}{c_2} = 3$  under electric field  $E_\infty = 50mV/s$  with different numbers of mesh elements: 3,821, 54,985, 6,102, 6,786, 8,563. Finally, 6,102 Lagrange elements are chosen to obtain a mesh-independent steady distance  $\bar{H}$  (within 0.5% change). The discretization methods used in this serial of simulations are given in Table 7-2. The numerical error tolerance applied is  $10^{-5}$ . The values of the parameters used in the numerical simulations are listed in Table 7-3.



**Figure 7-9. Schematic diagram of model system of dielectric Janus particles in a microchannel.**

Variables	Discretization method
Velocity	Second order
Pressure	First order
Electric potential	Second order
Displacement field of the particle	Second order

**Table 7-2. Discretization methods used in the simulations.**

Definition	Constant/Parameters	Values/Range
Permittivity of the vacuum	$\epsilon_0$ (F/ m)	$8.85 \times 10^{-12}$
Relative permittivity of the liquid medium	$\epsilon_m$	80
Viscosity of the liquid	$\mu$ (kg/m s)	$0.9 \times 10^{-3}$
Density of liquid	$\rho$ (kg/m <sup>3</sup> )	998
Zeta potential of the wall	$\zeta_w$ (mV)	-30
Diameter of the particle	d ( $\mu$ m)	5~15

**Table 7-3. Values of constants and parameters used in the simulations.**

At  $t=0$ , the particles start from a static state. Potentials are applied at inlet and outlets to set up the required electric field in each individual channel.

#### 7.4 Results and discussion

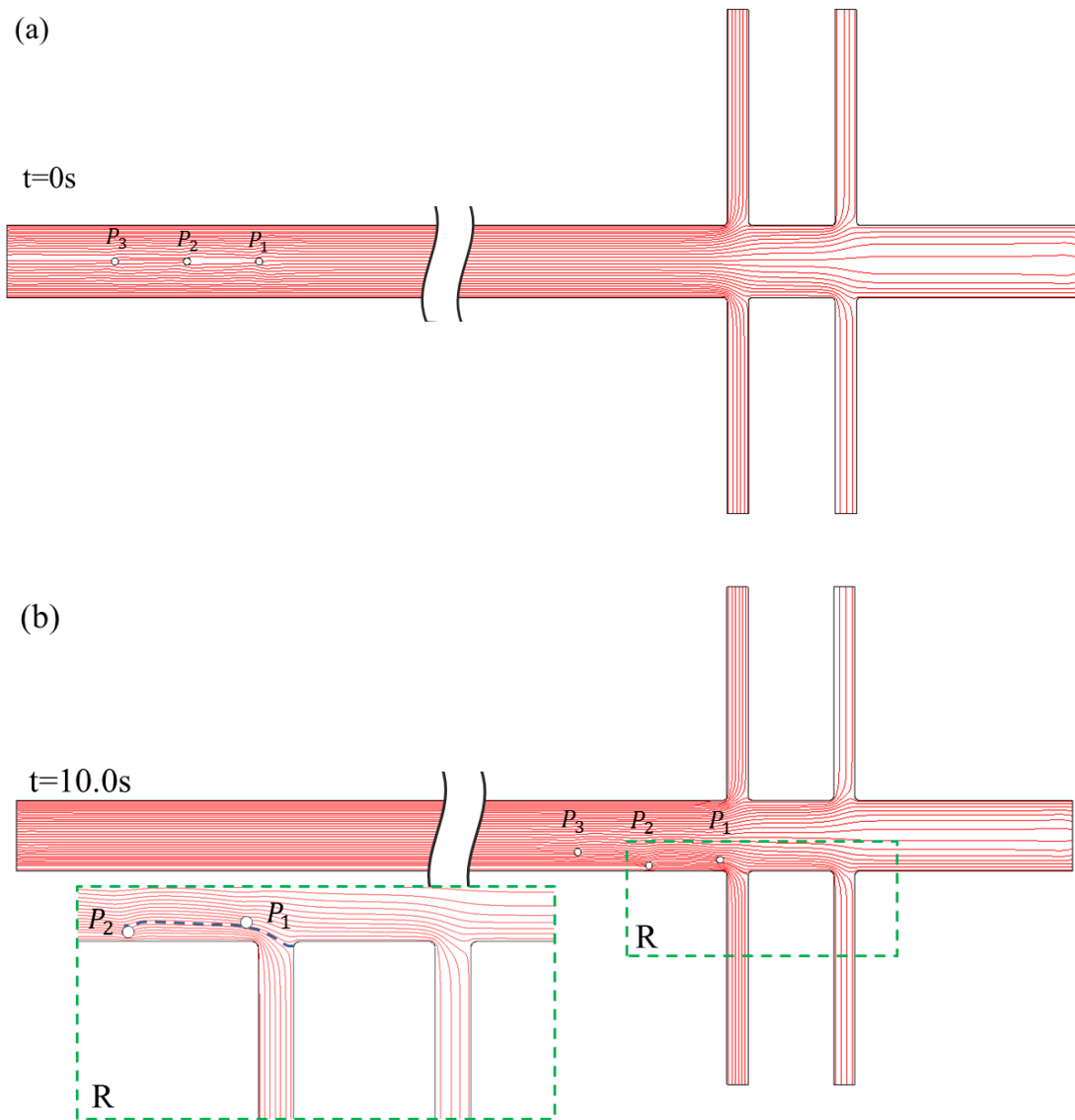
The results in the former section show that dielectric Janus particles may have different final separation distances from the channel wall, depending on their sizes and polarizability ratios. When the final separation distance is reached, the Janus particles will keep this distance and follow their respective streamlines in the bulk liquid electroosmotic flow (EOF). Therefore, it is possible to separate these particles based on their different trajectories. In order to demonstrate this possibility, this study considers that dielectric Janus particles of different sizes and polarizability ratios  $\frac{C_1}{C_2}$  are released in the electroosmotic flow (EOF) in uniform DC electric field. To minimize the interference from adjacent particles, the Janus particle solution is considered sufficiently diluted, and the space between adjacent particles in this numerical model is defined as 10 folds of the particle diameter. As demonstrated before, the Janus particle align itself from a random initial orientation angle with the electric field in a very short time, less than

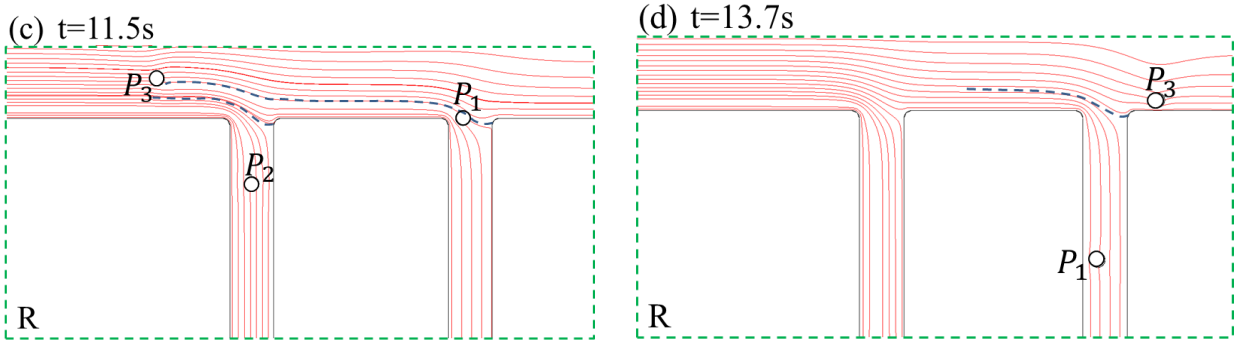
1 second, for simplicity, this reorientation process is neglected and the initial orientation angle of all the particles is assumed as  $\alpha = 0^\circ$ .

Figure 7-10 shows the separation process of three dielectric Janus particles of the same size,  $10\mu\text{m}$  and different polarizability ratios,  $P_1: \frac{c_1}{c_2} = 2$ ,  $P_2: \frac{c_1}{c_2} = 3$ ,  $P_3: \frac{c_1}{c_2} = 1.5$ , respectively. The particles are released at the center line of the channel with an initial spacing of  $10d$ . In the uniform DC electric field, given the selected zeta potential of the channel walls (Table 7-2), the EOF is much stronger than the ICEOF around the particles, and hence the vortices around the particles are hardly visible in this scale (particle diameter  $d = 10\ \mu\text{m}$ ) as shown in Figure 7-10.

At  $t=10.0\text{s}$ , all three Janus particles have reached their final separation distance from the wall. There are two pairs of branch channels downstream. The flow rate of the electroosmotic flow in each pair of branch channels can be accurately controlled by controlling the local electric field strength in the branch channels. The dashed lines ending at the branch points in Figure 7-10 (b), (c) and (d) show the virtual boundaries of the split-streams entering each branch channel. The particles and the portion of the stream beyond these boundaries will pass by the branch channel, and the particle inside the boundary will follow the streamlines and be collected in the branch channel at the immediately downstream position. For example, in Figure 7-10 (b) and (c), at branch channel 1, particles  $P_1$  and  $P_3$  are outside the boundary of the split-stream that going in to branch channel 1, while particle  $P_2$  is inside this split-stream. Therefore, particles  $P_1$  and  $P_3$  will pass by the branch channel 1 and particle  $P_2$  will enter the branch channel 1. The remaining stream in the main channel is split again at branch channel 2. Since particle  $P_3$  is further away from the wall than particle  $P_1$  and is outside the boundary of the split-stream entering the branch channel 2, only particle  $P_1$  will enter the branch channel 2. Figure 7-9d shows the boundary of

the split-stream that goes into branch channel 2. As the particle 3 is outside this boundary, it moves with the rest stream into the exit of the main channel. Over all, the principle of this method is that the particle with the highest polarizability ratio moves most close to the wall and will be collected first; then the particle of the second highest polarizability ratio will be collected at the second branch channels, and so on.





**Figure 7-10. Separation of dielectric Janus particles in EOF in DC electric field.  $E_{\infty}=50V/cm$  in the main channel,  $E_{\infty} = 25V/cm$  in branch channels 1,  $E_{\infty} = 12V/cm$  in branch channels 2. Polarizability ratios of the three particles:  $P_1: \frac{c_1}{c_2} = 2$ ,  $P_2: \frac{c_1}{c_2} = 3$ ,  $P_3: \frac{c_1}{c_2} = 1.5$ ,  $d=10\mu m$ . (a) Particles are released in the channel center with a horizontal separation distance  $10d$ , (b) the trajectories and positions of the particles in 10 seconds, (c), (d) particles are separated and collected into branch channels independently following their individual streamlines.**

The portion of stream in each branch channel can be determined by referring to the position of each type of particle,  $\bar{H}_{P_i} + \frac{d}{W}$ . Because of the nature of the bulk-like EOF in the microchannel, the portion of the flow into each branch channel can be easily controlled. The flow rate in the main channel is denoted as  $Q_0$ , and the flow rates in branch channels 1 and 2 are denoted as  $Q_1$  and  $Q_2$ , respectively. Because the electroosmotic flow velocity, Eq. (1-7), is linearly proportional to the local tangential electric field in the channel, the portion of the flow stream entering each branch channel can be determined by the following flow rate ratio:

$$\frac{Q_i}{Q_0} = \frac{W_i E_i}{W_0 E_0} \quad (7-4)$$

For example, in Figure 7-9, the electric field strength in the main channel is set as  $E_{\infty}=50V/cm$ ,  $W_0 = 10 \times d$ , and the electric field in branch channels 1 and 2 are  $E_{\infty} = 25V/cm$  and  $E_{\infty} = 12V/cm$ ,  $W_i = 3 \times d$ , respectively. Once the portions of stream and the flow rates are determined for each branch channel, particles of multiple kinds can be separated and collected continuously and automatically.

In addition, Janus particles of the same polarizability ratio but different sizes have different separation distances from the channel wall. As shown in Figure 7-7, smaller Janus particles of the same polarizability ratio are closer to the wall. Therefore, Janus particles of the same polarizability ratio can be separated by size as shown in Figure 7-11. In this case, there are two dielectric Janus particles of the same polarizability ratio,  $\frac{C_1}{C_2} = 2$ , but different sizes: one particle,  $P_4$ , has a diameter  $d = 10\mu m$ , and another particle,  $P_5$ , has a diameter  $d = 5\mu m$ . The two particles are initially  $100 \mu m$  away from each other, and the initial orientation angle of the two particles is  $\alpha = 0^\circ$ . The electric fields applied through the main channel is  $E_{\infty} = 50V/cm$ , and the local electric field in the branch channels is  $E_{\infty} = 18V/cm$ . After the particles reach their final separation distances from the wall, the dashed line in Figure 7-11 (b) and (c) shows the boundary of the split-stream that goes to the branch channel. The particle  $P_4$  is outside this boundary and thus passes by the branch point. The particle  $P_5$  is inside this split-stream and follows this split-stream moving into the branch channel. Based on the principle demonstrated here, particles of more than two scales can be separated and collected continuously in different branch channels at downstream. The particles of the smallest size are collected into the first branch channel and the second smallest particles go into the second branch channel, and so on.

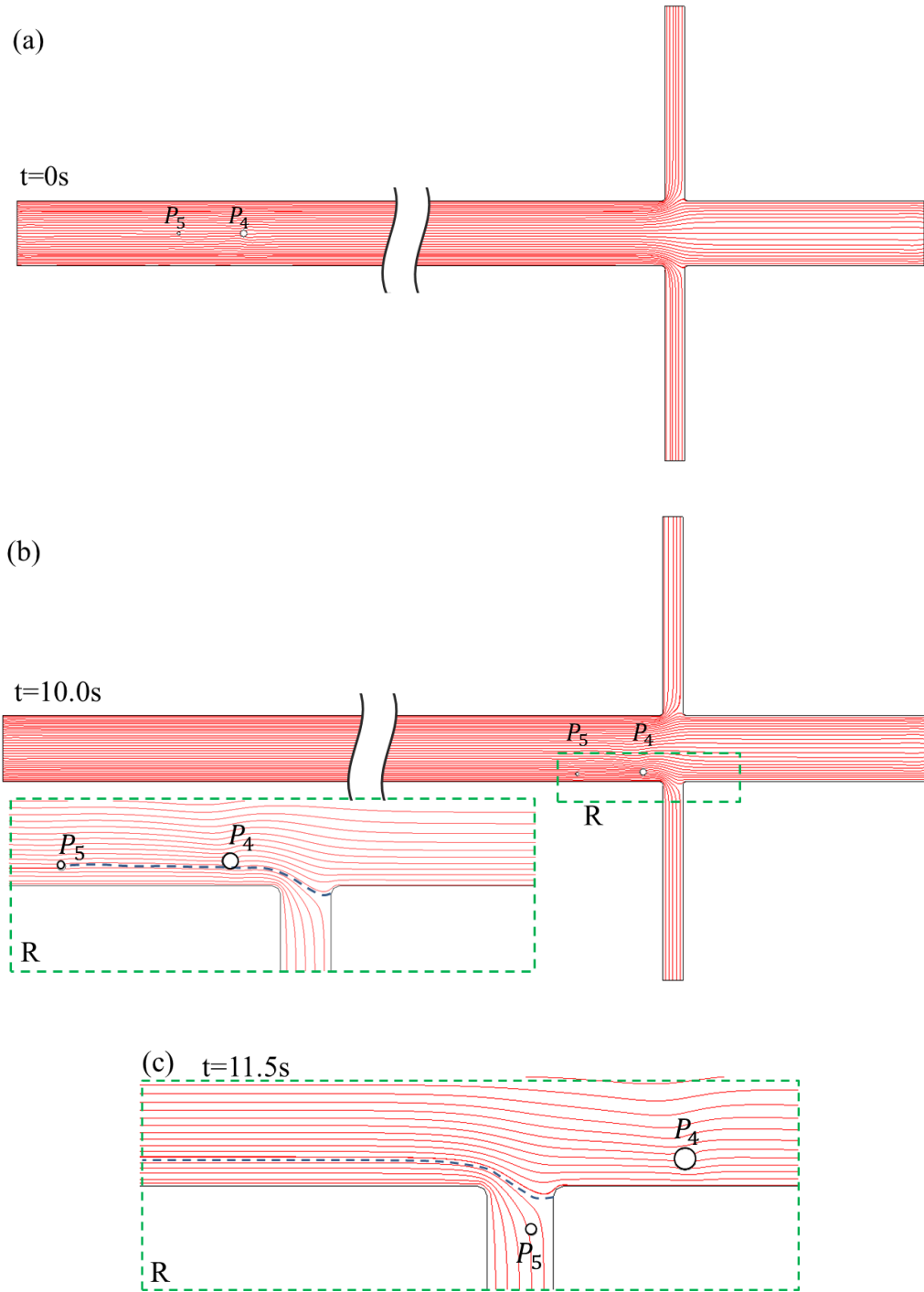


Figure 7-11. Separation of dielectric Janus particles by size.  $P_4$  and  $P_5$  have the same polarizability ratio,  $\frac{C_1}{C_2} = 2$ . The diameter of particle  $P_4$  is  $d= 10\mu\text{m}$ , the diameter of particle  $P_5$  is  $d= 5\mu\text{m}$ .  $E_\infty=50\text{V/cm}$ .



## 7.5 Conclusions

This paper proposed a novel dielectric Janus particle separation method by the polarizability ratio and the size of Janus particles. When dielectric Janus particles are suspended in an electrolyte solution and subjected to uniform DC electric field, the particles are polarized at different levels. The value of the induced surface potential and the ICEOF are dependent on the permittivity of the particle and the electrolyte solution, the size of the particle, the electric field strength and the orientation of the Janus particle in the electric field. When there is an angle between the two-hemisphere interface of the Janus particle and electric field direction, the asymmetric ICEOF around the particle drive the particle to rotate to align with the electric field in a short time period. Moreover, due to the different strengths of the vortices on the two sides of the particle, the interaction between the two vortices on each side of the particle and the channel walls pushes the particles to move towards one side of the walls depending on the initial orientation. The final separation distance of Janus particles from the wall is a function of the polarizability ratio and the size of the Janus particle and is predictable. Based on the fact that the different separation distances are critical to the trajectories of the particles in the laminar electroosmotic flow, dielectric Janus particles can be continuously separated by polarizability ratio and size. One possible commercial application of the dielectric Janus particle is micro carriers in targeted drug delivery. In a targeted drug delivery procedure, specific drugs need to be carried to diseased areas by designed routes [107]. The self-alignment phenomenon of the Janus particles guarantees that a specific drug can be loaded to a point on the Janus particle while the other surface of the particle maintains a different biological feature.

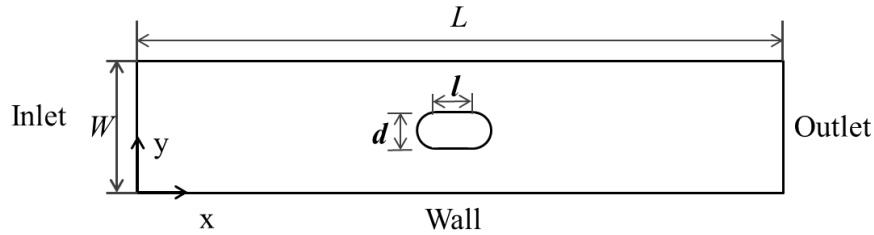
## Chapter 8

### Self-propelled heterogeneous particle

In electrophoretic separations, the electrophoretic velocity of a charged particle is determined by the intrinsic electrophoretic mobility of the particle  $\mu_e = \frac{\varepsilon_0 \varepsilon_r \zeta}{\mu}$ , where  $\zeta$  is the static zeta potential of the particle. However, target particle components normally have similar static potentials and the same sign. As a result, a long separation time and a significant separation section are always needed. We learned from the last chapter that, when a Janus particle line up with or vertical to the external electric field, the vortexes around the Janus particle drive the particle into translational motion and the velocity is polarizability-dependent. In this chapter, we build a polarizability-dependent self-propelled particle by attaching two hemispheres of high permittivity ( $\varepsilon_{p1}, \varepsilon_{p2}$ ) to a non-polarizable cylinder at the two ends. External electric field is applied along the spheroid axis of the particle. Since Eq. (3-7) doesn't apply to hemisphere surfaces, we use Eq. (5-1) to calculate the induced surface potential on the hemispheres. Besides the local EOF on the particle surface due to the zeta potential of the particle and the bulk EOF caused by the zeta potential on the wall, there are induced vortexes around the two polarizable hemispheres. The vortices on the high polarizable hemisphere are stronger than the vortices on the lower-polarizable side. The resulting motion of the particle under these three mechanisms is numerically studied. The impact of relevant parameters such as the polarizability of the two hemispheres and the liquid, the electric field strength, the size of the particle and the value of the static zeta potential are also investigated.

## 8.1 Computational domain and dimensions

Figure 8-1 is the 2D computational domain. The solid particle is suspended in aqueous electrolyte solutions in the channel, and electric field is applied through the channel. The particle is composed of one cylinder in the middle and two hemispheres at the two ends. The length of the cylinder is  $l$ , and the diameter of the cylinder is  $d$ . Different scales of the particle are used in these simulations, and the values are given in Table 8-1. The length of the micro channel section is  $L=100 \times l$ , and the width of the channel is  $W=20 \times d$ . The size of the domain is chosen to guarantee the flow is fully developed at the inlet and outlet while the particle travels in the concerned distance in this serial of simulations in this chapter. The zeta potential on the walls is constant, and the particle has a static zeta potential on the surface and local induced surface potential on the two ends. The translation velocity of the particle with polarizable ends  $C_1=1$ ,  $C_2=0.2$  is examined while the computational domain is divided into 1,678 elements, 2,158 elements, 2,650 elements, and 3,129 elements, respectively. The velocity of the particle reached a constant value (0.5% changes) when the number of mesh elements is 2,158 and more. Eventually, 2,200 Lagrange elements are generated for this series of simulations and mesh-dependency is eliminated. The particle is initially placed in the center of the domain parallel to the channel. The particle and the electrolyte are initially static. The 2D transient simulations in this chapter are performed with COMSOL 3.5a. The discretization methods used in this serial of simulations are given in Table 8-1. The numerical error tolerance is  $10^{-5}$ . The values of constants and parameters in this chapter are given in Table 8-2.



**Figure 8-1. The schematic diagram of the computational domain.**

Variables	Discretization method
Velocity	Second order
Pressure	First order
Electric potential	Second order
Displacement field of the particle	Second order

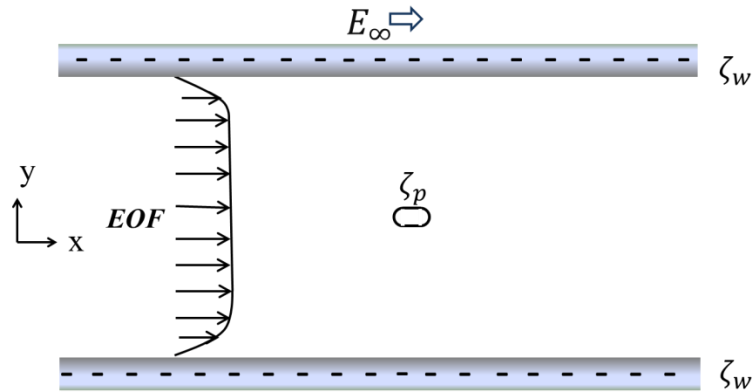
**Table 8-1. Discretization methods used in the simulations**

Definition	Constant/Parameters	Values/Range
Permittivity of the vacuum	$\epsilon_0$ (F/ m)	$8.85 \times 10^{-12}$
Relative permittivity of the liquid medium	$\epsilon_m$	80
Defined non-dimensional polarizability of the sphere	$C$	0~1
Viscosity of the liquid	$\mu$ (kg/m s)	$0.9 \times 10^{-3}$
Density of liquid	$\rho$ (kg/m <sup>3</sup> )	998
Zeta potential of the wall	$\zeta_w$ (mV)	-20,-30
Zeta potential of the particle	$\zeta$ (mV)	-10~-25
Diameter of the particle	$d$ ( $\mu$ m)	10~20
Length of the particle	$l$ ( $\mu$ m)	12~20
External electric field	$E_\infty$ (V/cm)	25~100

**Table 8-2. Values and ranges of constants and parameters in the simulations**

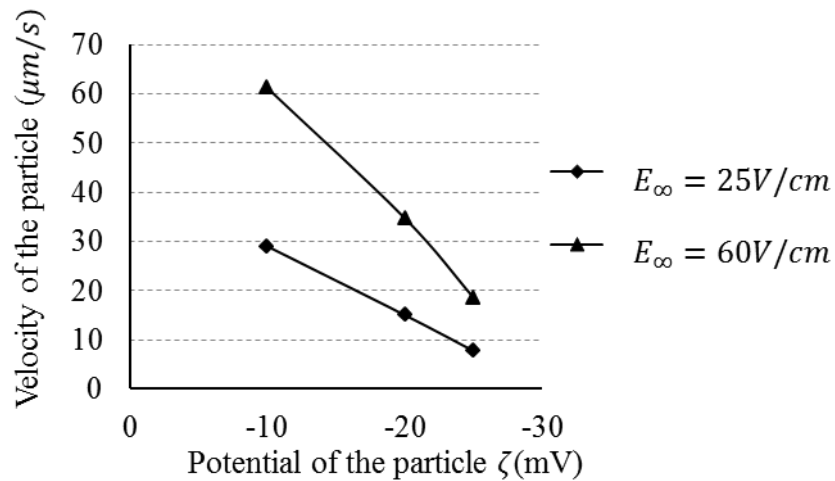
## 8.2 Results-immigration of homogeneous particle in uniform electric field

Consider a non-polarizable dielectric particle is suspended in an electrolyte in a straight channel. In this micro system, the channel wall presents a constant zeta potential  $\zeta_w$  and the particle also owns a zeta potential  $\zeta$ . When the particle is considered non-polarizable, the surface potential of the particle is solely the static zeta potential of the particle  $\zeta_p = \zeta$ . Assume  $\zeta_w$  is negative as in many cases in microfluidic studies, once apply electric field through the channel in the  $x$ -direction, there is linear electroosmotic flow (EOF) generated throughout the channel in the direction of the electric field, and the velocity of the EOF is determined by  $\vec{V} = -\frac{\epsilon_0 \epsilon_r \zeta_w}{\mu} \vec{E}_{\parallel}$ . At the same time, the potential  $\zeta_p$  on the particle leads to a slipping velocity on the surface which is calculated by  $\vec{V} = -\frac{\epsilon_0 \epsilon_r \zeta_p}{\mu} \vec{E}_{\parallel}$ . Resulted from the viscosity of the liquid, the particle tends to move in response to the bulk flow and the local slipping velocity on the particle surface (shown in Figure 8-2).



**Figure 8-2.** Dielectric particle suspended in an electrolyte in a straight channel. The channel wall is negatively charged and the zeta potential is  $\zeta_w$ . The potential of the particle is  $\zeta_p$ . Uniform electric field  $E_{\infty}$  is applied though the channel.

While both the zeta potential on the channel wall and the non-polarizable particle are negative, the immigration velocity and direction of the particle are given in Figure 8-3. The zeta potential on the channels wall is  $\zeta_w = -30mV$ , and the zeta potential on the particle ranges from  $\zeta = -10mV$  to  $\zeta = -25mV$ . The EOF of the bulk liquid exerts a driving force on the particle in the positive  $x$ -direction; in contrast, the slipping velocity on the particle provides a pushing effect in the negative  $x$ -direction. Both the EOF of the bulk liquid and the local EOF on the particle surface are linearly related to the electric field strength and the surface potential. While the absolute value of the surface potential of the particle is smaller than the zeta potential of the wall, the bulk EOF dominates, and particle moves in the direction of the bulk EOF. Under electric field strength  $E_\infty = 25V/cm$  and  $E_\infty = 60V/cm$ , the particle moves in the  $x$ -direction with different velocities. The particle migrates faster under higher electric field (e.g.  $E_\infty = 60V/cm$ ), because the EOF of the bulk liquid is proportional to the electric field. The velocity approaches zero while the zeta potential on the particle equivalent to the zeta potential of the wall.



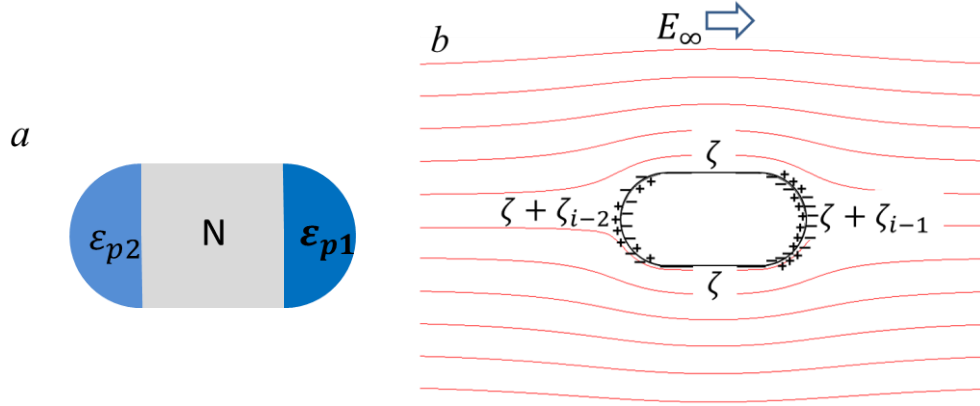
**Figure 8-3.** The translational velocity of a particle with static zeta potential  $\zeta$ . Zeta potential on the wall  $\zeta_w = -30mV$ . Electric field is applied in the  $x$ -direction.

### 8.3 Results-immigration of heterogeneous particle in uniform electric field

When the particle is dielectric heterogeneous, where the two hemispheres are polarizable, the ICEOF induced by the electric field around the particle contributes to the immigration of the particle. It has been proved in the last chapter that, the asymmetric ICEOF around a dielectric heterogeneous particle exerts a torque and net force on the particle depending on the orientation of the particle. In this chapter, the particle is placed parallel to the electric field, so that the torque is absent. The heterogeneous particle undergoes pure translational motion.

#### 8.3.1 Dielectric heterogeneous particle

The hemisphere on the right side has a permittivity  $\varepsilon_{p1}$ , the hemisphere on the left side has a permittivity of  $\varepsilon_{p2}$ , and the middle part of the particle is non-polarizable. The permittivity of the electrolyte is  $\varepsilon_m$ . The particle including the dielectric ends presents a static uniform zeta potential  $\zeta$  in the electrolyte. When the suspended particle is subjected to a uniform electric field, there exists static electric double layer on the surface of the non-polarizable cylinder, and induced electric double layer on the surfaces of the two ends. The induced surface potential on the two hemispheres are calculated by Eq. (5-1)  $\zeta_{i-1} = C_1(-\phi + \frac{\int_A \phi dA}{A})$  with  $C_1 = \frac{\varepsilon_{p1}}{\varepsilon_p + \varepsilon_m}$  on the  $\varepsilon_{p1}$  surface, and  $\zeta_{i-2} = C_2(-\phi + \frac{\int_A \phi dA}{A})$  with  $C_2 = \frac{\varepsilon_{p2}}{\varepsilon_p + \varepsilon_m}$  on the  $\varepsilon_{p2}$  surface. Accordingly, on the non-polarizable surface  $\zeta_p = \zeta$ , and at the two ends  $\zeta_p$  equals to the superimposition of the static potential  $\zeta$  and the induced surface potential  $\zeta_p = \zeta + \zeta_{i-1}$ ,  $\zeta_p = \zeta + \zeta_{i-2}$ . Assuming the hemisphere on the right side is more polarizable than the left part  $\varepsilon_{p1} > \varepsilon_{p2}$ . Figure 8-4a shows the structure of the heterogeneous particle, and Figure 8-4b illustrates the external electric field around the particle and the signs of the charges on the particle surface.

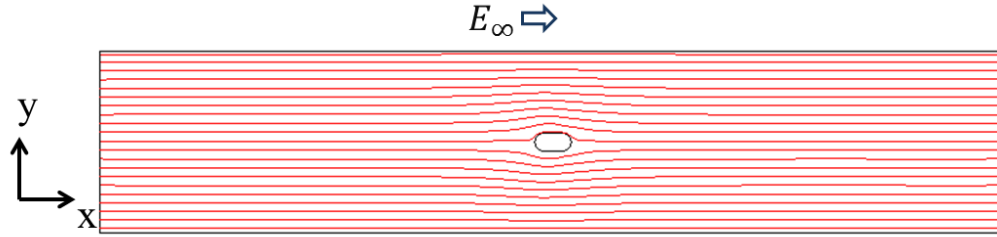


**Figure 8-4. Heterogeneous particle with non-polarizable cylinder in the middle, dielectric hemisphere  $\epsilon_{p1}$  on the right, and dielectric hemisphere  $\epsilon_{p2}$  on the left,  $\epsilon_{p1} > \epsilon_{p2}$ , (a) the length of the cylinder is  $l$  and the diameter is  $d$ . (b) electric field around the particle and the induced charges on the particle. Uniform electric field  $E_\infty$  is applied. The static zeta potential on the particle is a constant  $\zeta$ , and the induced surface potential on the hemisphere on the right is  $\zeta_{i-1}$ , and  $\zeta_{i-2}$  on the other side.**

### 8.3.2. Immigration of the heterogeneous particle in uniform electric field in EOF

When the zeta potential on the wall is  $\zeta_w = -30mV$ , and the zeta potential on the particle is  $\zeta = -20mV$ , the EOF of the bulk liquid and the EOF on the particle surface exert driving effect on the particle in opposite directions. Additionally, the ICEOF generates a driving force pointing to low-polarizable end. The streamlines in the computational domain under electric field  $E_\infty = 60V/cm$  are shown in Figure 8-5. Due to the small scale of the particle, the bulk EOF is much stronger than the local ICEOF around the particle so the ICEOF is invisible in Figure 8-5. However, the effects of the ICEOF to the immigration of the particle are noticeable as indicated in Figure 8-6.





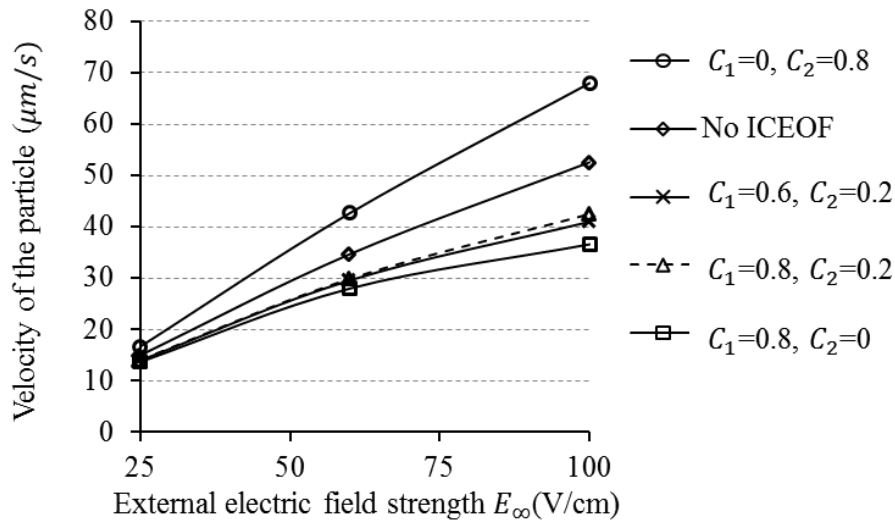
**Figure 8-5. Streamlines around a heterogeneous dielectric particle. Static zeta potential on the wall  $\zeta_w = -30mV$ , static zeta potential on the particle  $\zeta = -20mV$ , electric field  $E_\infty = 60V/cm$  applied in the  $x$ -direction.  $C_1=0.8$ ,  $C_2=0$ .**

Figure 8-6 plots the translational velocity of the particle under the effect of ICEOF and in the absence of ICEOF. Since the absolute value of  $\zeta_w$  is higher than the zeta potential on the particle, the EOF of the bulk liquid is the critical mechanism affecting the particle. According to Figure 8-3, in the absence of ICEOF, the particle moves in the  $x$ -direction, and the velocity increases with the external electric field strength.

However, when the two hemispheres are made of highly polarizable dielectric materials, there are induced vortices around the hemisphere surfaces. The ICEOF around the two ends of the particles affect the particle in opposite directions: the vortices on the right push the particle in the negative  $x$ -direction, and the vortices on the left side push the particle in the positive  $x$ -direction. The net force from these two effects is directly determined by the difference between the polarizability of the two ends. For example, when  $\epsilon_{p1} > \epsilon_{p2}$ , which means the vortexes induced by the field at the right side are stronger than the ones on the left side. The net effect tends to drive the particle move in the negative  $x$ -direction. The translational velocities of the particles with different combinations of polarizable hemispheres are investigated. It is obvious that, though the EOF of the bulk liquid is still the dominant mechanism, the velocity of the particle is

slowed down by the ICEOF. With polarizability combination ( $C_1=0.6, C_2=0$ ), ( $C_1=0.8, C_2=0.2$ ), the translational velocities of the particles are similar, that is because the polarizability difference in these two cases are the same. The most noticeable modification in velocity is made by a set of hemispheres of polarizability ( $C_1=0.8, C_2=0$ ), in which, the translational velocity of the particle in the  $x$ -direction at  $E_\infty = 100V/cm$  is  $U_p = 36.6\mu m/s$ . Comparing with particle velocity  $U_p = 52.6\mu m/s$  without ICEOF, the immigration is slowed down by 30%.

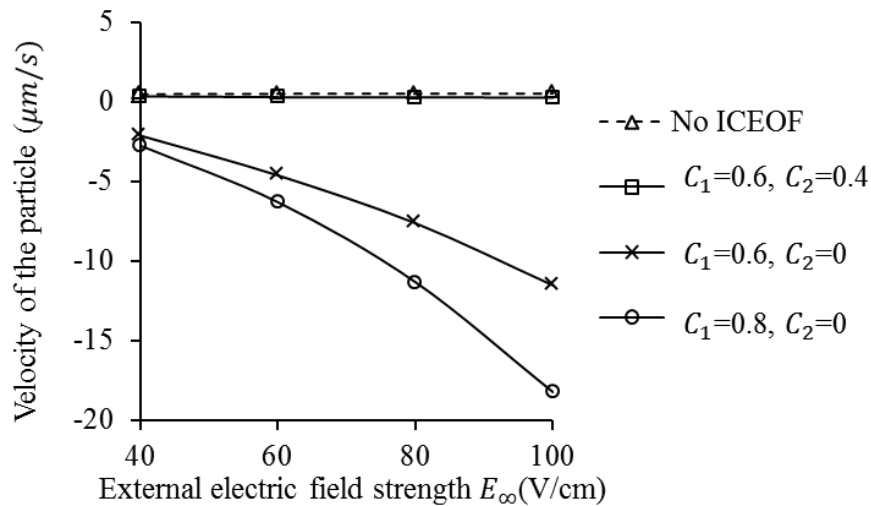
Similarly, when  $\varepsilon_{p1} < \varepsilon_{p2}$ , the vortexes on the right side of the particle are stronger than that on the left side of the particle. The resulting driving effect is in the  $x$ -direction, which is the same as the direction of the particle motion. Under electric field  $E_\infty = 100V/cm$ , the velocity of the particle with  $C_1=0, C_2=0.8$  is  $U_p = 68.0\mu m/s$ , which is 29% higher than the velocity of the particle without ICEOF.



**Figure 8-6.** The translational velocity of the particle without ICEOF and with ICEOF of different strengths around the two ends of the particle. Zeta potential of the wall  $\zeta_w = -30mV$ ; zeta potential on the particle  $\zeta = -20mV$ . The combinations of the defined

polarizability ( $C_1=0, C_2=0.8$ ), ( $C_1=0.6, C_2=0$ ), ( $C_1=0.8, C_2=0.2$ ), and ( $C_1=0.8, C_2=0$ ). The size of the particle is  $d=l=10\mu\text{m}$ .

On the other hand, when the zeta potential of the particle and the zeta potential of the wall are equal to each other  $\zeta_w = \zeta_p = -20\text{mV}$ , the effects from the bulk flow and the local slipping velocity on the particle surface are comparative. The resulted velocity of the particle is almost zero. In this case, the additional hydrodynamic force from the vortices on the particle directly determines the direction and velocity of the particle. Figure 8-7 gives the translational velocity of the particle with equal zeta potential to the zeta potential on the wall and hemispheres of different polarizability ( $\varepsilon_{p1} > \varepsilon_{p2}$ ) at the ends. While the two ends are non-polarizable or similarly polarizable (e.g.  $C_1=0.6, C_2=0.4$ ), the velocity of the particle is almost zero. Comparing with ( $C_1=0.6, C_2=0$ ) and ( $C_1=0.8, C_2=0.2$ ), polarizability ( $C_1=0.6, C_2=0.4$ ) provides the minimal polarizability difference, and the resulted velocity of the particle still close to zero. On the other hand, with larger polarizability on the right side, and the left side non-polarizable (e.g. ( $C_1=0.6, C_2=0$ ) and ( $C_1=0.8, C_2=0$ )), the heterogeneous particle moves in the negative  $x$ -direction. The velocity of the particle increases exponentially with the electric field strengths.



**Figure 8-7. The velocity of the particle with different polarizable hemispheres in uniform electric field. Zeta potential on the wall and the particle are  $\zeta_w = -20mV$  and  $\zeta = -20mV$  respectively. The motion of the particles is in the negative x-direction with  $(C_1=0.6, C_2=0)$ ,  $(C_1=0.6, C_2=0.4)$  and  $(C_1=0.8, C_2=0.2)$ . The scale of the particle is  $d=l=10\mu m$ .**

Table 8-3 lists the translational velocity of particles of different scales under electric field strength  $E_\infty = 60V/cm$ , with  $\zeta_w = \zeta_p = -20mV$ . The scale of the particle influences the particle motion in two ways. On one hand, smaller size leads to weaker vortexes of the ICEOF. On another hand, the reduced contacting area between the particle and the liquid diminishes the viscous resistance from the neighboring liquid. We study the motion of the particle under three scales:  $(d=l=10 \mu m)$ ,  $(d=20, l=20 \mu m)$ , and difference ratio  $(d=20 \mu m, l=10 \mu m)$ .

$(\mu m/s)$	No ICEOF	$C_1=0.6$ $C_2=0.4$	$C_1=0.6$ $C_2=0.2$	$C_1=0.6$ $C_2=0$	$C_1=0.8$ $C_2=0.2$	$C_1=0.8$ $C_2=0$
$d=l=10 \mu m$	0.4	0.3	-2.0	-4.6	-3.6	-6.3
$d=l=20 \mu m$	0.2	-1.5	-6.6	-12.0	-10.2	-16.4
$d=20, l=10 \mu m$	0.2	-1.9	-8.4	-14.7	-13.4	-20.0

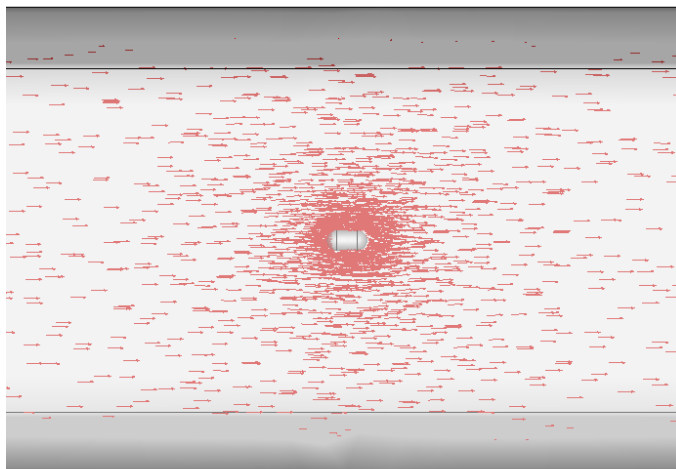
**Table 8-3. The translational velocities of the dielectric particles with two hemispheres of different polarizabilities at the ends.  $E_\infty = 60V/cm$ ,  $\zeta_w = \zeta = -20mV$ .**

We compare the direction and the value of translational velocity of the particles of three different sizes and six sets of polarizable ends. Since  $C_1 > C_2$  in these six cases, the ICEOF on the heterogeneous particle induces hydrodynamic force opposite to the x-direction. The driving effect from the ICEOF is more obvious when the particle size is larger. The velocity of a twice larger particle ( $d=20 \mu m$ ) is around three times as the velocity of the particle of smaller size ( $d=10 \mu m$ ). Meanwhile, the particle of larger diameter and shorter length gains the biggest

driving effect from the ICEOF. Among all the simulation results, dielectric polarizability ( $C_1=0.6, C_2=0.4$ ) provides the minimal driving effect. While the polarizability differences are more significant (e.g. ( $C_1=0.8, C_2=0$ ), ( $C_1=0.8, C_2=0.2$ ), ( $C_1=0.6, C_2=0$ ), ( $C_1=0.6, C_2=0.2$ )), the particles move in the negative  $x$ -direction. The driving effect provided by ( $C_1=0.8, C_2=0$ ) is the most significant. Though particles with polarizable ends ( $C_1=0.8, C_2=0.2$ ), and polarizable ends ( $C_1=0.6, C_2=0$ ) have the same polarizability difference, ( $C_1=0.6, C_2=0$ ) leads to more dramatic effect than the other.

#### 8.4 2D numerical validation

A 3D numerical model is built with FLEUNT 12.0 to validate the 2D numerical simulations in this chapter. After mesh-independency study, 146,030 unstructured meshes are originally generated by GAMBIT 2.40. First order upwind spatial discretization and first order implicit transient simulation are utilized. The numerical error tolerance is  $10^{-6}$ . The parameters used in this 3D model are given in Table 8-1. The third dimension of the computational domain is  $20 \times d$ , which is the same as the width of the channel. Figure 8-8 shows the velocity vector on a slice surface at the center of the domain. Specific values of parameters are: electric field  $E_\infty = 100V/cm$ ; zeta potential on the channel wall:  $\zeta_w = -30mV$ ; zeta potential on the particle  $\zeta = -20mV$ ; the defined polarizability of the heterogeneous particle ( $C_1=0, C_2=0.8$ ). The numerical result of the translational velocity is  $U_p = 65.5\mu m/s$ , which is 3.6% lower than the 2D simulation result  $U_p = 68.0\mu m/s$  (shown in Figure 8-6).



**Figure 8-8. The velocity vector of the flow field. Zeta potential on the channel wall:  $\zeta_w = -30mV$ ; zeta potential on the particle  $\zeta = -20mV$ ; the defined polarizability of the heterogeneous particle ( $C_1=0, C_2=0.8$ ).  $E_\infty = 100V/cm$**

## 8.5 Conclusions

In this chapter, we did simulation study of the self-propulsion effects of a dielectric heterogeneous particle in uniform electric fields. Two polarizable hemispheres of different polarizabilities are attached to a non-polarizable cylinder to compose a dielectric heterogeneous particle. Since both the particle and the channel wall are assumed inherently possess static zeta potentials, the particle moves with an intrinsic velocity under the influence of the EOF of the bulk liquid and the local EOF on the particle surface. At the meantime, the vortices around the particle induced by the electric field give rise to a net force acting on the particle. Simulation results show that, the intrinsic velocity of the particle is altered at a variety of levels owing to the polarizability-dependent ICEOF around the particle. The change of the velocity induced by the ICEOF is a function of the polarizability of the two hemispheres, the size of the particle and the electric field strength. This self-propulsion effect can be used in particle manipulation operations.

Through assembling object particles with different polarizable ends, particles' electrophoretic motilities can be diversified and the differences can be enhanced. As a result, the operation time and the dimension of the electrophoretic separation system can be optimized.

## Chapter 9

### Conclusions and future work

This thesis involves the theoretical and numerical study of the induced-charge electroosmotic flow (ICEOF) of dielectric particles in uniform electric field. The ICEOF pattern around homogeneous dielectric particles and heterogeneous dielectric particles were studied. The time-dependent immigration of suspended dielectric particles under the influence of ICEOF were also investigated using transient simulations.

#### 9.1 Conclusions

The key contributions include:

The analytical expression for the induced surface potential of dielectric particles was derived for the first time. Unlike the induced surface potential of metal particles, which is only determined by the geometry of the particle and the external electric field, the induced surface potential of a dielectric particle is sensitive to the polarizability of the dielectric system as well. The corresponding ICEOF slipping velocity is also found dependent on the polarizability.

The symmetric ICEOF of a homogeneous particle doesn't contribute to the immigration of the particle. However, the interaction between the ICEOF around two closely located particles is a function of the polarizabilities of the particles. In the case of heterogeneous dielectric particles which consist of multiple components, the induced surface potential is spatially varying. We found the electric field-actuated polarizability-dependent rotation of the heterogeneous particles.

Two novel particle separation methods were developed by employing the fundamental phenomena demonstrated in this research. The first is for homogeneous particles. The particles suspended in a straight channel are induced into a narrow stream section between the solid



channel walls and vortices. Due to the interaction between the wall and the ICEOF of the particle, the traces of the particles are deviated at certain degrees depending on the strengths of the ICEOF. When the polarizability of a particle is significant enough, the particle will be trapped into the vortex; otherwise, the particle flows downstream. This method can be accomplished by simple channel design and less labor and the result is sensitive to the electric field.

A novel particle separation method for heterogeneous Janus particles was also developed. We numerically studied the rotation and alignment of Janus particles made of two different dielectric halves in uniform electric fields. Unlike metallic-dielectric particles, dielectric Janus particles rotate to line up with the electric field. Meanwhile, the vortices on the two sides of the particle push the particle to move perpendicular to the wall. At steady state, particles of different polarizability ratios keep equilibrium distances from the wall. Consequently, particles of different polarizability ratios can be independently collected into different branch channels.

We built a self-propelled heterogeneous dielectric particle for the first time. When the particle is parallel to the electric field, the ICEOF around the two polarizable ends of the particle exerts a hydrodynamic force pointing to the low polarizable side. This driven effect can be controlled by the polarizabilities of the two ends, the size of the particle and electric field strength. However, the direction of the force always points to the end of weak polarizability. This strategy can be used to alter the intrinsic electrophoretic motilities of target particles to enhance particle manipulation efficiency.

## 9.2 Future work

This thesis research can be further developed in many aspects. Several of the possibilities are discussed in the following.

- Conduct experiments to verify the simulation results in this research.

The results of the simulation research in this thesis can be used to determine the optimum operation conditions such as the external electric field strength, the dimensions of the channels, the sizes of the particles etc. Homogeneous dielectric particles and heterogeneous particles of high polarizability may not be available commercially, so particle fabrication techniques should be developed and used to synthesize object particles in the lab if possible. The concentration and pH of the aqueous solutions that will be employed in the experiments would affect the zeta potential on the channel wall; however, the polarizability of the artificial particles can be controlled. The experimental results would differ from the simulation results from this dissertation due to several practical issues such as the density difference between the object particles and the surrounding solution.

- Develop the mathematical expression of the induced surface potential on surfaces of anisotropic polarizability in uniform electric field and isotropic surfaces in non-uniform electric field.

In practical, the polarizability (the permittivity) of a material can be spatially varying due to the temperature difference, contamination issues, etc. In these cases, the dielectrics are not simply a composition of patches of polarizable dielectric materials, but might possess spatially linear-varying permittivity. When the permittivity of the surrounding liquid medium or the solid surface is not isotropic, the Laplace's equation does not apply, instead  $\nabla \cdot [\epsilon_r(-\nabla\phi)] = 0$  should be used

under the condition of zero free charges in the system. In others cases, due to the concentration gradient of the surrounding aqueous solutions or the geometry of the channel, the local electric field in the channel can be non-uniform. In these two scenarios, it is challenging to obtain the analytical solution of Laplace equation to express the induced surface potential on the solid-liquid interface. A future study of mathematical expressions of the induced surface potential of the isotropic dielectric systems is necessary.

- Consider the buoyance effect caused by the density difference between the suspended particles and the surrounding aqueous solution.

In the simulations throughout this thesis research, the densities of the particles are assumed the same as the surrounding aqueous solution, so the buoyance effect is neglected. However, in practical microfluidic operations, the target particles can have different densities than that of the carrier solution. This results in a buoyant force in the direction of the height of the channel. Though the particles would not sink to the bottom of the channel or reach the top of the channel due to the induced vortices around the particles, this buoyancy effect would affect the final positions of the particles [37] in the micro-channels. The effect of density difference should be studied through both numerical simulation and experimental study. The results can help to determine the operation conditions for the separation techniques mentioned in Chapter 6 and Chapter 7.

## References

- [1] P. Attard, *Adv. Chem. Phys.*, 1996, 92, 1-159,
- [2] T. Akagi and T. Ichiki, *Anal Bioanal Chem*, 2008, 391, 2433–2441
- [3] Y. Demircan, E. Özgür, H. Külah, *Electrophoresis*, 2013, 34, 1008–1027.
- [4] D. Li, *Electrokinetics in microfluidics*, Elsevier Press, 2004, 501-510,
- [5] T. M. Squires and M. Z. Bazant, *J. Fluid Mech.*, 2004, 509, 217–252.
- [6] A. S. Dukhin, *Colloids Surf., A*, 1993, 13, 29-48
- [7] Z. Wu and D. Li, *Electrochim. Acta.*, 2008, 53, 5827-5835
- [8] S. Baroni, *Phys. Rev.B*, 1986, 33, 7017-7021
- [9] K. Arnold, A. Herrmann, L. Pratsch and K. Gawrisch, *Biochim. Biophys. Acta*, 1985, 815, 515-518
- [10] J. Yang, Y. Huang, X. Wang, X-B. Wang, F. F. Becker, P. R. C. Gascoyne, *Biophys. J.*, 1999, 76, 3307-3314
- [11] S. Gabriely, R. W. Lau, C. Gabriel, *Phys. Med. Biol.*, 1996, 41, 2251–2269.
- [12] Y. Bai, Z.-Y. Cheng, V. Bharti, H. S. Xu and Q. M. Zhang, *Appl. Phys. Lett.*, 2000, 76, 3804.
- [13] J. Robertson, *Eur. Phys. J. Appl. Phys.*, 2004, 28, 265–291.
- [14] S. Roberts, *Phys. Rev.*, 1979, 76, 1215-1220.
- [15] M. A. Subramanian, D. Li, N. Duan, B. A. Reisner and A. W. Sleight, *J. Solid State Chem.*, 2000, 151, 323-325.
- [16] F. Nadal, F. Argoul, P. Hanusse, B. Pouligny and A. Ajdari, *Phys. Rev. E.*, 2002, 65, 061409
- [17] W. Li and R. W. Schwartz, *Phys. Rev. B.*, 2007, 75, 012104
- [18] V. G. Levich, *Physicochemical Hydrodynamics*. Englewood Cliffs, N.J.: Prentice-Hall, Inc., 1962
- [19] N. G. Green, A. Ramos, A. González, H. Morgan and A. Castellanos, *Phys. Rev. E.*, 2002, 66, 026305.
- [20] A. González, A. Ramos, N. G. Green, and A. Castellanos and H. Morgan, *Phys. Rev. E.*, 2000, 61, 4019

- [21] N. G. Green, A. Ramos, A. González, H. Morgan and A. Castellanos, *Physical Review E*, 2000, *61*, 4011
- [22] F. Zhang, Y. Daghighi and D. Li, *J. Colloid Interface Sci.*, 2011, *364*, 588–593.
- [23] A. D. Stroock, S. K. W. Dertinger, Ar. Ajdari, I. Mezic, H. A. Stone, G. M. Whitesides, *Science*, 2002, 295
- [24] P. Takhistov, K. Duginova, and H.-C. Chang, *J. Colloid Interface Sci.*, 2003, *263*, 133–143
- [25] C.-Y. Lee, C.-L. Chang, Y.-N. Wang and L.-M. Fu, *Int. J. Mol. Sci.*, 2011, *12*, 3263-3287
- [26] Y. Daghighi and D. Li, *Analytica Chimica Acta*, 2013, *763*, 28– 37
- [27] R. H. Liu, M. A. Stremler, K. V. Sharp, M. G. Olsen, J. G. Santiago, R. J. Adrian, H. Aref, and D. J. Beebe, *J. Microelectromech. Syst.*, 2000, *9*, (2).
- [28] V. Studer, A. Pe´pin, Y. Chen and A. Ajdari, *Analyst*, 2004, *129*, 944-949.
- [29] M. Mpholo, C. G. Smith and A.B.D. Brown, *Sensors and Actuators B*, 2003, *92*, 262–268
- [30] I. Gitlin, A. D. Stroock, G. M. Whitesides, and A. Ajdari, *Appl. Phys. Lett.*, 2003, *83*, 1486-1487.
- [31] A. Ramos, H. Morgan, N. G. Green and A. Castellanos, *J. Colloid Interface Sci.*, 1999, *217*, 420-422
- [32] A. Ramos, A. González, A. Castellanos, N. G. Green, and H. Morgan, *Phys. Rev. E.*, 2003, *67*, 056302
- [33] A. Ajdari, *Phys. Rev. E.*, 2000, *61*, R45-R48.
- [34] M. M. Gregersen, F. Okkels, M. Z. Bazant and H. Bruus, *New J. Phys.*, 2009, *11*, 075019
- [35] D. Saintillan, E. Darve and E. S. G. Shaqfeh, *J. Fluid Mech.*, 2006, *563*, 223–259.
- [36] R.W. O'Brien, L. R. White, *J. Chem. So., Faraday Trans.*, 1978, *74*, 1607-1626
- [37] Z. Wu, Y. Gao, D. Li, *Electrophoresis*, 2009, *30*, 773–781
- [38] G. Yossifon, I. Frankel and T. Miloh, *Phys. Fluids*, 2007, *1*, 068105
- [39] Y. Ben, H-C. Chang, *J. Fluid Mech.*, 2002, *461*, 229-238.
- [40] K. A. Rose, J. A. Meier, G. M. Dougherty, J. G. Santiago, *Phys. Rev. E.*, 2007, *75*, 011503
- [41] H. Sugioka, *Phys. Rev. E.*, 2010, *81*, 036301
- [42] H. Sugioka, *Phys. Rev. E.*, 2011, *83*, 025302(R)
- [43] M. S. Kili, M. Z. Bazant, *Electrophoresis*, 2011, *32*, 614–628
- [44] H. Zhao, H. H. Bau, *Langmuir*, 2007, *23*, 4053-4063

- [45] D. Saintillan, *Phys. Fluids*, 2008, 20, 067104
- [46] K. A. Rose, B. Hoffman, D. Saintillan, E. S. G. Shaqfeh and J. G. Santiago, *Phys. Rev. E.*, 2009, 79, 011402
- [47] E. Yariv, *EPL*, 2008, 82, 54004
- [48] Z. Wu and D. Li, *Electrochimica Acta*, 2009, 54, 3960
- [49] F. Nadal, F. Argoul, P. Hanusse, B. Pouligny and A. Ajdari, *Phys. Rev. E.*, 2002, 65, 061409
- [50] W. D. Ristenpart, I. A. Aksay, D. A. Saville, *J. Fluid Mech.*, 2007, 575, 83-109.
- [51] W. D. Ristenpart, P. Jiang, M. A. Slowik, C. Punckt, D. A. Saville and I. A. Aksay, *Langmuir*, 2008, 24, 12172-12180
- [52] W. D. Ristenpart, I. A. Aksay and D. A. Saville, *Langmuir*, 2007, 23, 4071-4080
- [53] J. D. Hoggard, P. J. Sides and D. C. Prieve, *Langmuir*, 2008, 24, 2977-2982
- [54] W. D. Ristenpart, I. A. Aksay and D. A. Saville, *Phys. Rev. Lett.*, 2003, 90, 128303/1
- [55] M. Mittal, P. P. Lele, E. W. Kaler and E. M. Furst, *J. Chem. Phys.*, 2008, 129, 064513
- [56] F. Ma, S. Wang, L. Smith and N. Wu, *Adv. Funct. Mater.*, 2012, 22, 4334-4343
- [57] F. Zhang and D. Li, *J. Colloid Interface Sci*, 2013, 410, 102-110
- [58] Q. Chen, J. K. Whitmer, S. Jiang, S. C. Bae, E. Luijten, and S. Granick, *Science*. 2011, 331, 199
- [59] M. Bradley and J. Rowe, *Soft Matter*. 2009, 5, 3114
- [60] B. Wang, B. Li, B. Dong, B. Zhao and C. Y. Li, *Macromolecules*. 2010, 43, 9234
- [61] F. Sciortino, A. Giacometti and G. Pastore, *PRL* 103(2009) 237801
- [62] St. Ebbens, M.-H. Tu, J. R. Howse and R. Golestanian, *Phys Rev E*. 2012, 85, 020401(R)
- [63] M. M. Moghani and B. Khomami, *Soft Matter.*, 2013, 9, 4815
- [64] J. de Graaf, N. Boon, M. Dijkstra and René van Roij, *J. Chem. Phys.* 2012, 137, 104910
- [65] W. Yang, V. R. Misko, K. Nelissen, M. Kong and F. M. Peeters, *Soft Matter*, 2012, 8, 5175
- [66] K. P. Yuet, D. K. Hwang, R. Haghgooie and P. S. Doyle, *Langmuir*, 2010, 26, 4281
- [67] S. Gangwal, O. J. Cayre and O. D. Velev, *Langmuir*, 2008, 24, 13312
- [68] T. Honegger, O. Lecarme, K. Berto and D. Peyrade, *J. Vac. Sci. Technol. B*, 2010, 28, C6114 (2010)
- [69] T. Honegger, O. Lecarme, K. Berton and D. Peyrade, *Microelectron Eng.* 2010, 87, 756.
- [70] S. Gangwal, O. J. Cayre, M. Z. Bazant and O. D. Velev, *PRL*, 2008, 100, 058302
- [71] A. M. Boymelgreen and T. Miloh, *Physi. Fluids*, 2011, 23, 072007

- [72] A. M. Boymelgreen and T. Miloh, *Electrophoresis*, 2012, 33, 870
- [73] Y. Daghighi, Y. Gao and D. Li, *Electrochimica Acta*, 2011, 56, 4254
- [74] Y. Daghighi, I. Sinn, R. Kopelman and D. Li, *Electrochimica Acta*, 2011, 87, 270
- [75] Y. Daghighi and D. Li, *Lab Chip*, 2011, 11, 2929
- [76] N. Pamme, *Lab Chip*, 2007, 7, 1644–1659.
- [77] D. Kohlheyer, J. C. T. Eijkel, A. van den Bergm, R. B. M. Schasfoort, *Electrophoresis*, 2008, 29, 977–993.
- [78] A. A. Elbashir, F. E. O. Suliman, B. Saad and H. Y. Aboul-Enein, *Biomed. Chromatogr.*, 2010, 24, 393–398.
- [79] J. S. Mellors, K. Jorabchi, L. M. Smith and J. M. Ramsey, *Anal. Chem.*, 2010, 82, 967–973.
- [80] G. B. Salieb-Beugelaar, K. D. Dorfman, A. van den Bergm and J. C. T. Eijkel, *Lab Chip*, 2009, 9, 2508–2523.
- [81] A. I. Lo´pez-Lorente, B. M. Simonet and M. Valca´rcel, *Trends Anal. Chem.*, 2011, 30 (1).
- [82] M. Vaher, M. Koel, J. Kazarjan and M. Kaljurand, *Electrophoresis*, 2011, 32, 1068–1073.
- [83] M. Hanauer, S. Pierrat, I. Zins, A. Lotz and C. Sönnichsen, *Nano letter*, 2007, 7, 2881–2885.
- [84] H. Shadpour and S. A. Soper, *Anal. Chem.*, 2006, 78, 3519–3527.
- [85] T. Rabillouda, M. Chevallet, S. Luche, C. Lelong, *J. Proteomics*, 2010, 73, 2064–2077.
- [86] N. Lewpiriyawong, C. Yang and Y.C. Lam, *Electrophoresis*, 2010, 31, 2622–263.
- [87] A. Lenshof and T. Laurell, *Chem. Soc. Rev.*, 2010, 39, 1203–1217.
- [88] K. Khoshmanesh, S. Nahavandi, S. Baratchi, A. Mitchell and K. Kalantar-zadeh, *Biosens. Bioelectron.*, 2011, 26, 1800–1814.
- [89] A. B. Fuchs, A. Romani, D. Freida, G. Medoro, M. Abonnenc, L. Altomare, I. Chartier, D. Guergour, C. Villiers, P. N. Marche, M. Tartagni, R. Guerrieri, F. Chatelaina and N. Manaresi, *Lab Chip*, 2006, 6, 121–126.
- [90] K. Khoshmanesh, C. Zhang, F. J. Tovar-Lopez, S. Nahavandi, S. Baratchi, K. Kalantar-zadeh and A. Mitchell, *Electrophoresis*, 2009, 30, 3707–3717.
- [91] J. G. Kralj, M. T. W. Lis, M. A. Schmidt and K. F. Jensen, *Anal. Chem.*, 2006, 78, 5019–5025.
- [92] X. Xuan, J. S. H. Lee and D. Li, *Lab Chip*, 2006, 6, 274–279
- [93] Y. Kang, D. Li, S. A. Kalams and J. E. Eid, *Biomed Microdevices*, 2008, 10, 243–249
- [94] G. H. Mark and R. Pethig, *Biotechnol. Bioeng.*, 1995, 45, 337–343

- [95] W.-K. Chen, The electrical engineering handbook, *Academic Press*, 2005, 508-509.
- [96] B. J. Kirby and E. F. Hasselbrink Jr, *Electrophoresis*, 2004, 25, 187–202.
- [97] B. J. Kirby and E. F. Hasselbrink Jr, *Electrophoresis*, 2004, 25, 203-213.
- [98] J. Robertson, *Eur. Phys. J. Appl. Phys.*, 2004, 28, 265–291.
- [99] Y. Chun and D. Li, *J. colloid Interface Sci.*, 2004, 272, 480–488.
- [100] Y. Chun and D. Li, *Microfluid Nanofluid*, 2004, 1, 52–61.
- [101] Z. Wu and D. Li, *Electrochimica Acta*, 2009, 54, 3960–3967.
- [102] F. Durst, S. Ray, B. Unsal and O. A. Bayoumi, *J FLUID ENG-T ASME*, 2005, 127, 1154-1160.
- [103] S. Marinela, D. H. Choia, R. Heuguetb, D. Agrawala and M. Lanagan, *Ceram. Int.* 2013, 39, 299
- [104] [http://repositorio.ul.pt/bitstream/10451/1643/10/19741\\_ulsd\\_re487\\_10\\_Chapter2.pdf](http://repositorio.ul.pt/bitstream/10451/1643/10/19741_ulsd_re487_10_Chapter2.pdf).  
Last accessed: August 21st, 2014.
- [105] T. Rimmel, M. Schulberg, S. Fujimura, H. Honma, H. Kobayashi, H. Kohno, S. Owens, R. Deslattes and J. Pedulla, *Advances in X-ray Analysis*, 2000, 43
- [106] A. Tkach, O. Okhay, P. M. Vilarinho and A. L. Kholkin, *J. Phys.: Condens. Matter*, 2008, 20, 415224
- [107] W. Gao and Joseph Wang, *Nanoscale*, 2014, 6, 10486.



## Appendix

### Journal papers from the results of this thesis:

1. Fang Zhang, Dongqing Li, '**Induced-charge electroosmotic flow around dielectric particles in uniform electric field**', Journal of Colloid and Interface Science, Published online: November 15<sup>th</sup>, 2013.
2. Fang Zhang, Dongqing Li, '**A novel particle separation method based on induced-charge electro-osmotic flow and polarizability of dielectric particles**', Electrophoresis, published online: Aug 19<sup>th</sup>, 2014
3. Fang Zhang, Dongqing Li, '**Separation of Dielectric Janus Particles Based on Polarizability-Dependent Induced-Charge Electroosmotic Flow**', accepted by Journal of Colloid and Interface Science: February 3<sup>rd</sup>, 2015.

## License agreement for Chapter 4

This is a License Agreement between Fang Zhang ("You") and Elsevier ("Elsevier") provided by Copyright Clearance Center ("CCC"). The license consists of your order details, the terms and conditions provided by Elsevier, and the payment terms and conditions.

Supplier	Elsevier Limited The Boulevard, Langford Lane Kidlington, Oxford, OX5 1GB, UK
Registered Company Number	1982084
Licensed content publisher	Elsevier
Licensed content publication	Journal of Colloid and Interface Science
Licensed content title	Induced-charge electroosmotic flow around dielectric particles in uniform electric field
Licensed content author	Fang Zhang, Dongqing Li
License number	3480800575245
Licensed content date	15 November 2013
Licensed content volume number	410
Licensed content issue number	n/a
Number of pages	9
Start Page	102
End Page	110
Type of Use	reuse in a thesis/dissertation
Portion format	full article both print and electronic
Are you the author of this Elsevier article?	Yes
Will you be translating?	No
Title of your thesis	Induced-charge electroosmotic flow of dielectric particles and its application
Expected completion date	Jan 2015
Estimated size	150

## License agreement for Chapter 6

This is a License Agreement between Fang Zhang ("You") and John Wiley and Sons ("John Wiley and Sons") provided by Copyright Clearance Center ("CCC"). The license consists of your order details, the terms and conditions provided by John Wiley and Sons, and the payment terms and conditions.

License number	3480800796153
License date	Oct 02, 2014
Licensed content publisher	John Wiley and Sons
Licensed content publication	Electrophoresis
Licensed content title	A novel particle separation method based on induced-charge electro-osmotic flow and polarizability of dielectric particles
Licensed copyright line	© 2014 WILEY-VCH Verlag GmbH & Co. KGaA, Weinheim
Licensed content author	Fang Zhang, Dongqing Li
Licensed content date	Aug 19, 2014
Start page	n/a
End page	n/a
Type of use	Dissertation/Thesis
Requestor type	Author of this Wiley article
Type of Use	Print and electronic
Portion format	full article
Will you be translating?	No
Title of your thesis	Induced-charge electroosmotic flow of dielectric particles and its application
Expected completion date	Jan 2015
Estimated size	150

## **License agreement for Chapter 7**

The manuscript “Separation of Dielectric Janus Particles Based on Polarizability-Dependent Induced-Charge Electroosmotic Flow’ (IDJCIS-14-3482R1) authored by Fang Zhang and Dongqing Li is in press for publication in Journal of colloid and interface science.